ICEYE

DATA CALIBRATION AND VALIDATION

Version 1.0
Released: 22 June 2020

www.ICEYE.com

EXECUTIVE SUMMARY

ICEYE's constellation consists of several smallsat SAR sensors orbiting Earth with very high temporal resolution.

The use of different satellites requires a large calibration effort to allow the users to have the correct information about each satellite's capabilities.

The calibration allows the characterization of the elevation antenna pattern to be determined and therefore to calculate the calibration constant for each SAR system.

ICEYE has performed the calibration of every operational satellite, specifically ICEYE-X2, ICEYE-X4 and ICEYE-X5, and has validated the results using distributed targets in the Amazon and Congo forests as well as a dedicated Corner Reflector site. For this purpose, dedicated datasets have been acquired after the March 2020 SAR system update for each satellite. The intention is to repeat the calibration cycle periodically to increase constellation fidelity as the ICEYE fleet evolves.

This document provides detailed information on the calibration component with the validation activities presented here being only a partial data validation. This is to enable a more comprehensive calibration and validation campaign to be performed during the commissioning phase of each new ICEYE satellite. It will also facilitate more streamlined, and therefore routine and ongoing calibration validation of operational satellites throughout their lifetime.

It is shown in this document that the validation performed over the Congo forest converges towards the calibration results, showing a good agreement between the backscattering of the Amazon and the Congo forest, as summarized in section 3.2.4

The validation performed over the Corner Reflector site allowed only a partial validation, as shown in section 3.2.5 due to the lack of Spotlight images acquired over the Amazon forest and a smaller number of ICEYE-X2 images, as summarized in Table 3.

TABLE OF CONTENTS

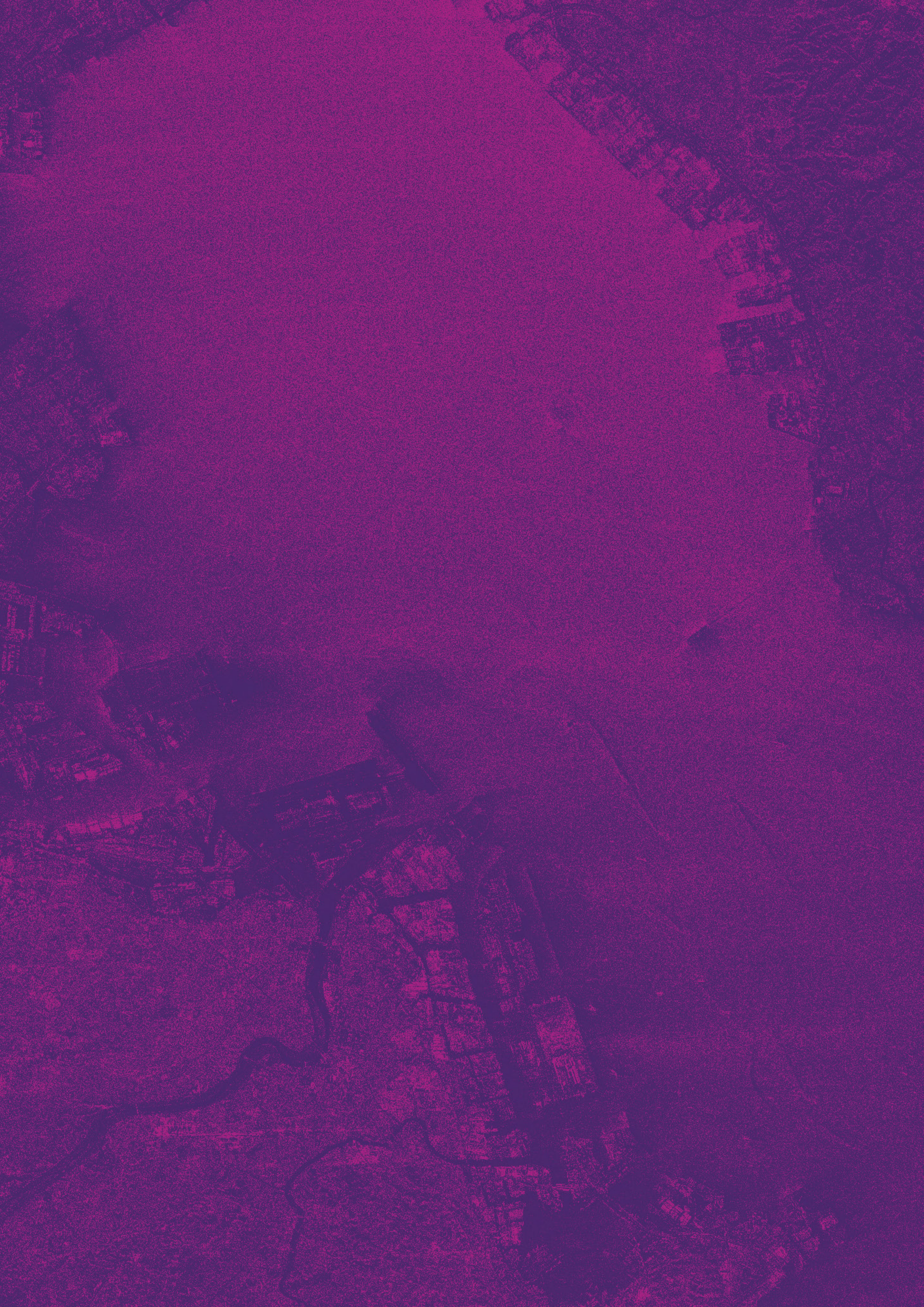

1. INTRODUCTION

1.1 PURPOSE AND SCOPE

ICEYE's constellation consists of several smallsat SAR sensors orbiting Earth with a goal of 3 hour access worldwide for acquiring SAR imagery in several imaging modes.

ICEYE X-band data can be used to easily retrieve the backscattering coefficient of distributed and point-like targets.

This document describes the calibration and validation methodologies used to generate calibrated data from Level 1 (L1) ICEYE products and to validate them.

In the first section, the calibration is used to estimate the elevation antenna pattern and the calibration constant, and has been performed by acquiring images over the Amazon forest and the Congo forest in regions that have homogeneous backscatter.

The next section covers the validation and has been performed using point-like targets over the Rosamond Corner Reflector Array (RCRA) area, located on the dry Rosamond lake bed and used by the JPL for SAR calibration, and distributed targets over the Congo forest, which has homogeneous backscatter similar to the Amazon forest, with the purpose of verifying the antenna pattern compensation and the calibration constant calculation.

The calibration and validation results of X2, X4 and X5 satellites are presented in the final section.

2. CALIBRATION THEORY

▶ CALIBRATION THEORY

CONTENTS

This section summarizes the auxiliary data conventions used in the Auxiliary Data Specification documents.

2.1 RADIOMETRIC CALIBRATION

Radiometric calibration is the process needed to associate unequivocally the received signal with the geophysical parameter of interest. In the case of SAR, the parameter of interest is the Backscattering Coefficient.

The calibration can be internal and external, and must compensate effects due to:

- the atmosphere (delay and oscillations of the signal during tropospheric and ionospheric propagation),
- the antenna (distribution of radiated energy in range and in azimuth),
- the electronic (variation of transmitted power and receiver gain),
- the processor (contribution due to the implemented algorithm).

Ignoring any atmospheric influence, the received power from the radar and the backscattering coefficient are related through the radar equation:

$$P_{rec} = \frac{P_t \cdot G_r \cdot G^2(\theta) \cdot \lambda^2}{(4\pi)^3 R^4} \cdot C_{proc} \cdot (\sigma^0 \delta x \delta R_g) \tag{1}$$

Where:
P_t = Transmitted power from the radar
G_r = Gain of the radar receiver
θ = Incidence angle
$G^2(\theta)$ = Two-way antenna pattern
λ = Wavelength
R = Slant range
σ^0 = Backscattering coefficient per area unit
C_{proc} = Processing constant
δx = Azimuth resolution
δR_g = Ground range resolution

▶ CALIBRATION THEORY

CONTENTS

Grouping the known terms in the constant K_{proc}, we obtain:

$$P_{rec} = K_{proc} \frac{P_t \cdot G_r \cdot G^2(\theta)}{R^4 \sin sin \ \theta} \cdot \sigma^0 \qquad (2)$$

The calibration process calculates the backscattering coefficient σ^0. It can be performed using the transmitting and receiving radar chain, the two-way antenna pattern, the distance between radar and target and the incidence angle.

ICEYE's calibration chain is used to estimate the two-way Antenna Pattern and the product $K_{proc} \cdot P_t \cdot G_r$.

Note that ICEYE calibration is selected to be

$$K = \frac{1}{K_{proc}}$$

2.2 ICEYE DATA RADIOMETRIC CALIBRATION ON DISTRIBUTED TARGETS

ICEYE uses the external calibration for the calculation of the backscattering coefficient using distributed targets for the calculation of the two-way antenna pattern $G^2(\theta)$.

The Amazon forest is selected as distributed target. The Congo forest is tested as a second candidate for distributed target.

Note that the ICEYE SAR processor compensates the following effects:

- Range spread loss;
- Elevation antenna pattern (the estimation method is explained in the next section);
- Azimuth antenna pattern in ScanSAR and spotlight modes;
- Sensor settings variations (receiver gain, transmit power, duty cycle)

The intensity value of the image is defined through the Digital Numbers DN:

$$|DN|^2 = I^2 + Q^2 = (|I + jQ|)^2 \quad (3)$$

with I and Q representing the real and imaginary amplitude of the complex data.

The intensity value is proportional to the radar brightness β^0:

$$\beta^0 = K \cdot |DN|^2 \cdot FSL \cdot \frac{1}{G^2(\theta)} \quad (4)$$

Where K is the calibration constant and $FSL = \frac{R^3}{R^3_{Ref}}$ is the Free Space Loss factor.

The radar brightness β^0 is proportional to the backscattering coefficient σ^0:

$$\sigma^0 = \beta^0 \cdot \sin sin\theta - NESZ = K \cdot |DN|^2 \sin sin\ \theta - NESZ \quad (5)$$

where NESZ is the Noise Equivalent Sigma Zero.

Assuming that the FSL has been compensated, the gamma nought results:

$$\gamma^0(\theta) = K \cdot |DN|^2 \cdot \frac{1}{G^2(\theta)} \tan tan\ \theta \quad (6)$$

The Amazon forest is a homogeneous scatterer and it is assumed that $\tan tan\ \theta$ gamma nought is constant in elevation. It means that if the profile is not constant, it is due to the elevation antenna pattern $G^2(\theta)$.

The antenna pattern is estimated through the following steps.

1. A set of images acquired over the reference site in the Amazon forest is selected.
2. The gamma nought is calculated for any image:
   $\gamma^0(\theta) = |DN|^2 \cdot \tan\theta$
3. The homogeneity of the images is analyzed, due to the fact that in the acquired scenes there are regions present that are non-homogeneous caused by rocks, rivers, topography and meteorological effects. The non-homogeneous areas are filtered out. The filtering is performed following the steps:
   - The histogram of the image is calculated with the mean μ and the standard deviation σ.
   - The histogram is limited between $[0, \mu+4\sigma]$ and the data values are scaled to $[0,255]$.
   - Two methods can be applied to reduce the speckle in the images: multilooking or image smoothing using a Gaussian kernel.
   - A global thresholding algorithm based on an adaptive gaussian filter is used to generate the threshold T below which the data can be masked.
   - The image is then masked using the threshold:
     $I_{masked} = I(I>T)$.

   The masking is required to exclude the areas not pertaining to the isotropic vegetation.
4. The gamma nought profile in range is obtained calculating the mean of filtered gamma nought in azimuth.
5. The elevation antenna pattern (AP) is calculated from the single image fitting the gamma profile with a sinc-squared function.

▶ CALIBRATION THEORY

CONTENTS

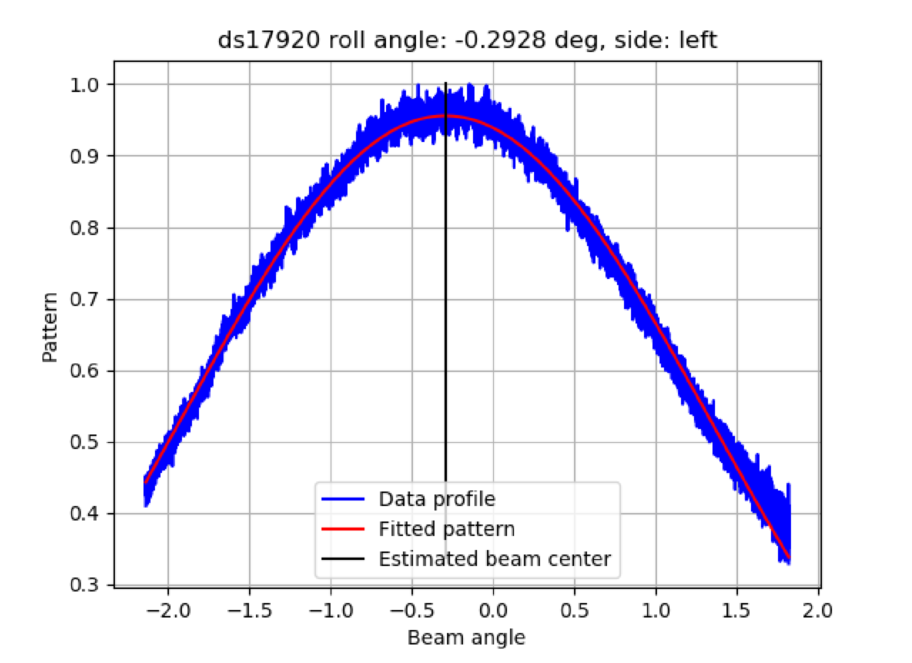

Figure 1. Antenna pattern fitting using sinc square function

6. The roll angle is calculated from the position of the maximum of the AP. The profile is shifted by the corresponding roll angle α to align the maximum with the beam center.
7. The procedure is repeated for a number of calibration acquisitions and mean of all the results is taken as the Elevation Antenna Pattern $G^2\ (\theta)$.

▶ CALIBRATION THEORY

CONTENTS

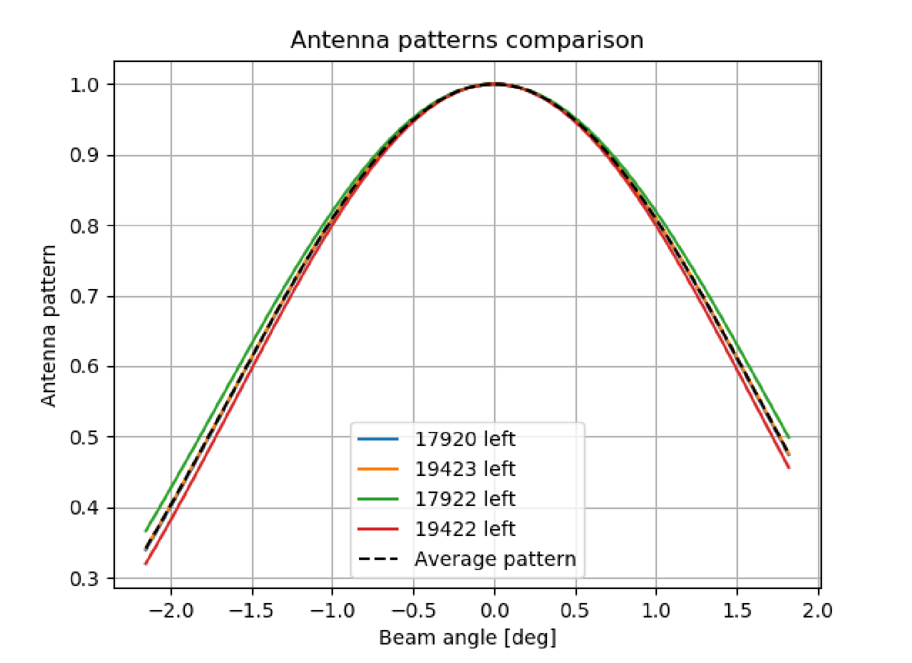

Figure 2. Comparison of the antenna pattern fittings of different images and the final mean

The antenna pattern $G^2(\theta)$ is used to calibrate the image amplitude. The calibration is performed through the following steps:

1. Gamma nought without calibration or correction is calculated from the received data;

$$\gamma^{0\prime}(\theta) = |DN|^2 \tan(\theta) \tag{7}$$

2. The antenna pattern correction is applied to the gamma nought:

$$\gamma^{0\prime\prime}(\theta) = |DN|^2 \tan(\theta) \cdot \frac{1}{G^2(\theta)} \tag{8}$$

3. The non-homogeneous areas, like rocks, rivers, topography, meteorological effects, are filtered out. The filtering is performed following the steps:
   - The histogram of the image is calculated with the mean μ and the standard deviation σ.
   - The histogram is limited between $[0, \mu+3\sigma]$ and the data values are scaled to $[0,255]$.

▶ CALIBRATION THEORY

CONTENTS

- Two methods can be applied to reduce the speckle in the images: the multilooking or image smoothing using a Gaussian kernel.
- A global thresholding algorithm based on adaptive Otsu binarization is used to generate the threshold T below which data can be masked.
- The image is masked using the threshold: $I_{masked} = I(I>T)$.

4. It is assumed that the value of the mean backscattering coefficient of the Amazon forest is constant RCS_{forest} (in dB RCS_{forest} = -6.5 dB); the calibration constant is obtained from:

$$K = \frac{RCS_{forest}}{\gamma^{0''}(\theta)} \qquad (9)$$

Where $\gamma 0''(\theta)$ is the mean of all the gamma nought values.

5. The histogram for the calibration constant values for a given dataset is calculated. The peak of the K distribution is located and a 2nd degree polynomial is fitted around this peak. The real peak is then identified as a maximum of the fitted polynomial.
6. The calibration coefficient is then calculated for a dataset with a sufficient number of images to ensure the statistic validity.

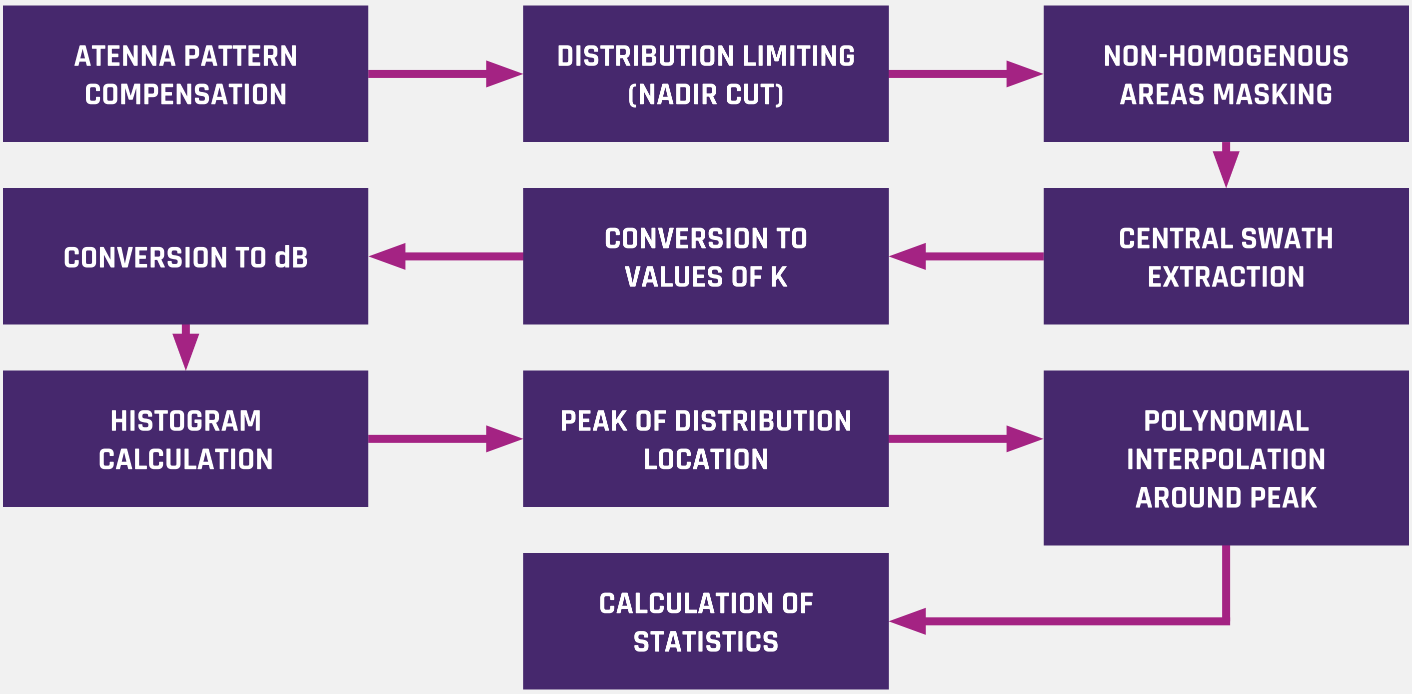

Figure 3. Scheme of the calibration constant estimation.

▶ CALIBRATION THEORY

CONTENTS

2.3 ICEYE CALIBRATION ON POINT-LIKE TARGETS

The acquisition of images on targets with known Radar Cross Section (RCS) is a fundamental test for calibration purposes. The Corner Reflectors used for ICEYE Point Target calibrations are located in California in the Rosamond Corner Reflector Array (RCRA) area. Here, in the dry Rosamond lake bed there are 38 trihedral Corner Reflectors with different size, orientations and elevations.

The 3 CR types are initially designed for 3 frequency bands:

1. 4.8 meter trihedral for P-band, constructed with Aluminum with larger 0.5” (12.7mm) round holes, and 48% open surface area. The larger holes are still compatible with L-band, but in principle not with X band that has a wavelength of 3.11 cm. In fact, the hole diameter must be less than one sixth of the radar wavelength in order to not affect the RCS of the CR.
2. 2.4 meter trihedral for L-band, constructed with Aluminum with staggered round holes of size 0.09375” (2.4 mm). Even if designed for L-band, the CR seems to be compatible with X-band systems.
3. 0.7 meter trihedral for Ka-band constructed with 12 (2.053 mm) gauge aluminum solid sheets.

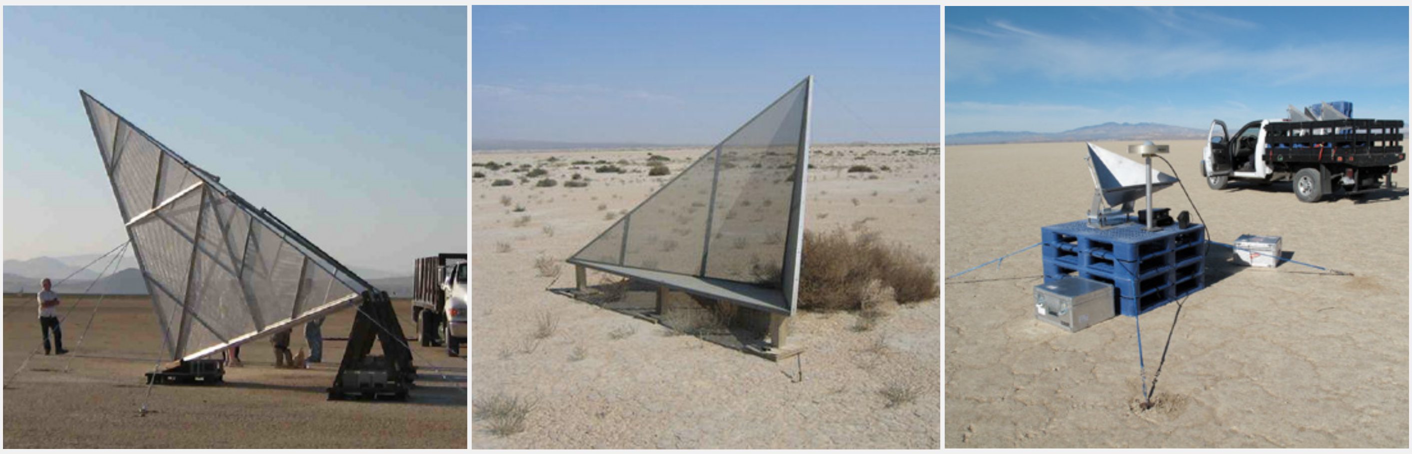

Figure 4. Three types of CR with trihedral shape in the Rosamond area, respectively 4.8 m, 2.4 m and 0.7 m size.

▶ CALIBRATION THEORY

CONTENTS

2.3.1 THEORETICAL RCS OF TRIHEDRAL CORNER REFLECTORS

The theoretical RCS can be calculated analytically with good accuracy for standard Corner Reflector [5].

The RCS of the trihedral CR depends on the size and wavelength.

$$\sigma_{trihedral}(\alpha, \lambda) \leq \frac{4\pi a^4}{3\lambda^2} \qquad 10$$

If the radar is not aligned with the CR orientation, the RCS will depend on the misalignment of the CR with the Line Of Sight direction, and will be function of azimuth and elevation angles of the corner reflector:

$$\sigma_{trihedral}(\psi, \phi) = \{ \frac{4\pi a^4}{\lambda^2} \cdot \left(\frac{4c_1c_2}{c_1+c_2+c_3} \right)^2 for \qquad 11$$

$$c_1 + c_2 \leq c_3 \quad \frac{4\pi a^4}{\lambda^2} \cdot \left(c_1+c_2+c_3 - \frac{2}{c_1+c_2+c_3} \right)^2 for$$

$$c_1 + c_2 > c_3$$

Where c1, c2 and c3 are each assigned one of $\{c_1c_2c_3 = \{\sin sin\ \varphi$ $\cos cos\ \varphi$ $\sin sin\ \psi$ $\cos cos\ \varphi$ $\cos cos$ $\cos cos\ \varphi$ such that $c_1 \leq c_2 \leq c_3$.

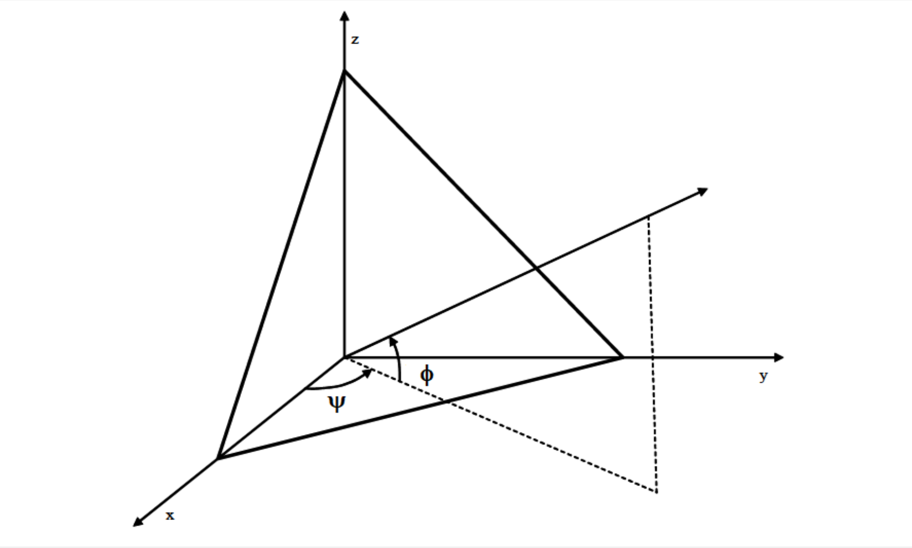

Figure 5. CR geometry definition for the calculation of RCS

▶ CALIBRATION THEORY

CONTENTS

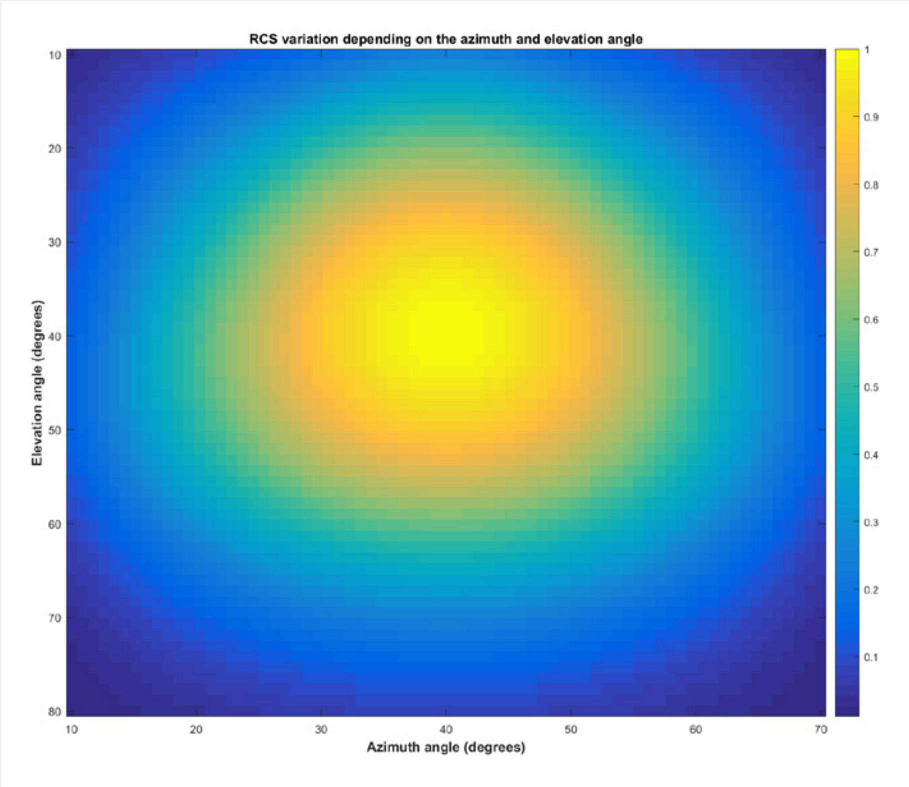

Figure 6. RCS of trihedral CR in function of the misalignment in azimuth and elevation

Let φ_{CR} , ψ_{Look} and ψ_{CR} respectively be the CR elevation, the geographical look orientation and the geographical CR orientation.

The angle $\Delta\varphi$ is the misalignment in elevation, and is calculated as $90 - \theta - \varphi_{CR}$. The maximum RCS is obtained at 35°, as shown in Figure 6.

The angle $\Delta\psi$ is the misalignment in azimuth, and is calculated as $\psi_{Look} - \psi_{CR} + 45$. The maximum RCS is obtained at 45°.

▶ CALIBRATION THEORY

CONTENTS

The geographical line of sight orientation is obtained by projecting the pointing vector target-satellite onto the plane passing through the target's position and tangent to the Earth ellipsoid.

It is obtained in the following steps:

Let $P_{sat} = (x_s y_s z_s)$ and $P_{target} = (x_t y_t z_t)$ which are the satellite position and target position in ECEF (Earth-Centered Earth-Fixed) coordinate system respectively.

The pointing vector from target to satellite is:

$$P_{ts} = P_{sat} - P_{target} = (x_s - x_t y_s - y_t z_s - z_t) \quad (12)$$

The vector must be projected on the local coordinate system. It is obtained through the ECEF system rotation depending on the latitude and longitude.

Let $V_{rot} = (-\sin sin\ \vartheta_{long}\ \cos cos\ \vartheta_{long}\ 0)$, the vector for the rotation of the plane (x,y), where ϑ_{long} is the longitude.

Let $P_{target\_norm} = P_{target}\ /\ max\ \{\ P_{target}\ \}$, the normalized vector position.

The conversion local to the ECEF system is obtained through the rotational matrix:

$$R_{local2ECEF} = [\ V_{rot}\ P_{target\_norm} \times V_{rot}\ P_{target\_norm}\ ] \quad (13)$$

Transposing the rotational matrix we obtain the rotational matrix for the conversion from ECEF coordinates to local system coordinates:

$$R_{ECEF2local} = R_{local2ECEF}^{\ T} \quad (14)$$

The projection of the pointing vector onto the local coordinates is calculated as:

$$P_{ts\_local} = R_{ECEF2local} \cdot P_{ts} = [\ V_{rot}\ P_{target} \times V_{rot}\ P_{target}\ ]\ [\ x_s - x_t y - y_t z_s - z_t\ ] = [x_{local}\ y_{local}\ z_{local}] \quad (15)$$

The geographical orientation is:

$$\psi_{Look} = tan^{-1}\left(\frac{y_{local}}{x_{local}}\right) \qquad 16$$

2.3.2 RADIOMETRIC CALIBRATION OF POINT TARGETS

In the validation the RCS of the CR $\sigma trihedral\ (\psi,\ \phi)$ must be compared with the measured RCS from the images.

The RCS is calculated from:

$$\sigma = K\ \frac{I_P \cdot P_A}{C_F}\ sin(\theta) \qquad 17$$

Where I_P is the total power of the IRF mainlobe, P_A the product pixel area and C_F is the relative power in the point target sidelobes. The relative power in sidelobes is calculated as

$$C_F = \frac{1}{1+ISLR}$$

where ISLR is the 2D Integrated Side Lobe Ratio. The Pixel area is calculated as $P_A = \Delta a \cdot \Delta r$, where Δa and Δr are respectively the pixel spacing in azimuth and in range.

To calculate the total power of the IRF mainlobe I_P, it is necessary to remove the background radar cross-section contribution.

It can be done following the steps:

1. Take a sub-image around the CR.
2. Calculate the intensity $I = |DN|^2$
3. Select 4 areas shown in Figure 7 to calculate the background mean and calculate the mean value.
4. Interpolate the image and subtract the mean background value from I.
5. Integrate the main peak in 2D. The main peak is represented by the colored area in Figure 8.

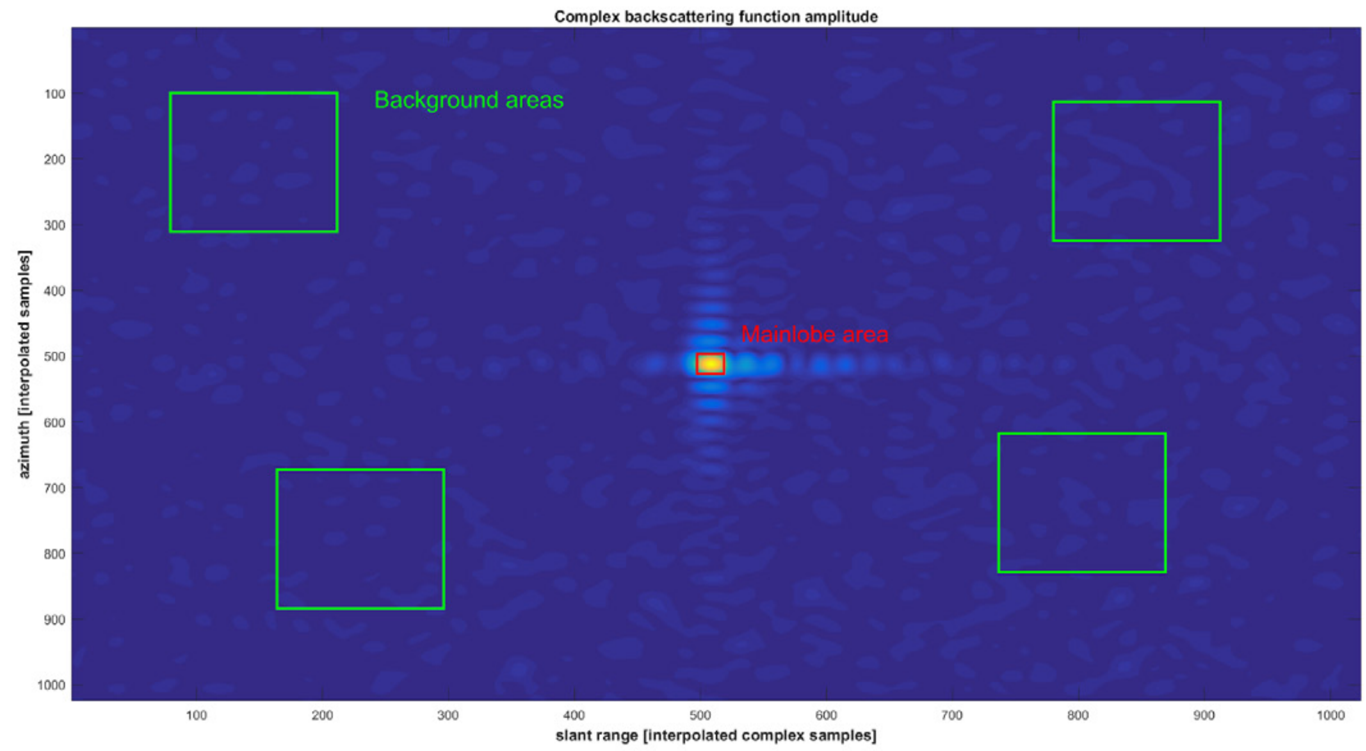

Figure 7. Definition of mainlobe area and background areas for RCS calculation

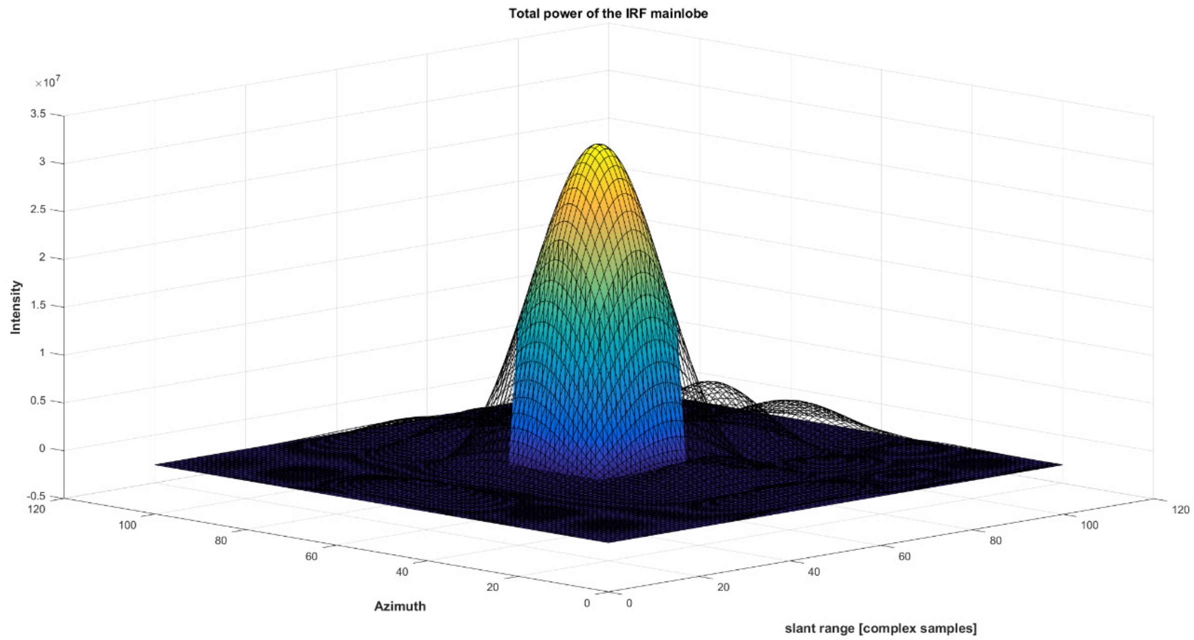

Figure 8. Mainlobe area to integrate for the calculation of I_P

2.3.3 CORNER REFLECTORS SELECTION AND FILTERING PARAMETERS CALCULATION

The precise measurement of RCS can easily be undermined by the presence of unknown and uncharacterised errors. Typical sources for error are multi path, undesired reflections and insufficient knowledge of the nature and form of the Corner Reflectors used for this analysis.

An approach to reduce these errors sources is to analyse the statistical trend of the results for a large amount of data with the aim of finding which Corner Reflectors are the best candidates for RCS calculations and to filter the parameters that provide more accurate results .

A key reference parameter related to the quality of the RCS calculation is the ratio between the theoretical RCS value and the measured RCS:

$$R_{\sigma} = \frac{\sigma_{trihedral}(\psi, \phi)}{\sigma^0} \tag{18}$$

The selection of the best CR candidates for validation purposes has been performed by processing a large number of datasets for each satellite, calculating the RCS of the Corner Reflectors and analysing the statistical parameters of the parameter R_{σ} for every Corner Reflector.

After the Corner Reflector selection, the RCS of the CRs is calculated with dedicated parameters that should filter out the RCS estimations most affected by large errors.

In this analysis four parameters related to the measurement quality have been investigated.

It should be noted that the dataset used for the selection of reliable RCS measurements is different by the dataset that has been used to validate the calibration results.

2.3.3.1 AZIMUTH SPECTRUM PHASE PARAMETERS

The first two parameters for RCS quality estimation exploit the azimuth spectrum of the focused target.

The justification in the use of the azimuth spectrum is related to the spectral phase behaviour for stable targets. Good candidates will present a phase that follows a polynomial behaviour (preferably linear), while the phase will be noisy in the presence of ground clutter or if deviating for a polynomial trend in the presence of multipath.

The selection of suitable CRs is performed in the following steps.

1. The azimuth profile $P_{az}(s)$, where s is the azimuth time, corresponding to the peak in the interpolated matrix is calculated. Note that the Doppler spectrum has been previously centered.
2. The Fourier Transform is calculated from the azimuth profile $FFT\ \{P_{az}\} = S_{az}(f_D) = A_{az}\ (f_D) \cdot e^{j\phi_{az}(f_D)}$, where f_D is the Doppler frequency.
3. The normalized amplitude of the spectrum $A_{az}\ (f_D)$ is used to calculate the frequency range of the signal.
4. The spectral phase $\phi_{az}(f_D)$ is calculated in the frequency range found in the previous step. The phase must be unwrapped; before the unwrapping, the signal has to be basebanded:
   $\phi^{uw}_{az}(f_D) = unwrap\ \{\phi_{az}(f_D) \cdot e^{j\pi f_{Di}}\}$ with $f_{Di} = 1, 2, \ldots N_{az}$ and N_{az}
   the points used to calculate the FFT. It is done to avoid undesired phase jumps of π.
5. The unwrapped phase is fitted with a polynomial function of third degree and the phase is corrected subtracting the fitted polynomial function to the original phase.
   The Mean Square Error MSE from the fitting and the original phase and the standard deviation of the corrected phase σ are calculated. The two parameters for RCS quality estimation are named σ_{CASP} (Standard Deviation of the Corrected Azimuth Spectral Phase) and MSE_{CASP} .
6. The Corner Reflector is qualified as good target for calibration if: $MSE \leq MSE_{th}$ and $\sigma_{CASP} \leq \sigma_{CASP_{th}}$.

Figure 9 and Figure 10 show two examples of bad and good Corner Reflectors for calibration. As it is possible to observe, the good CR has a low standard deviation of phase and the phase behaviour follows a polynomial trend.

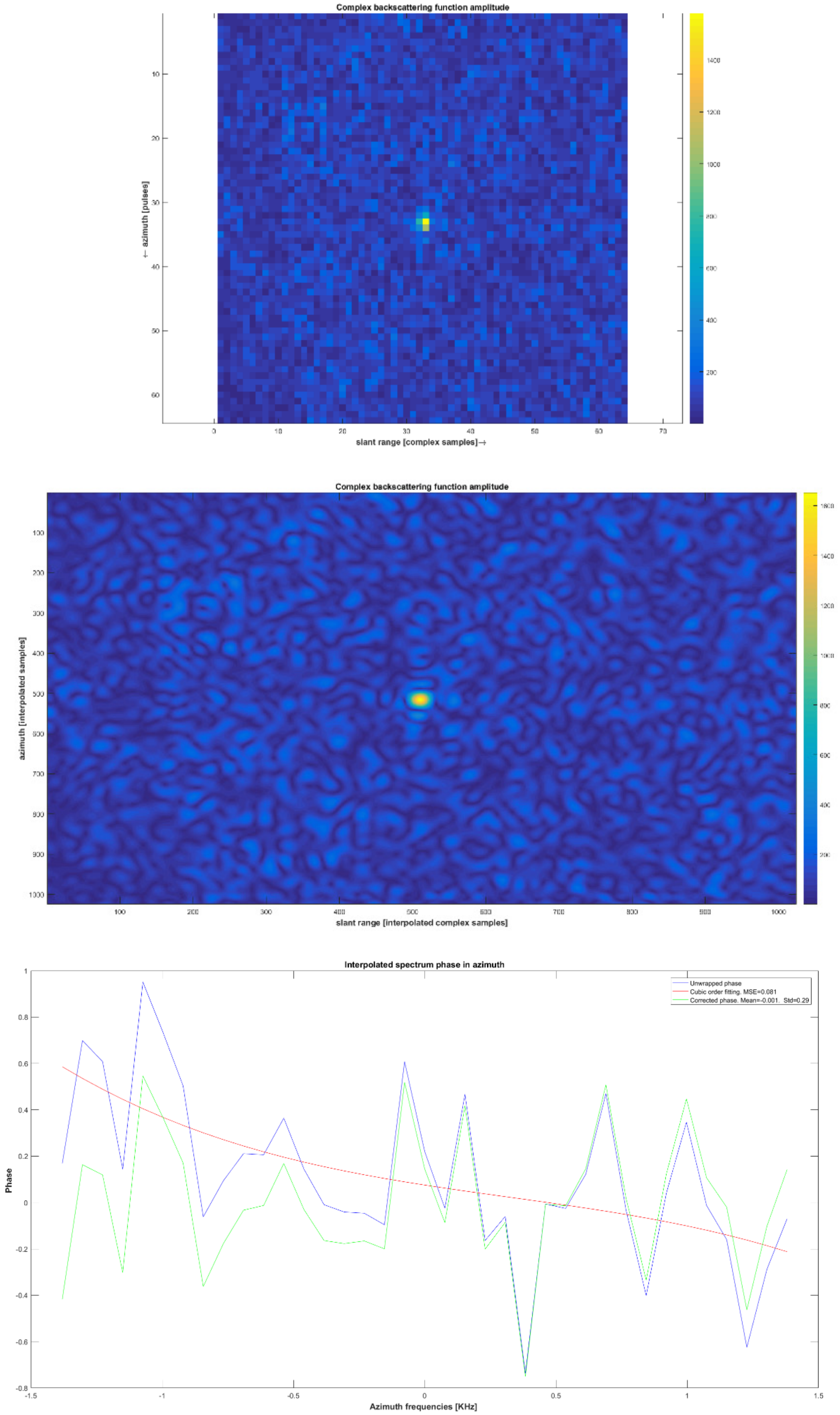

Figure 9. Example of CR excluded for calibration. Amplitude image (top), interpolated image (middle) and azimuth spectral phase (bottom)

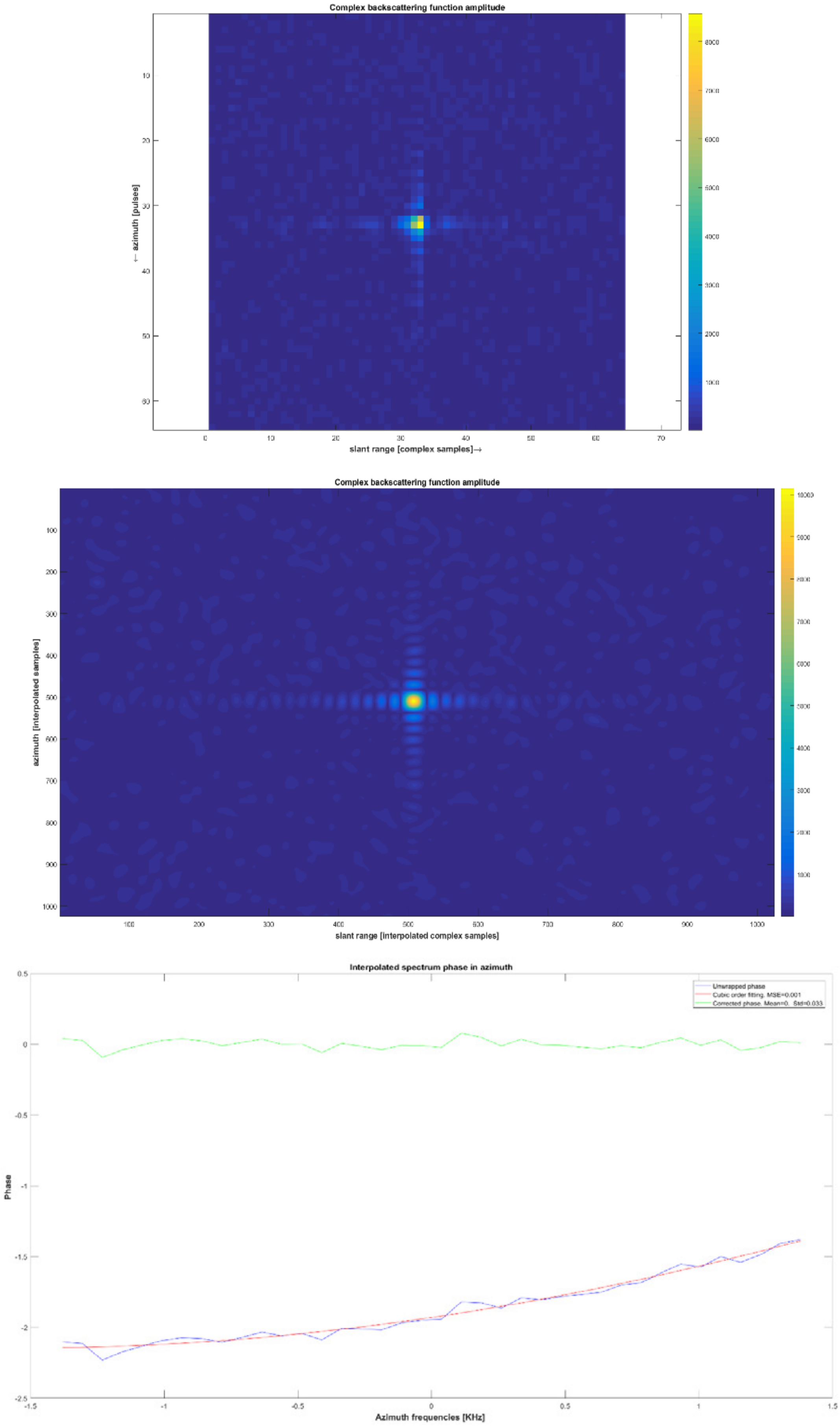

Figure 10. Example of good CR for calibration. Amplitude image (top), interpolated image (middle) and azimuth spectral phase (bottom)

2.3.3.2 SUBAPERTURE PEAK POSITION PARAMETER

The maximum backscattering of the Corner Reflector should correspond to the time in which the azimuth misalignment with the CR is null. If the azimuth misalignment is not too large, the maximum backscattering should occur in the central portion of synthetic aperture.

The generation of subapertures has been performed to calculate the variation of the peak intensity of the targets and to measure the corresponding peak position.

The selection of quality check of CRs is performed in the following steps.

1. Centring of the azimuth spectrum.
2. Generation of multiple sub-apertures with the 50% of the total bandwidth and with centers that cover the full azimuth spectrum.
3. Interpolation of each subaperture and intensity peak calculation.
4. Analysis of the peaks and selection of the subaperture with highest peak.

2.3.3.3 STANDARD DEVIATION OF THE GRADIENT OF THE 2D SPECTRAL PHASE

This parameter quantifies the phase noise in the 2D spectrum. If the phase has low noise, it is possible to unwrap the phase in 2 dimensions with continuity.

The STD of the gradient of the 2D spectral phase is calculated in the following steps.

1. The 2D Fourier Transform is calculated from the interpolated matrix over the IRF mainlobe I_M:
   $FFT2\{I_M\} = S_{2D}(f_D, f) = A_{2D}(f_D, f) \cdot e^{j\phi_{2D}(f_D, f)}$, where f_D is the Doppler frequency and f the range frequency.
2. The spectral phase $\phi_{2D}(f_D, f)$ is calculated in the frequency range found in the previous step. Before the unwrapping, the signal has to be basebanded in both dimensions. The 2D unwrap is performed by:
   $\phi_{2D}^{uw}(f_D, f) = unwrap\{\phi_{2D}(f_{Di}, f_i) \cdot e^{j\pi f_{Di}} \cdot e^{j\pi f_i}\}$
   with $f_{Di} = 1,2,\ldots N_{az}$, $f_i = 1,2,\ldots N_{rg}$, where N_{az} and N_{rg} are respectively the points used to calculate the FFT in azimuth and range.

▶ CALIBRATION THEORY

CONTENTS

3. The unwrapped phase is subsampled in both direction and the gradient $\nabla\,\phi_{2D}^{uw}(f_D, f)$ is calculated. The standard deviation of the gradient measures the phase continuity of the IRF. The parameter is named σ_{ASPG} (STD of the Azimuth Spectral Phase Gradient).
4. The Corner Reflector is qualified as good target for calibration if: $\sigma_{ASPG} \leq \sigma_{ASPG_{th}}$.

Figure 11 and Figure 12 show two examples of phase with and without noise.

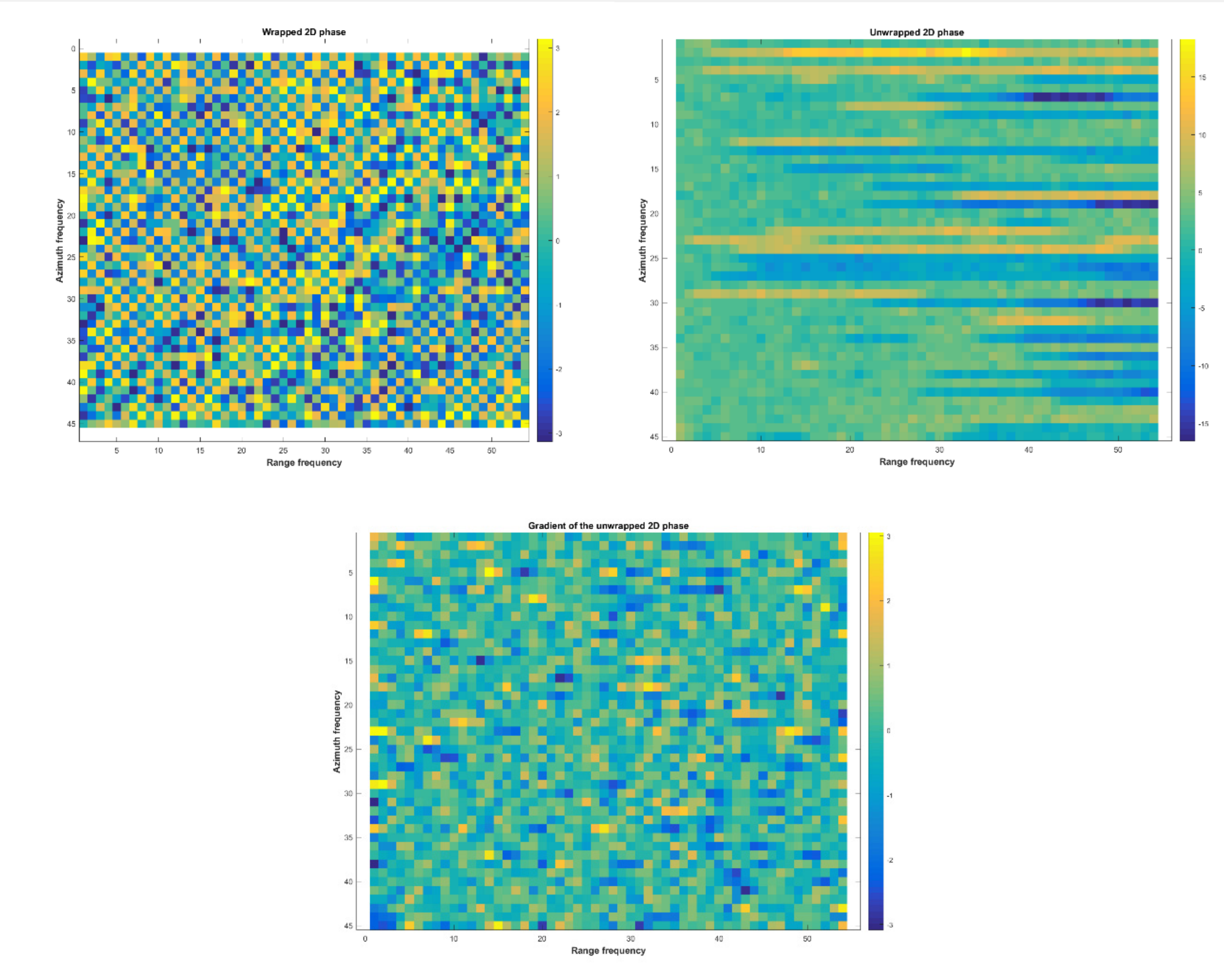

Figure 11. Example of CR excluded for validation. Wrapped phase (top left), unwrapped phase (top right) and gradient (bottom)

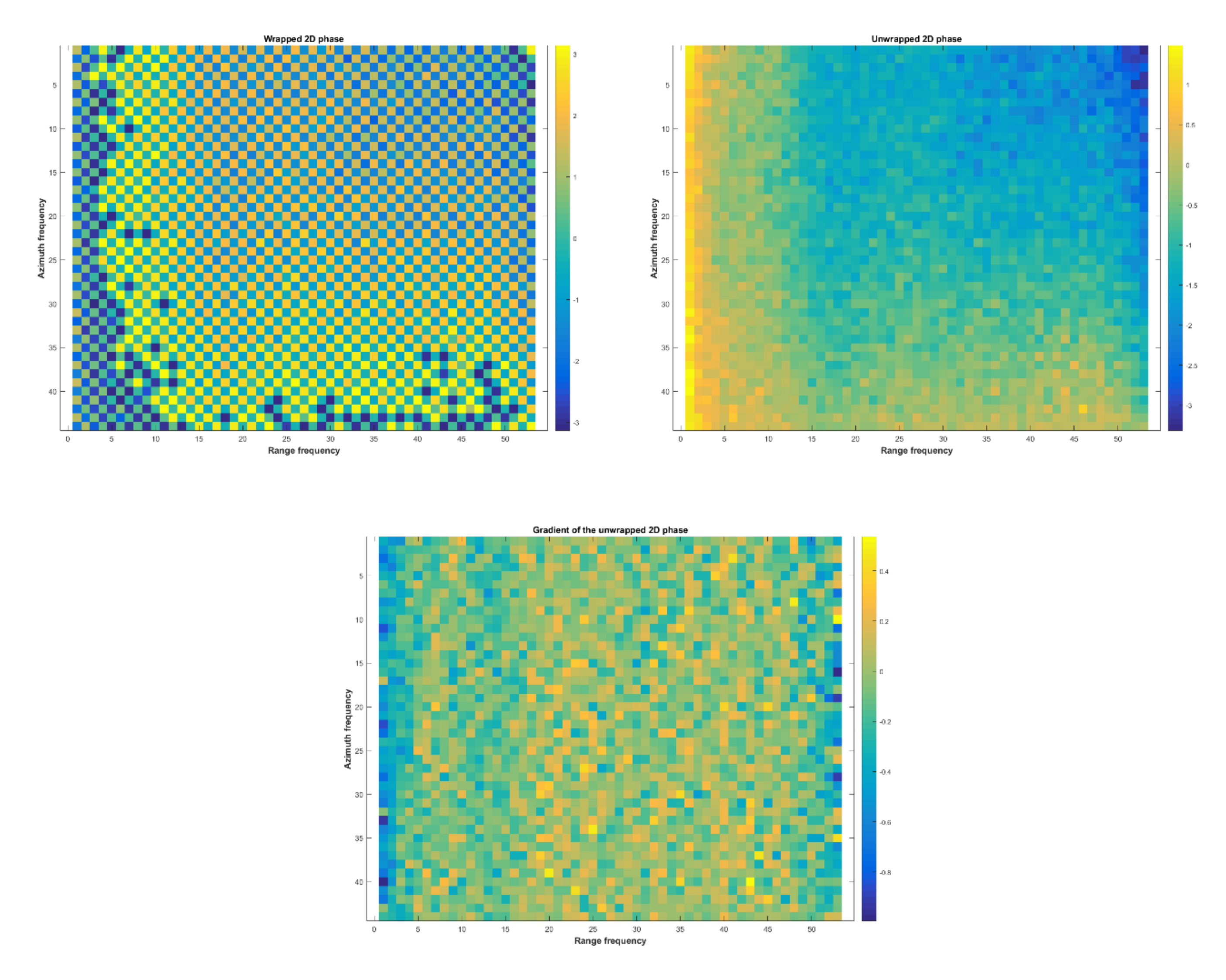

Figure 12. Example of CR selected for validation. Wrapped phase (top left), unwrapped phase (top right) and gradient (bottom)

3. CALIBRATION & VALIDATION OF ICEYE SENSORS

3.1 CHOICE OF TESTS SITES

3.1.1 ICEYE CALIBRATION ON DISTRIBUTED TARGETS: AMAZON FOREST

As discussed in Sec. 2.2, the calibration activities have been performed in the Amazon forest, which is the most typical distributed target. Figure 13 shows the typical area used for the ICEYE sensors calibration.

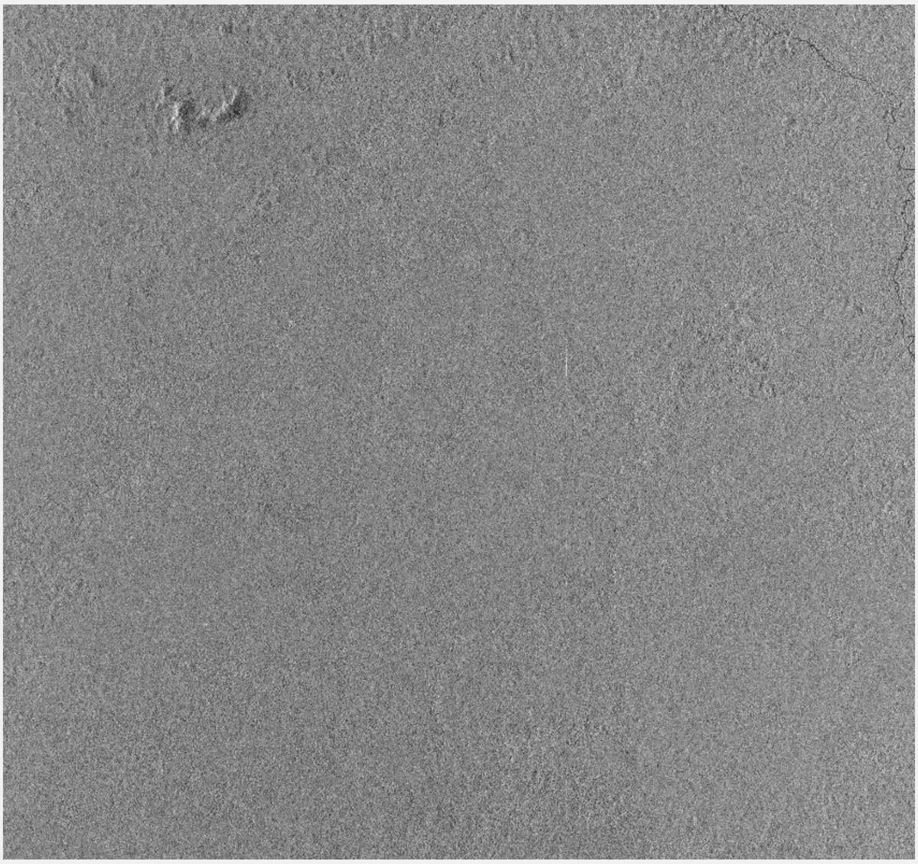

Figure 13. Test site in the Amazon forest.

3.1.2 ICEYE VALIDATION ON DISTRIBUTED TARGETS: CONGO FOREST

The Congo forest is used to validate the antenna pattern and the calibration constant previously retrieved from the Amazon forest, allowing an independent verification.

It is here assumed that the Congo forest has similar density and tree types as the Amazon forest, for which the Gamma nought has backscattering constant in elevation.

For the antenna pattern, the residual range profile is analyzed to validate it, while the calibration constant is validated using the pixels from the Area Of Interest.

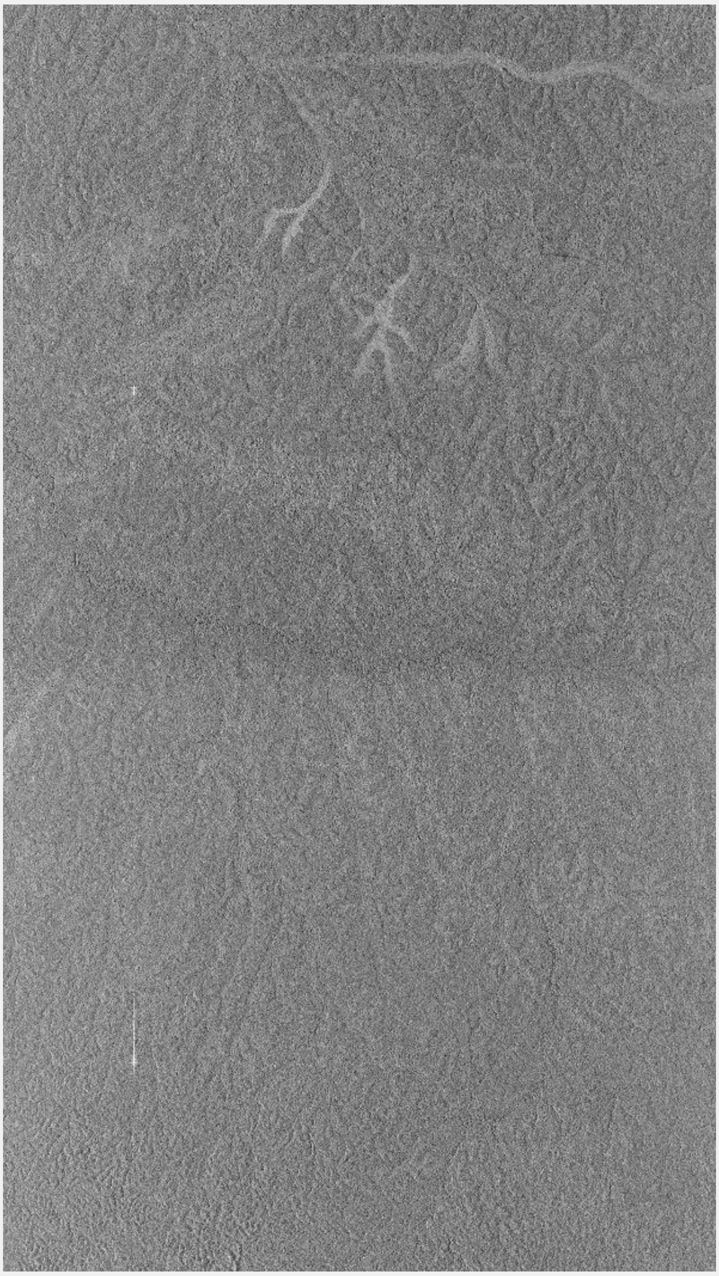

Figure 14. Test site in the Congo forest.

▶ CALIBRATION & VALIDATION OF ICEYE SENSORS

3.1.3 ICEYE VALIDATION ON POINT TARGETS: ROSAMOND CORNER REFLECTOR ARRAY

The validation phase on point targets has been performed in the Rosamond Corner Reflector Array (RCRA) area in California. Here, in the dry Rosamond lake bed there are 37 Corner Reflectors with different size (0.7 m, 2.4 m and 4.8 m), used by the JPL for SAR calibration, as shown in Figure 15.

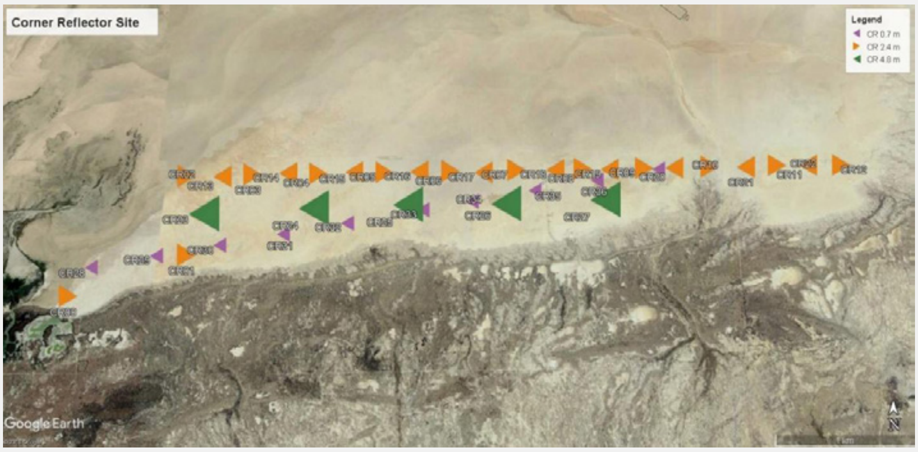

Figure 15. Test site in the Rosamond Corner Reflector Array area

3.2 CALIBRATION AND VALIDATION RESULTS

This section presents the results obtained during the phases of calibration and validation.

For the calibration, firstly the results for elevation antenna pattern and secondly the results for calibration constant will be presented.

The validation has been performed on point targets and distributed targets.

For the Corner Reflector Analysis, firstly the results of the selection of reliable Corner Reflectors and filtering parameters has been shown. Secondly, the validation results to verify the quality of calibration has been proposed.

For the distributed target, the Congo forest has been used to compare the results in terms of antenna pattern estimation and calibration constant calculation.

3.2.1 ANTENNA ELEVATION BEAM CALIBRATION

3.2.1.1 RESULTS FOR X2 SATELLITE

The results for the antenna pattern of X2 satellite are shown in the following figures in right and left looking mode.

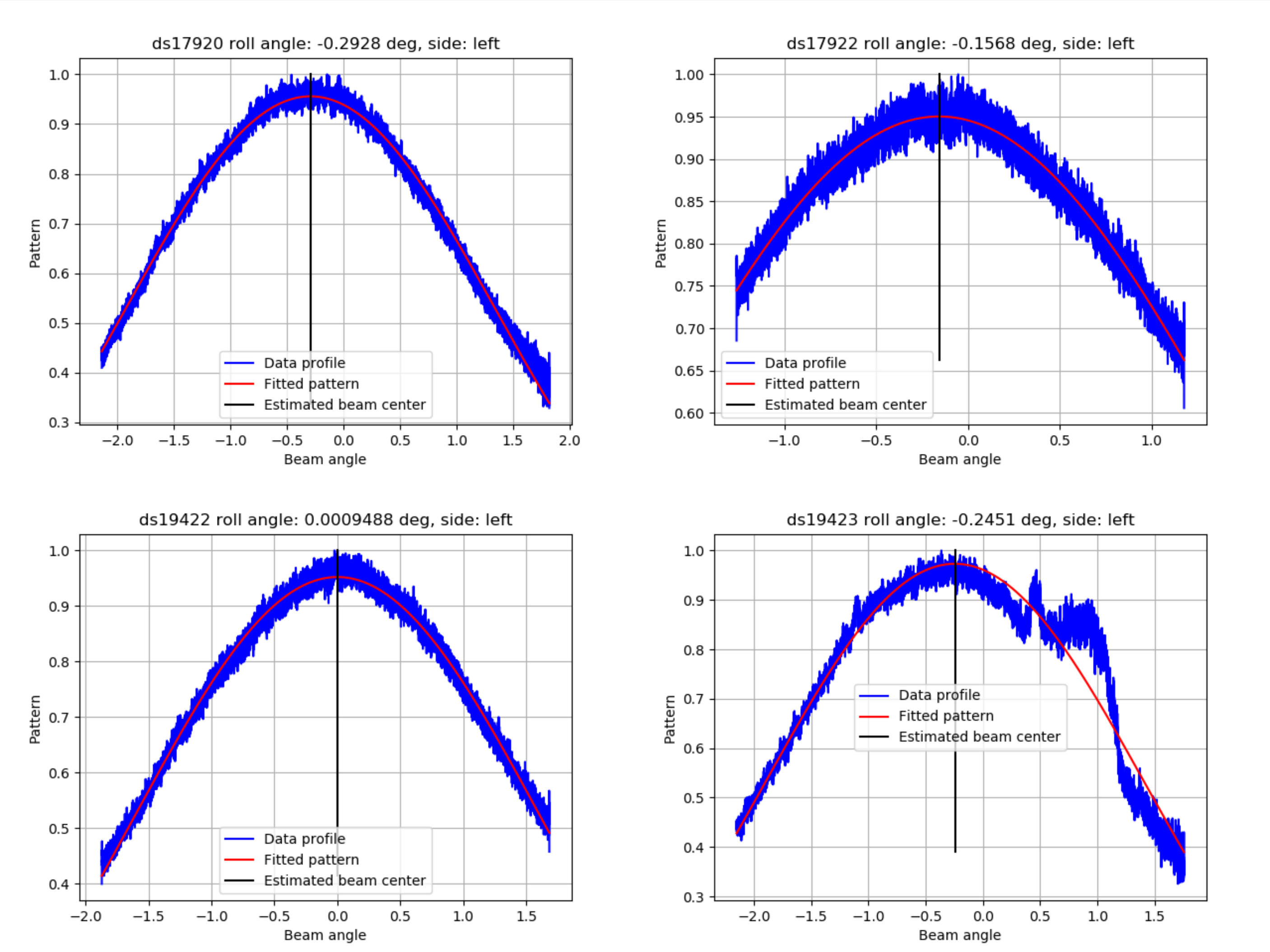

Figure 16. Chosen antenna calibration results for X2 satellite: left looking data profiles

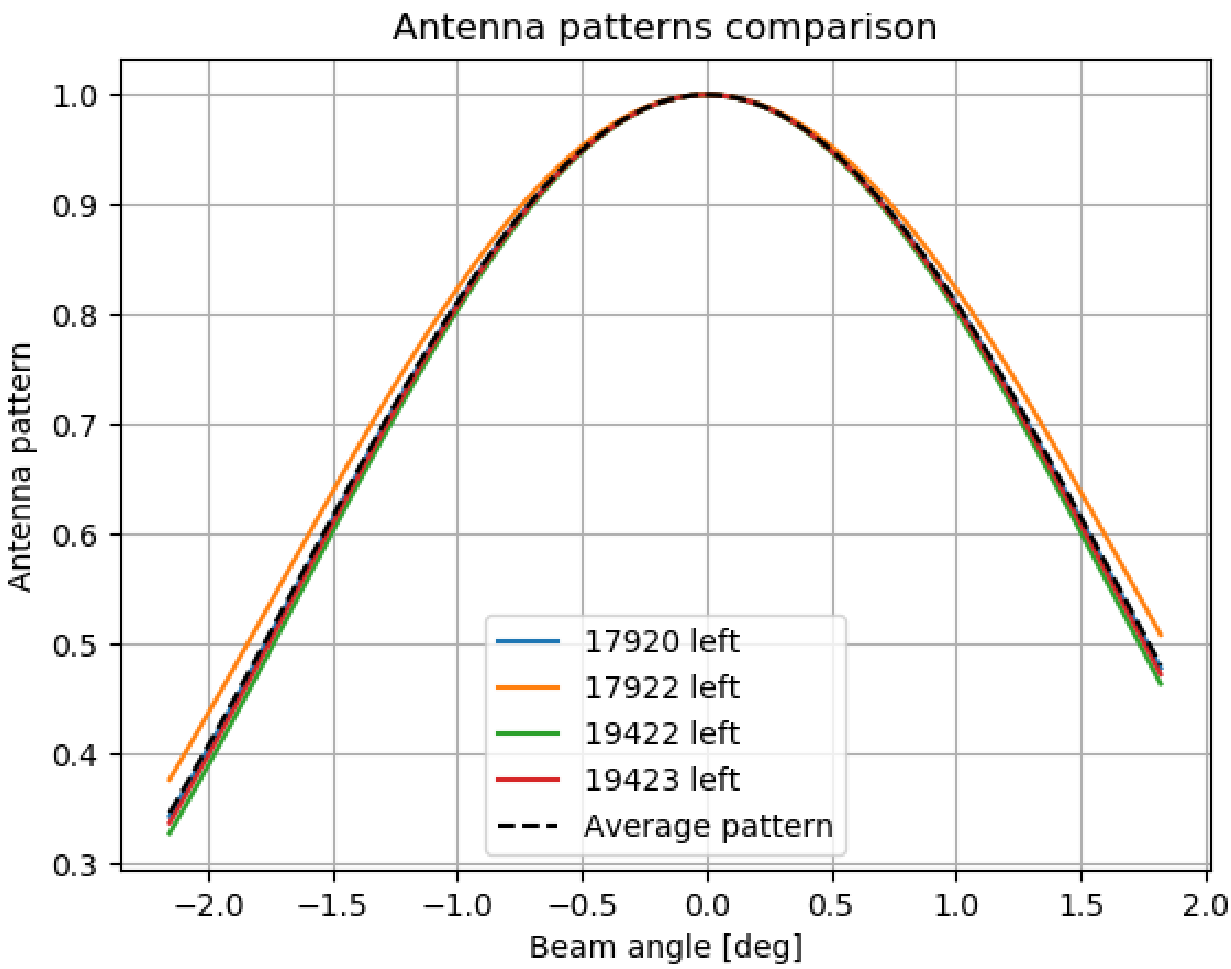

Figure 17. Comparison of antenna pattern fittings for X2 (left looking)

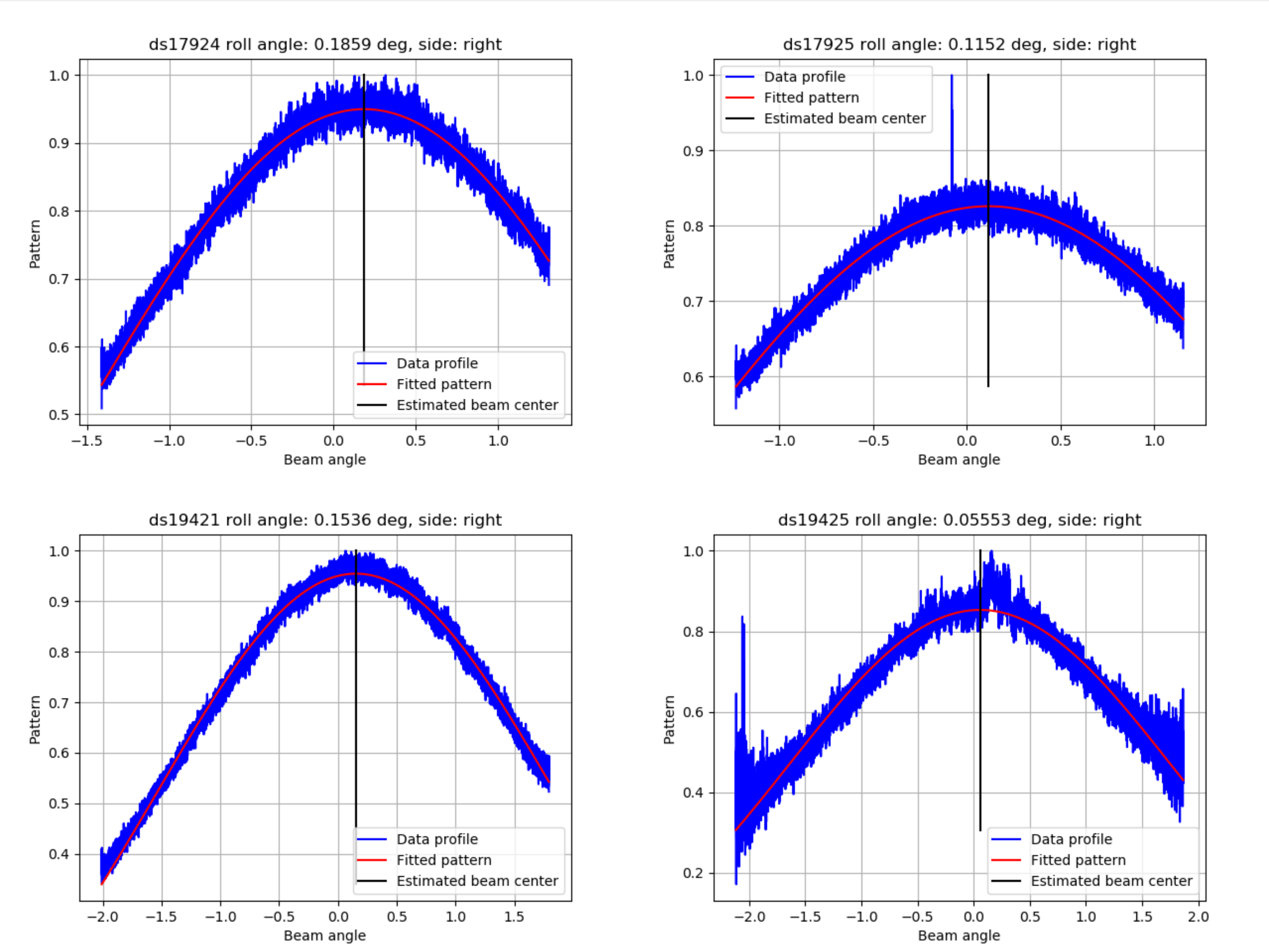

Figure 18. Chosen antenna calibration results for X2 satellite: right looking data profiles

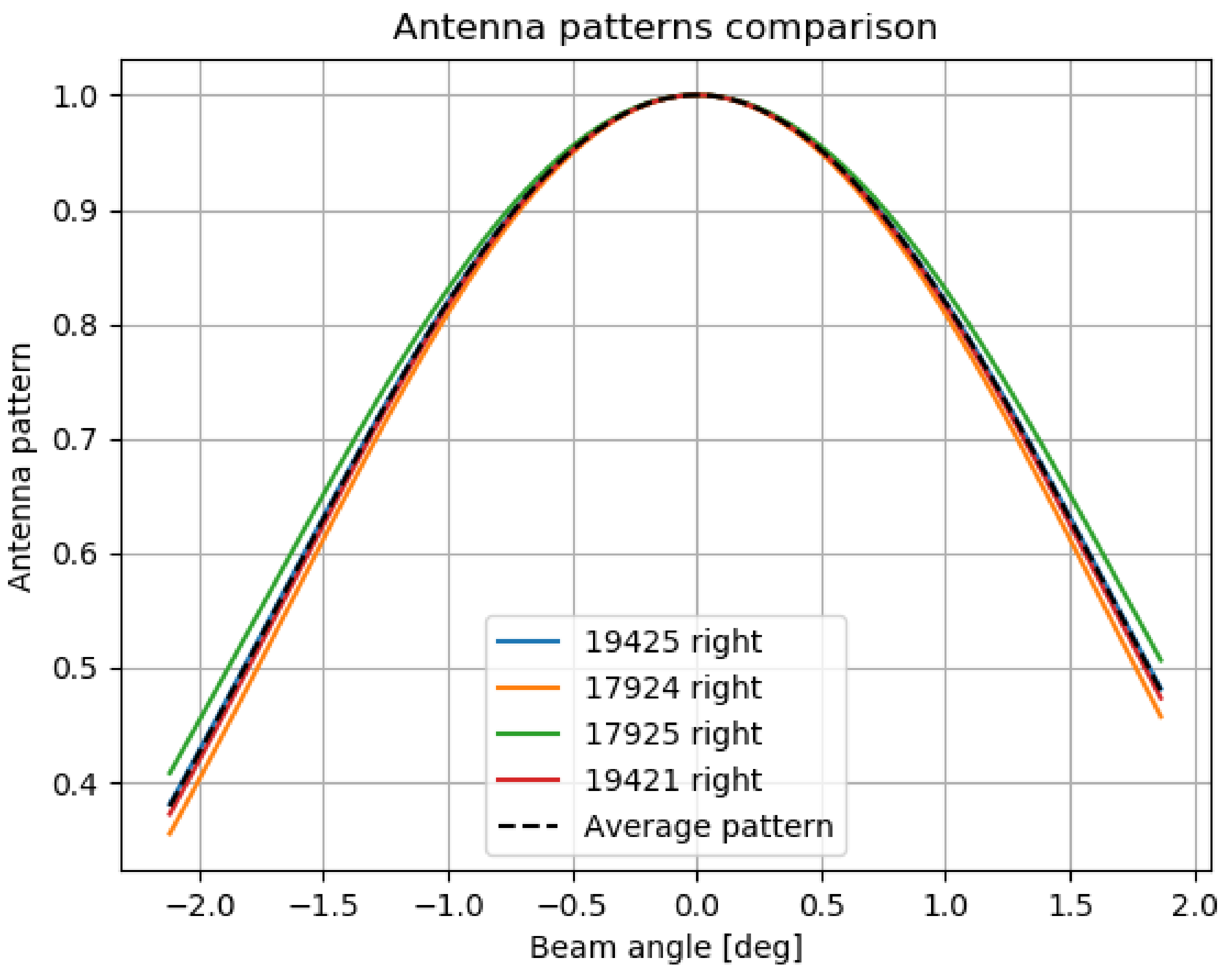

Figure 19. Comparison of antenna pattern fittings for X2 (right looking)

The comparison between ideal and measured antenna pattern is shown in results for the antenna pattern of X2 satellite are shown in Figure 20.

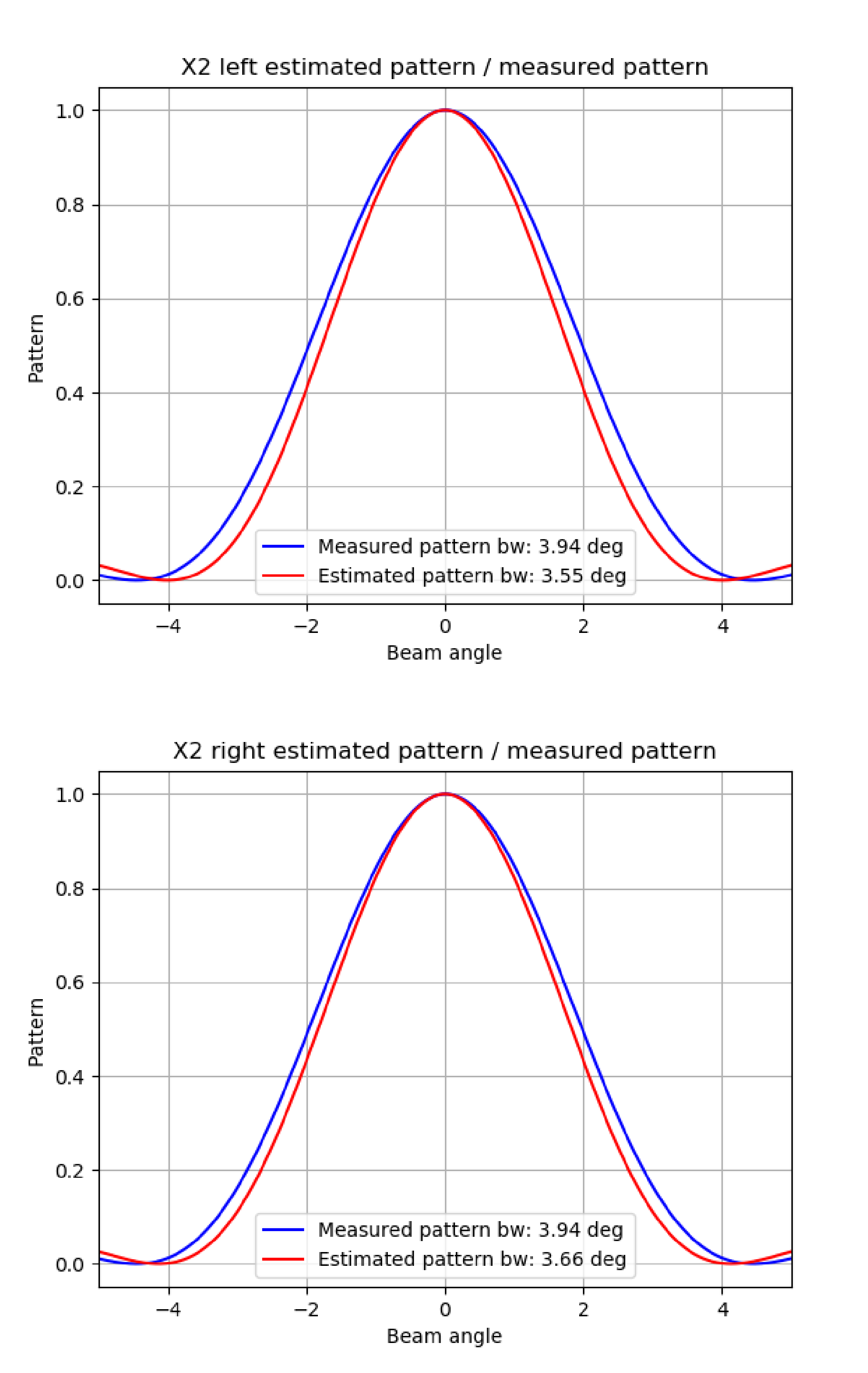

Figure 20. Comparison between ideal and measured antenna pattern for X2 (left and right looking)

3.2.1.2 RESULTS FOR X4 SATELLITE

The results for the antenna pattern of X4 satellite are shown in the following figures in right and left looking mode.

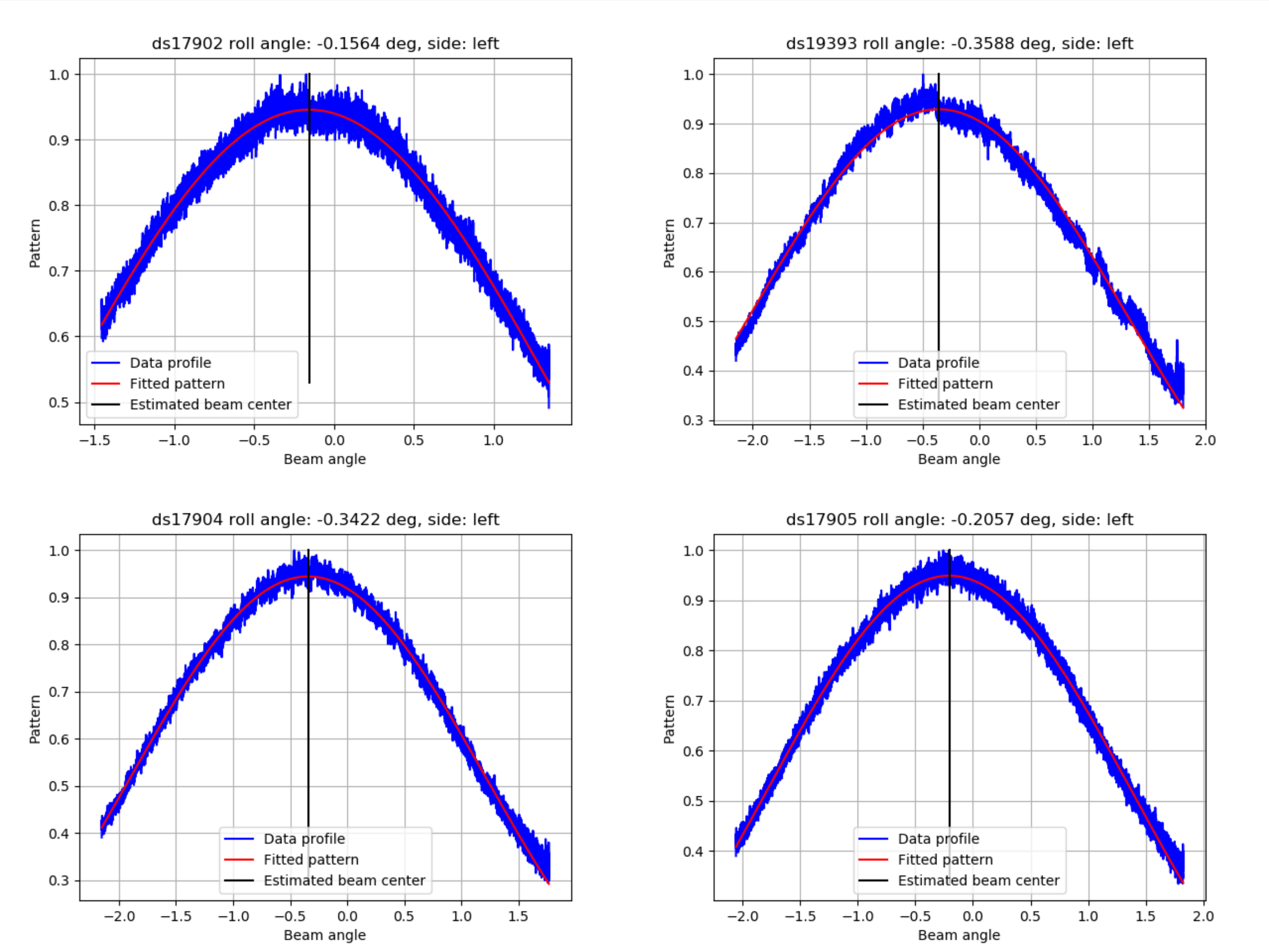

Figure 21. Chosen antenna calibration results for X4 satellite: left looking data profiles

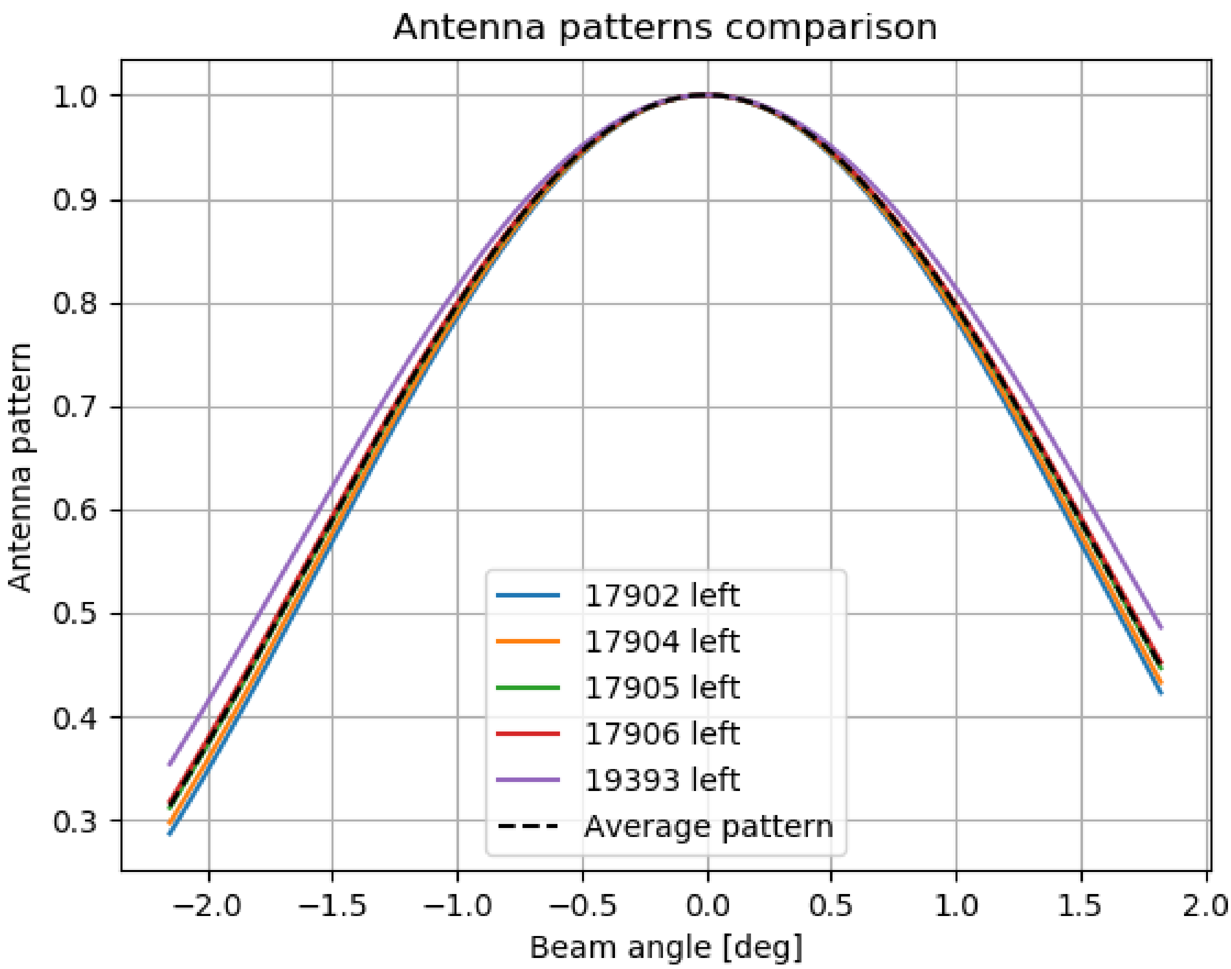

Figure 22. Comparison of antenna pattern fittings for X4 (left looking)

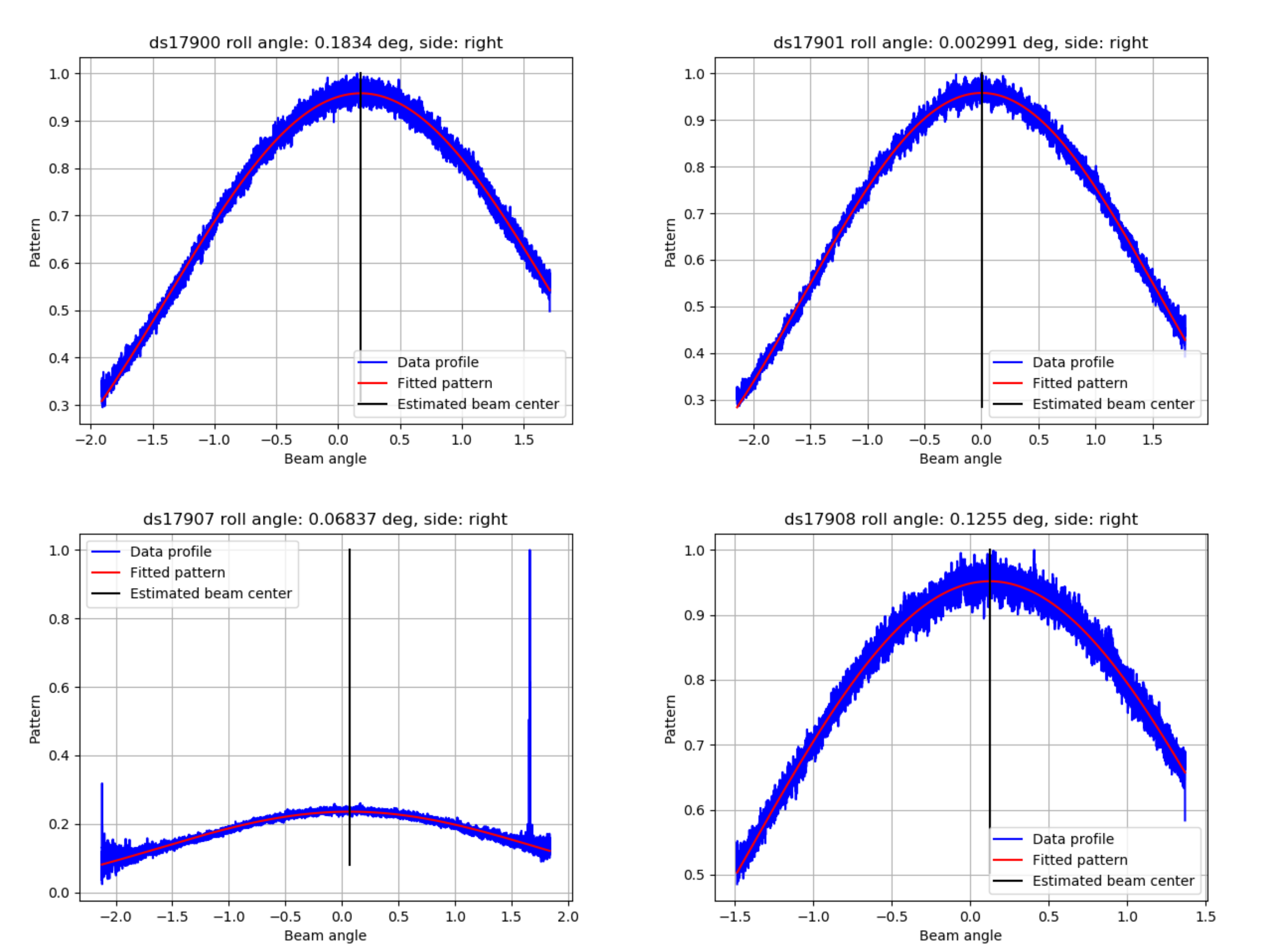

Figure 23. Chosen antenna calibration results for X4 satellite: left looking data profiles

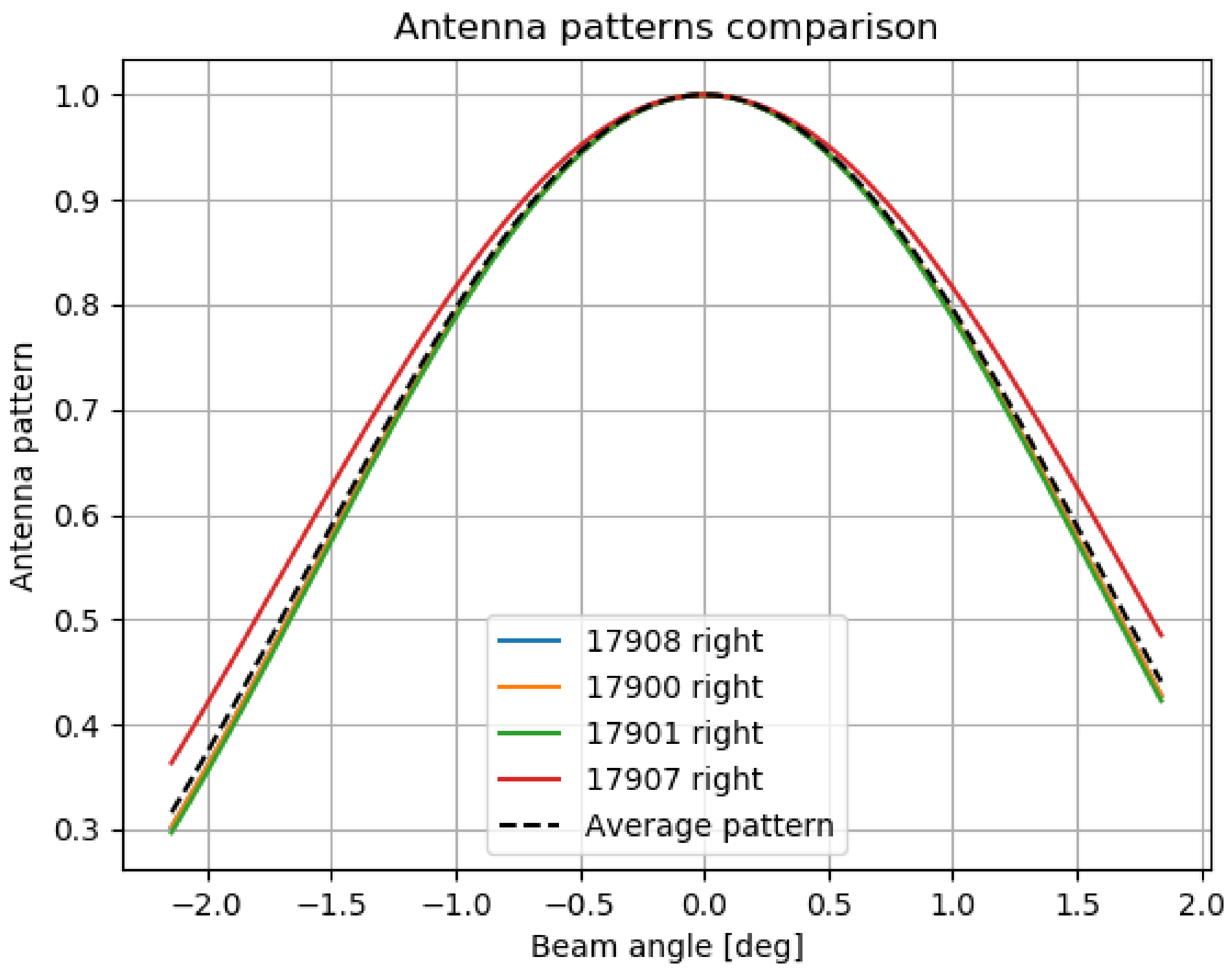

Figure 24. Comparison of antenna pattern fittings for X4 (right looking)

▶ CALIBRATION & VALIDATION OF ICEYE SENSORS

The comparison between ideal and measured antenna pattern is shown in results for the antenna pattern of X4 satellite are shown in Figure 25.

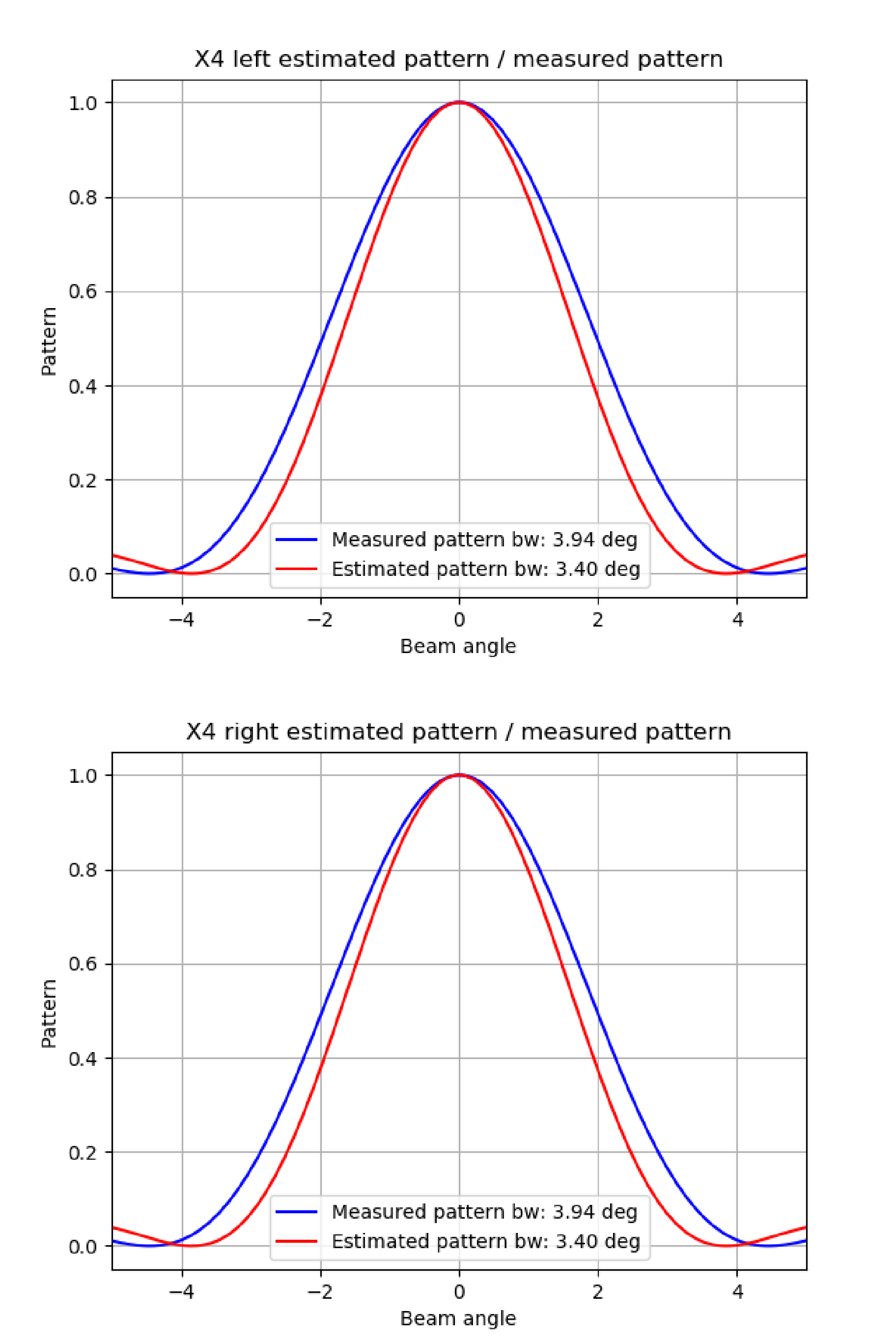

Figure 25. Comparison between ideal and measured antenna pattern for X4 (left and right looking)

3.2.1.3 RESULTS FOR X5 SATELLITE

The results for the antenna pattern of X5 satellite are shown in the following figures in right and left looking mode.

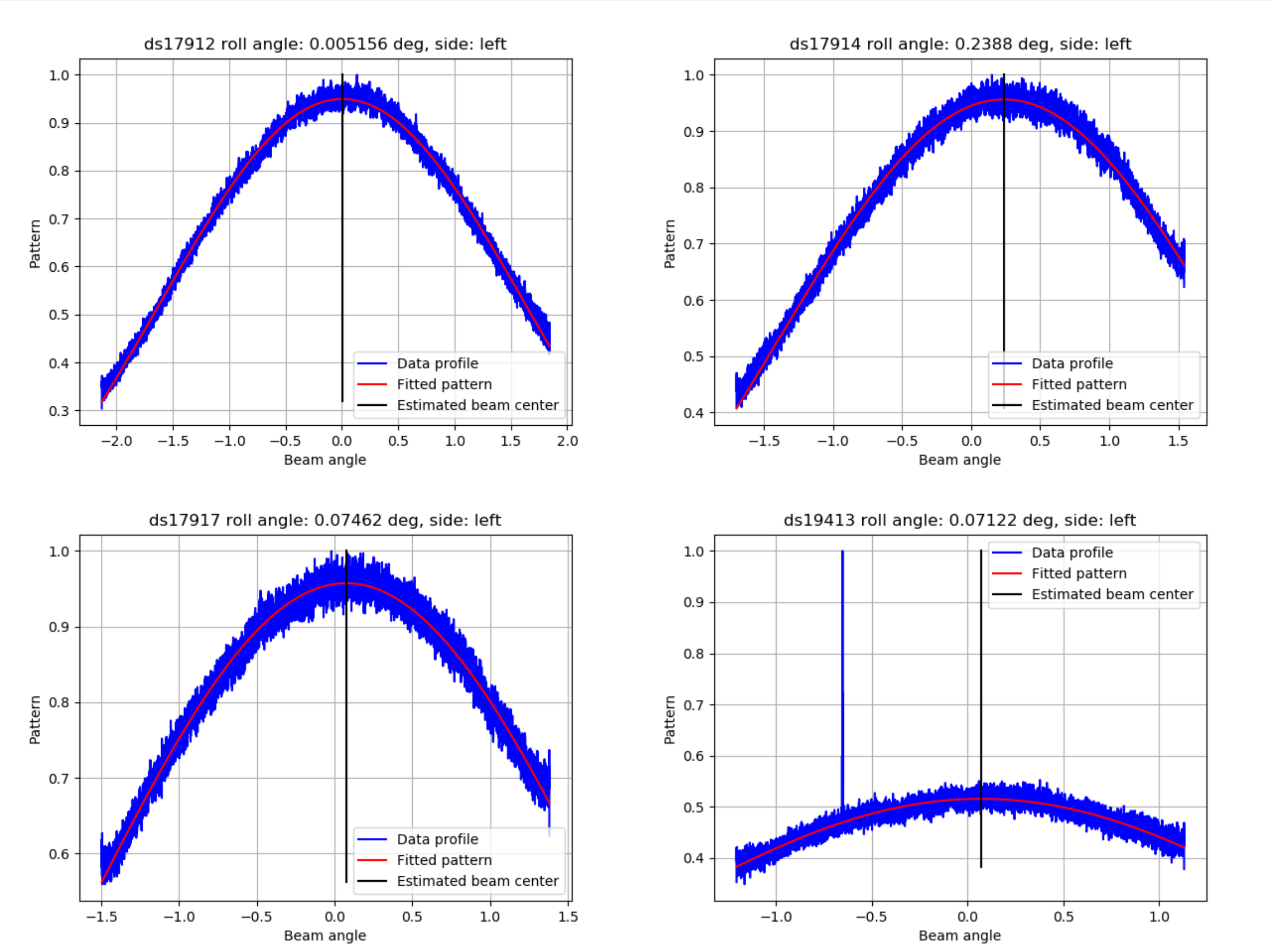

Figure 26. Chosen antenna calibration results for x5 satellite: left looking data profiles

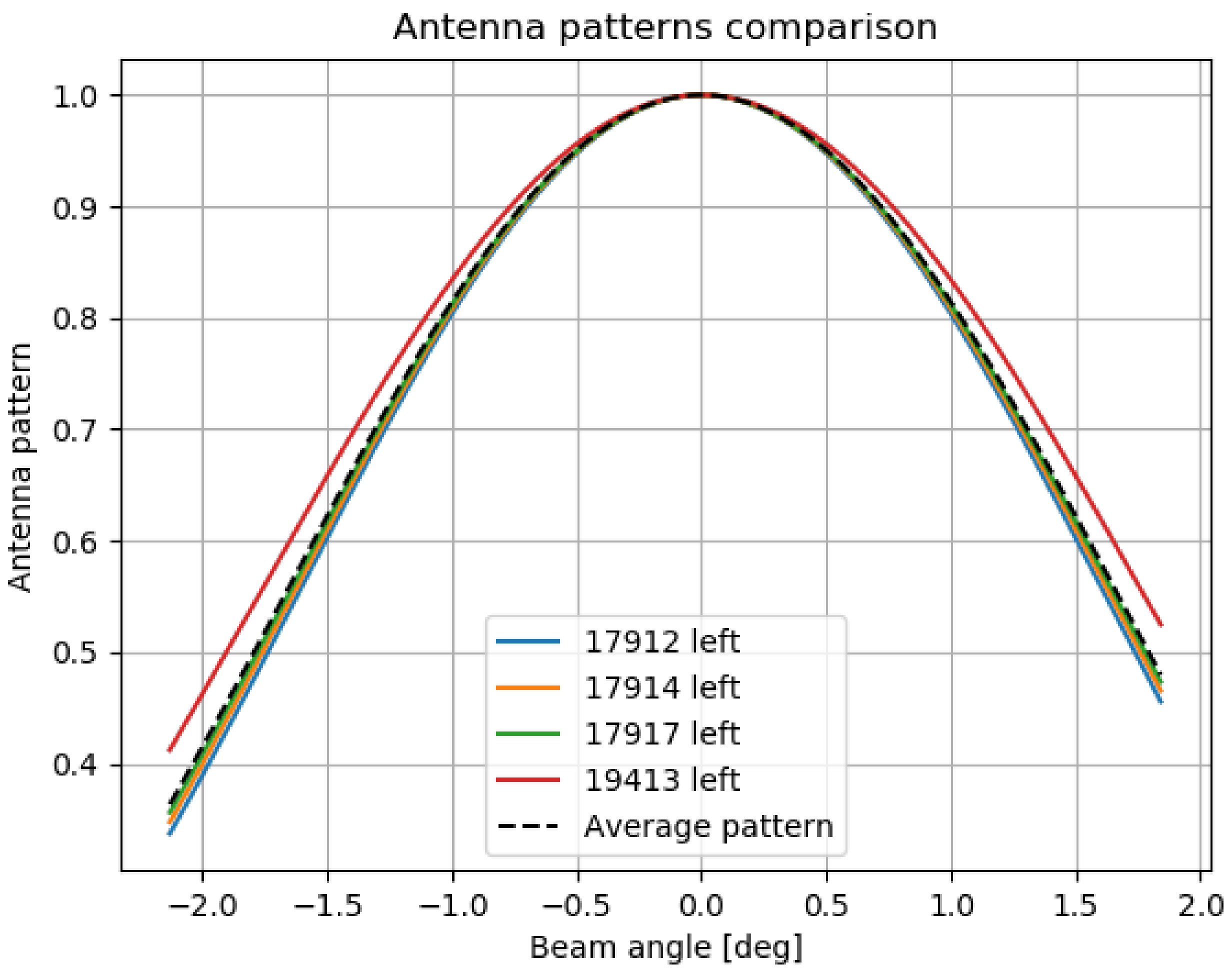

Figure 27. Comparison of antenna pattern fittings for X5 (left looking)

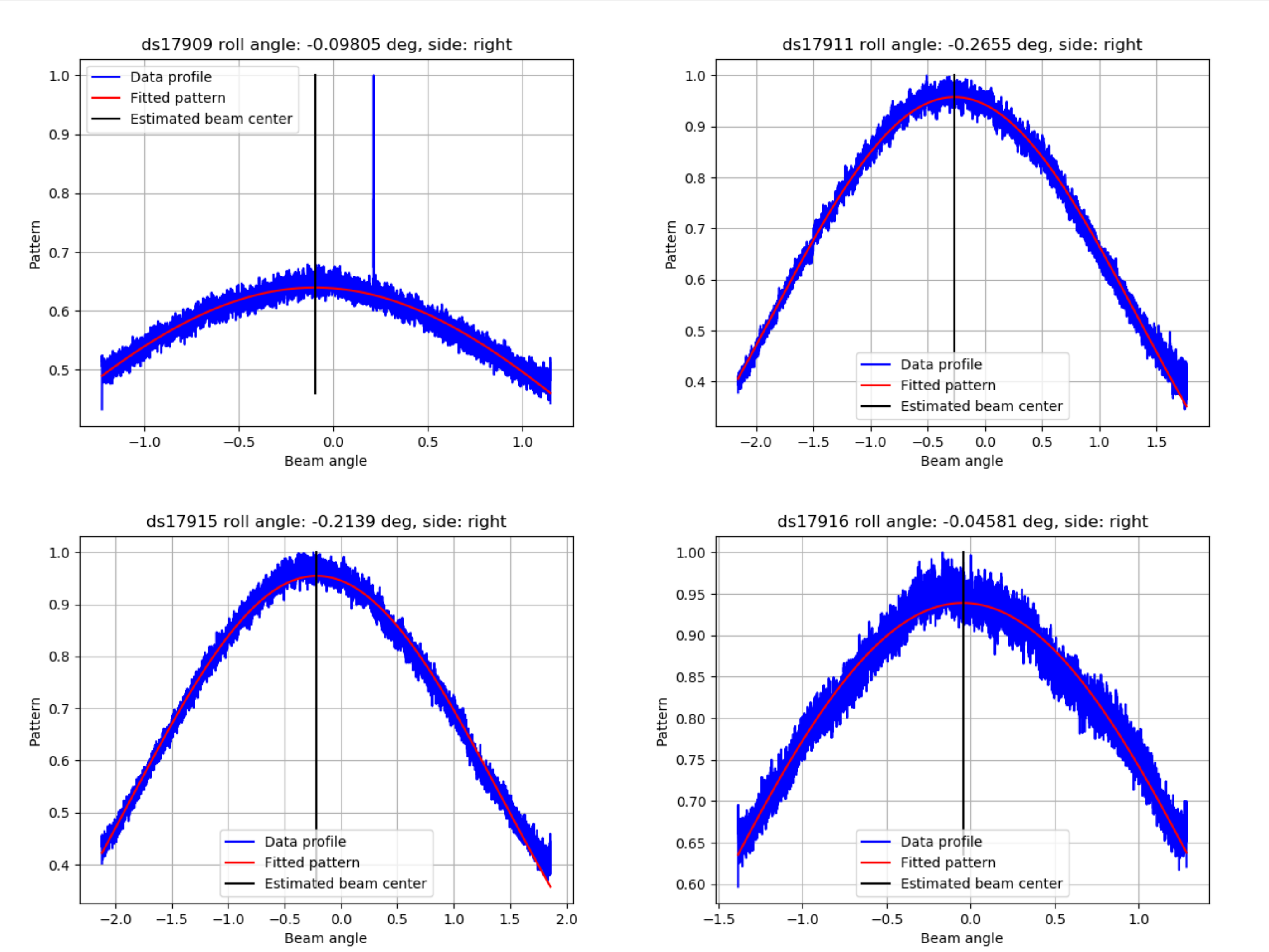

Figure 28. Chosen antenna calibration results for X5 satellite: left looking data profiles

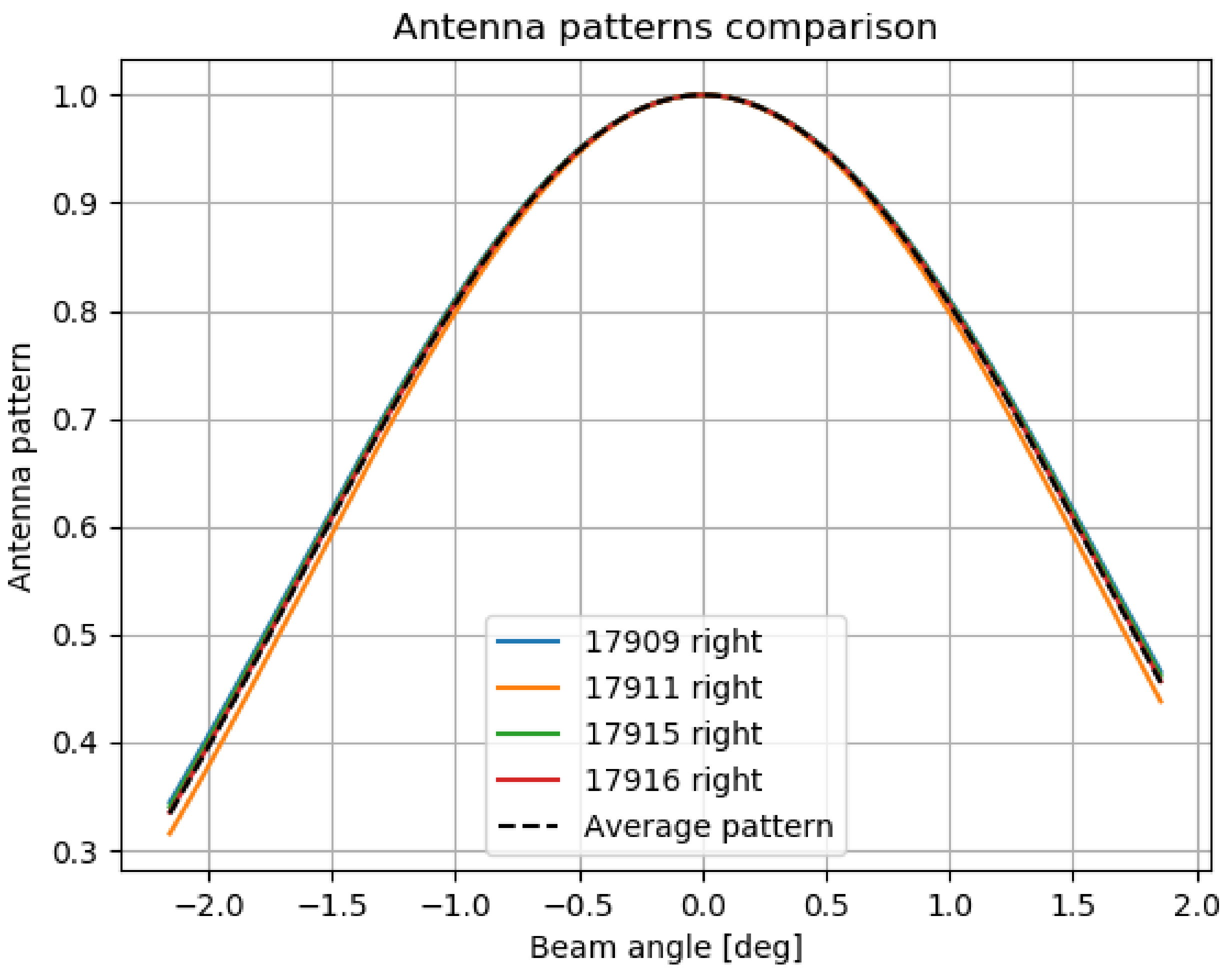

Figure 29. Comparison of antenna pattern fittings for X5 (right looking)

CALIBRATION & VALIDATION OF ICEYE SENSORS

The comparison between ideal and measured antenna pattern is shown in results for the antenna pattern of X5 satellite are shown in Figure 30.

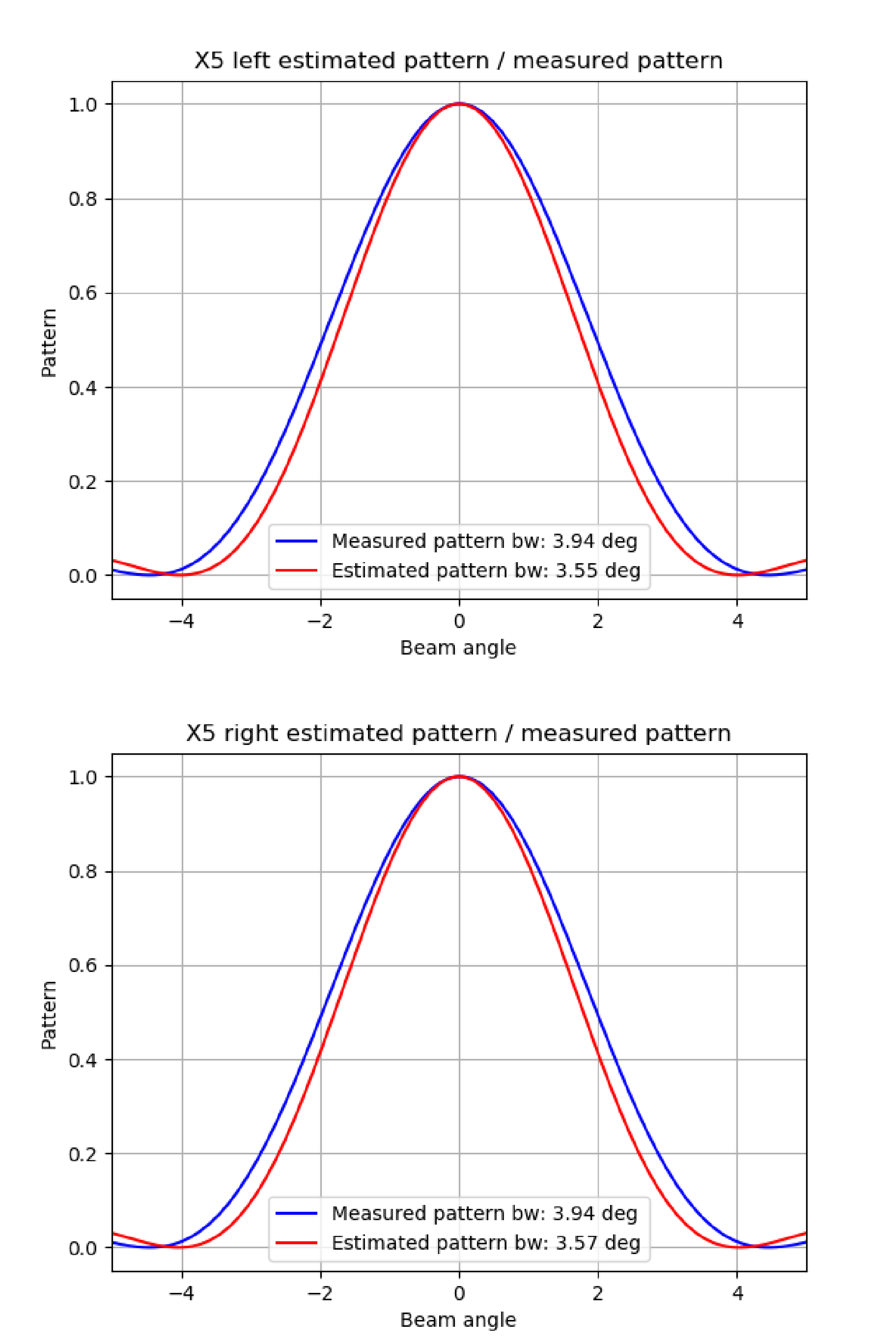

Figure 30. Comparison between ideal and measured antenna pattern for X5 (left and right looking)

3.2.2 CALIBRATION: CALIBRATION COEFFICIENT CALCULATION (AMAZON AND CONGO FORESTS)

3.2.2.1 RESULTS FOR X2 SATELLITE

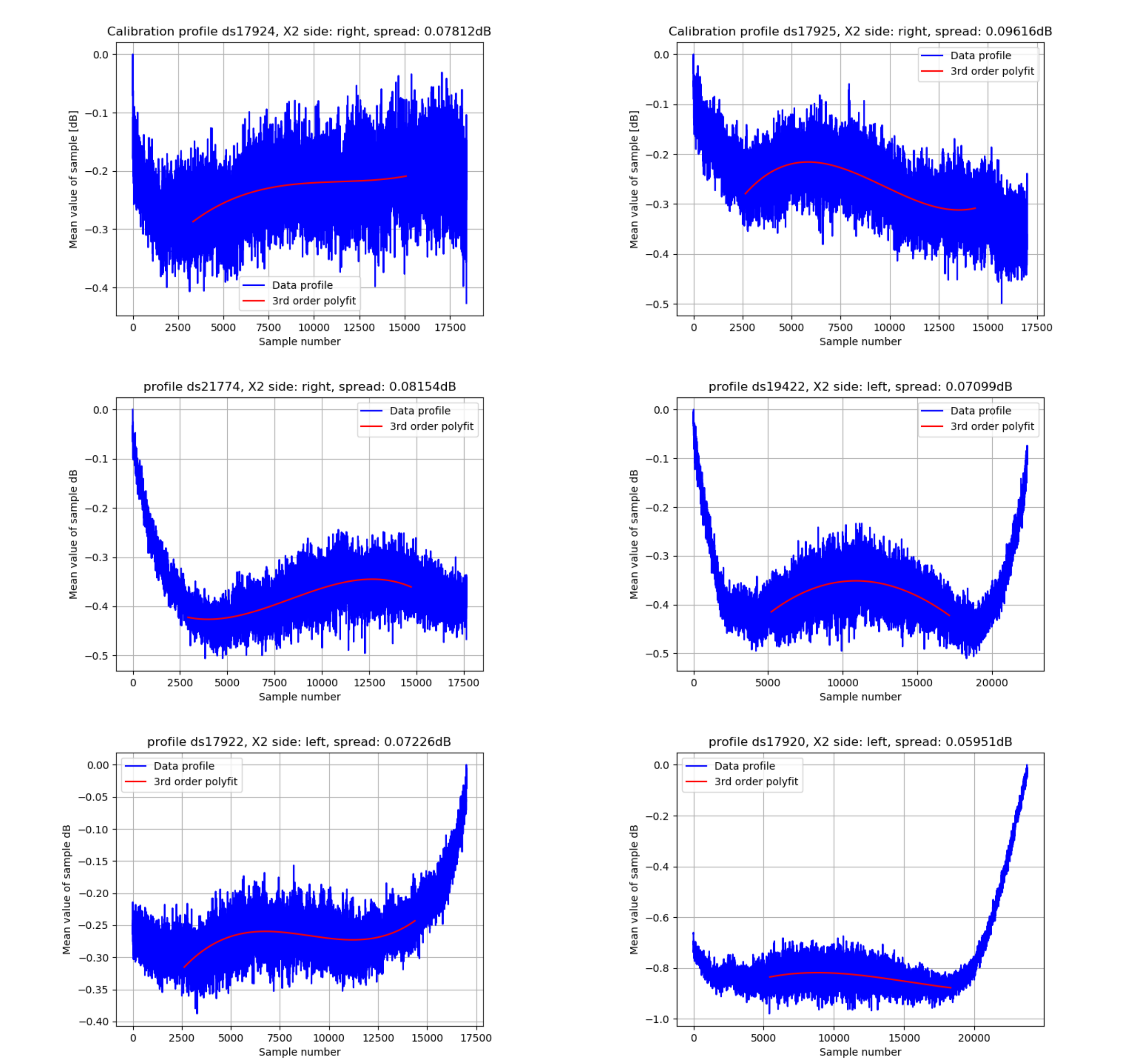

Figure 31. Radiometric calibration results. Amplitude are profiles compensated by antenna pattern and non-homogenous areas masking. 3rd order polynomial fitting reflects 30 km swath length.

▸ CALIBRATION & VALIDATION OF ICEYE SENSORS

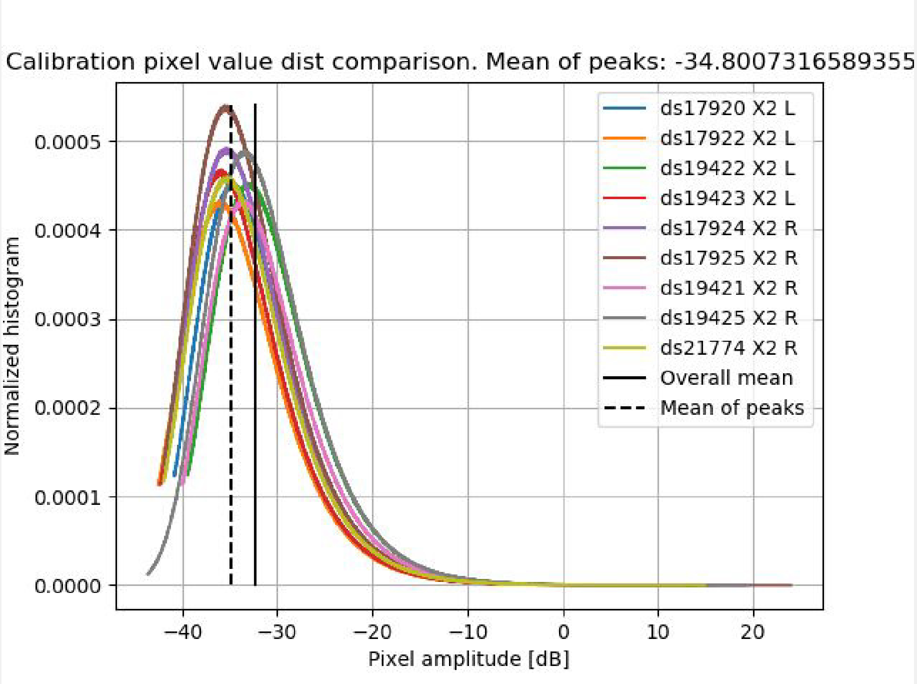

Figure 32. Comparison of calibration coefficient distributions for X2 satellite. Pixel amplitudes are scaled relative to mean RCS of forest (-6.5 dB)

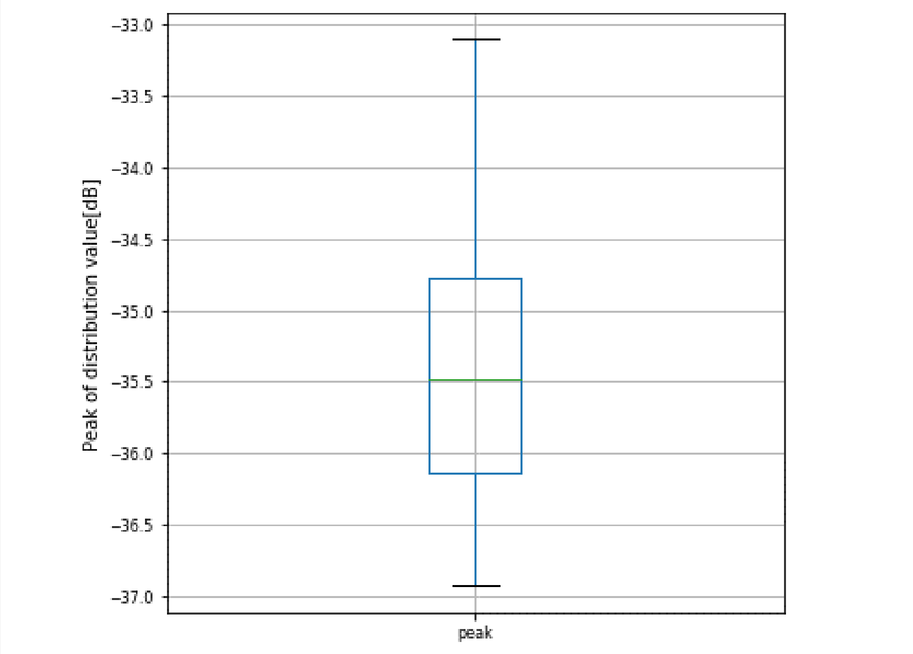

Figure 33. Boxplot of peak values of distribution of data for 37 X2 satellite acquisitions. Data is expressed in decibels (dB) scaled relative to mean RCS of forest (-6.5 dB)

3.2.2.2 RESULTS FOR X4 SATELLITE

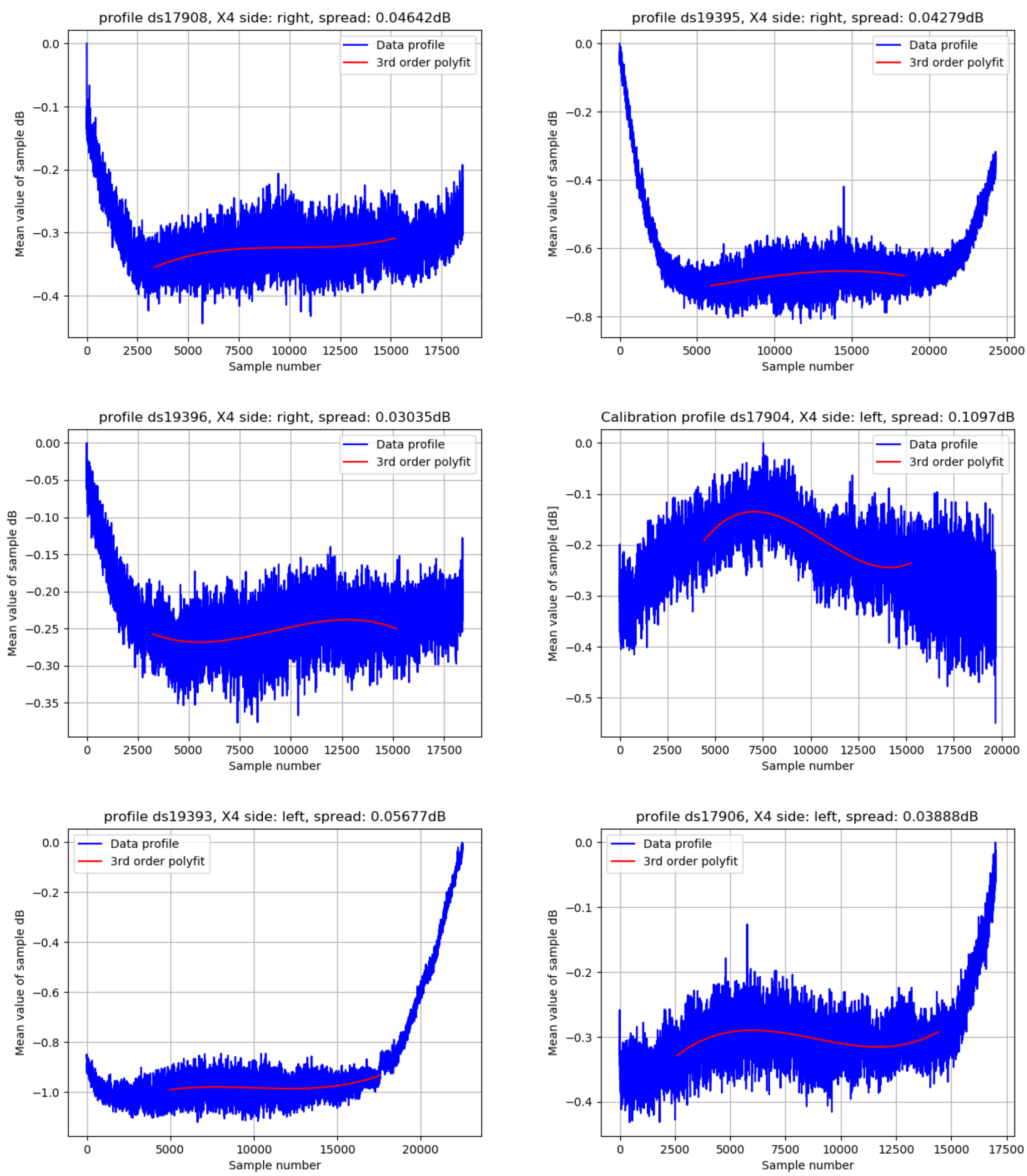

Figure 34. Radiometric calibration results. Amplitude profiles are compensated by antenna pattern and non-homogenous areas masking. 3rd order polynomial fitting reflects 30 km swath length.

▶ CALIBRATION & VALIDATION OF ICEYE SENSORS

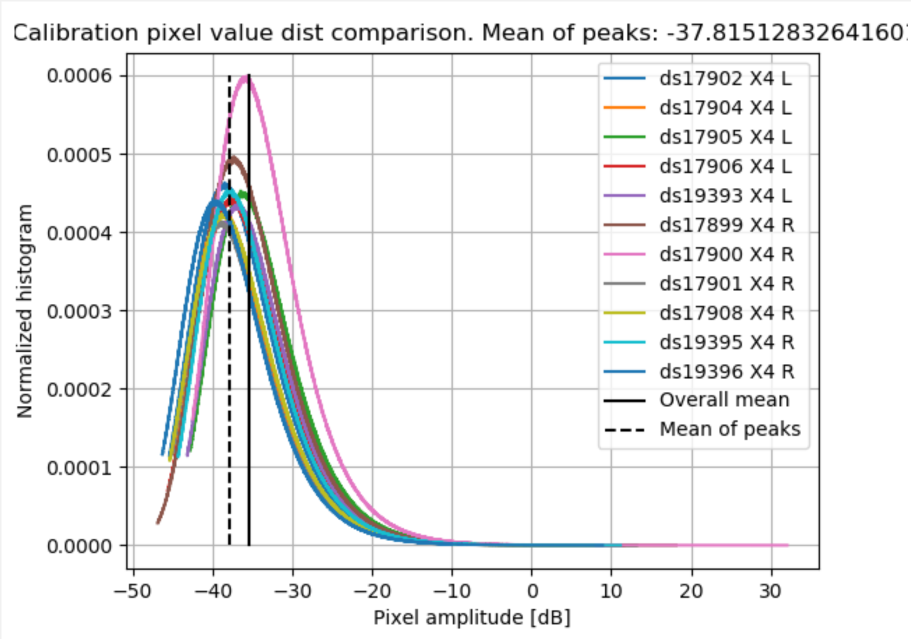

Figure 35. Comparison of calibration coefficient distributions for X4 satellite. Pixel amplitudes are scaled relative to mean RCS of forest (-6.5 dB)

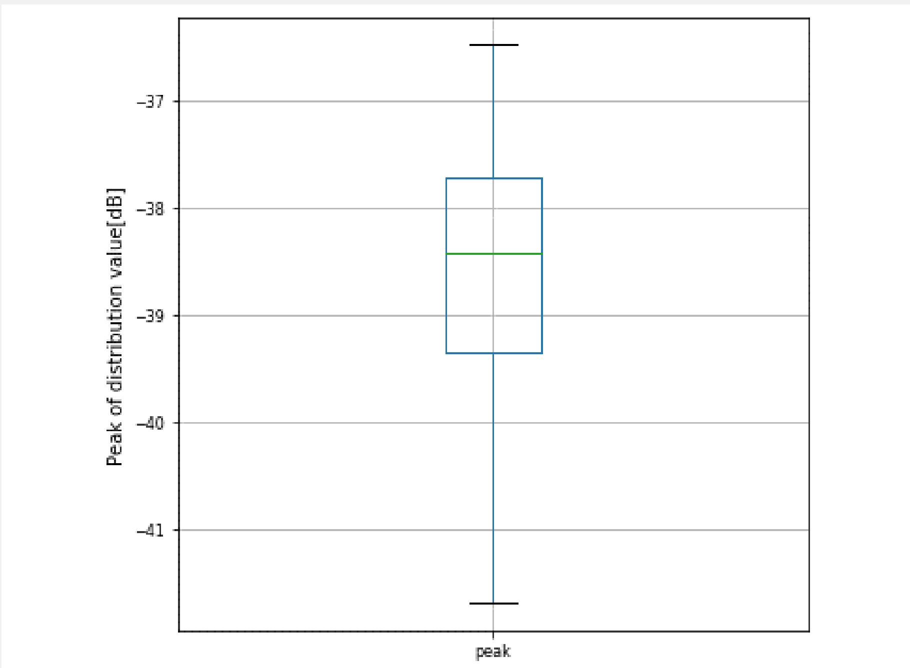

Figure 36. Boxplot of peak values of data distribution for 38 X4 satellite acquisitions. Data is expressed in decibels (dB) scaled relative to mean RCS of forest (-6.5 dB)

3.2.2.3 RESULTS FOR X5 SATELLITE

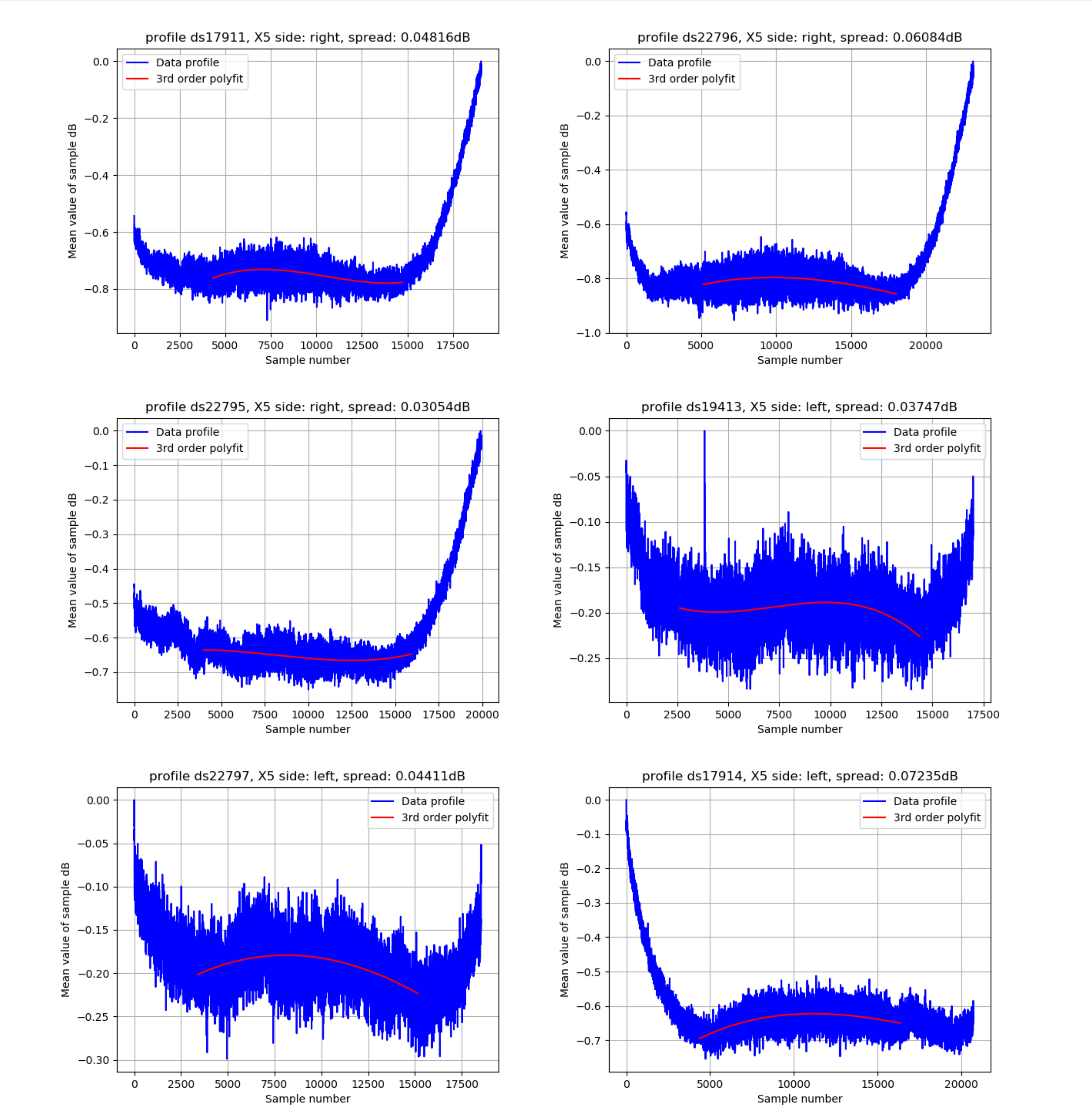

Figure 37. Radiometric calibration results. Amplitude profiles are compensated by antenna pattern and non-homogenous areas masking. 3rd order polynomial fitting reflects 30 km swath length.

▶ CALIBRATION & VALIDATION OF ICEYE SENSORS

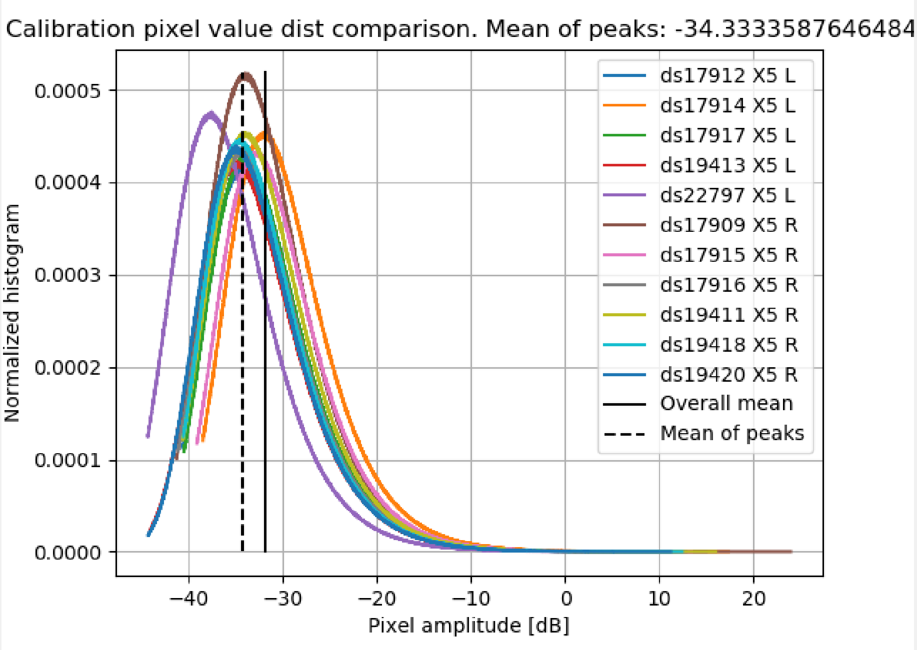

Figure 38. Comparison of calibration coefficient distributions for X5 satellite. Pixel amplitudes are scaled relative to mean RCS of forest (-6.5 dB)

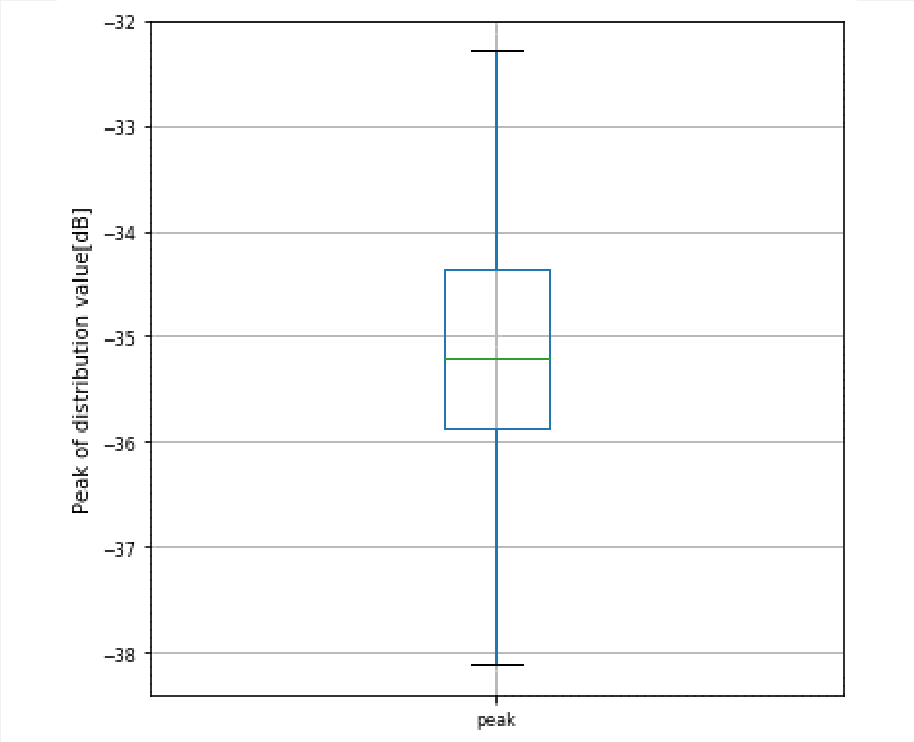

Figure 39. Boxplot of peak values of data distribution for 40 X5 satellite acquisitions. Data is expressed in decibels (dB) scaled relative to mean RCS of forest (-6.5 dB)

CALIBRATION & VALIDATION OF ICEYE SENSORS

3.2.2.4 SUMMARY OF BEAM CALIBRATION

In section 3.2.1 antenna pattern estimation results for all three satellites have been presented. Obtained results converge well with antenna pattern measurement results from the laboratory tests. What is more, pattern shapes estimated from left and right looking acquisitions are similar which confirms correctness of used method.

Table 1 shows the calibration factors CF calculated during the calibration taking the median and the mean value of the peak position of the K distribution. The calibration constant is then calculated as:

$$K = \frac{CF}{\delta_x \cdot \delta_{sr} \cdot F_{scale}} \quad (19)$$

where δ_x is the azimuth resolution, δ_{sr} the slant range resolution and F_{scale} the scale factor related to the dynamic range of DN values.

SATELLITE	CF CALIBRATION MEDIAN	CF CALIBRATION MEAN	CURRENT CF CALIBRATION STRIPMAP	CURRENT CF CALIBRATION SPOTLIGHT
X2	2.83*e-04	2.91*e-04	3.19*e-04	1.1*e-04
X4	1.44*e-04	1.37*e-04	9.639*e-05	6.291*e-05
X5	3.02*e-04	3.09*e-04	3.19*e-04	1.1*e-04

Table 1. Calibration factor for X2, X4 and X5 satellites

3.2.3 SELECTION OF RELIABLE CORNER REFLECTORS AND FILTERING PARAMETERS FOR RCS CALCULATION

This section presents the results for the selection of reliable Corner Reflectors. The Corner Reflectors used for validation are selected if the condition is satisfied: $|R_\delta - 1| < 0.4$.

The regression analysis of the filtering parameters has been performed to show the correlation between the parameter mean and the result quality. The analysis will select the filtering parameters to use in the validation.

3.2.3.1 RESULTS FOR X2 SATELLITE

A set of 4 images have been acquired on the site for Corner Reflector selection: ds23761, ds24146, ds24345, ds25093, ds25937.

The results per Corner Reflectors are presented in Figure 40.

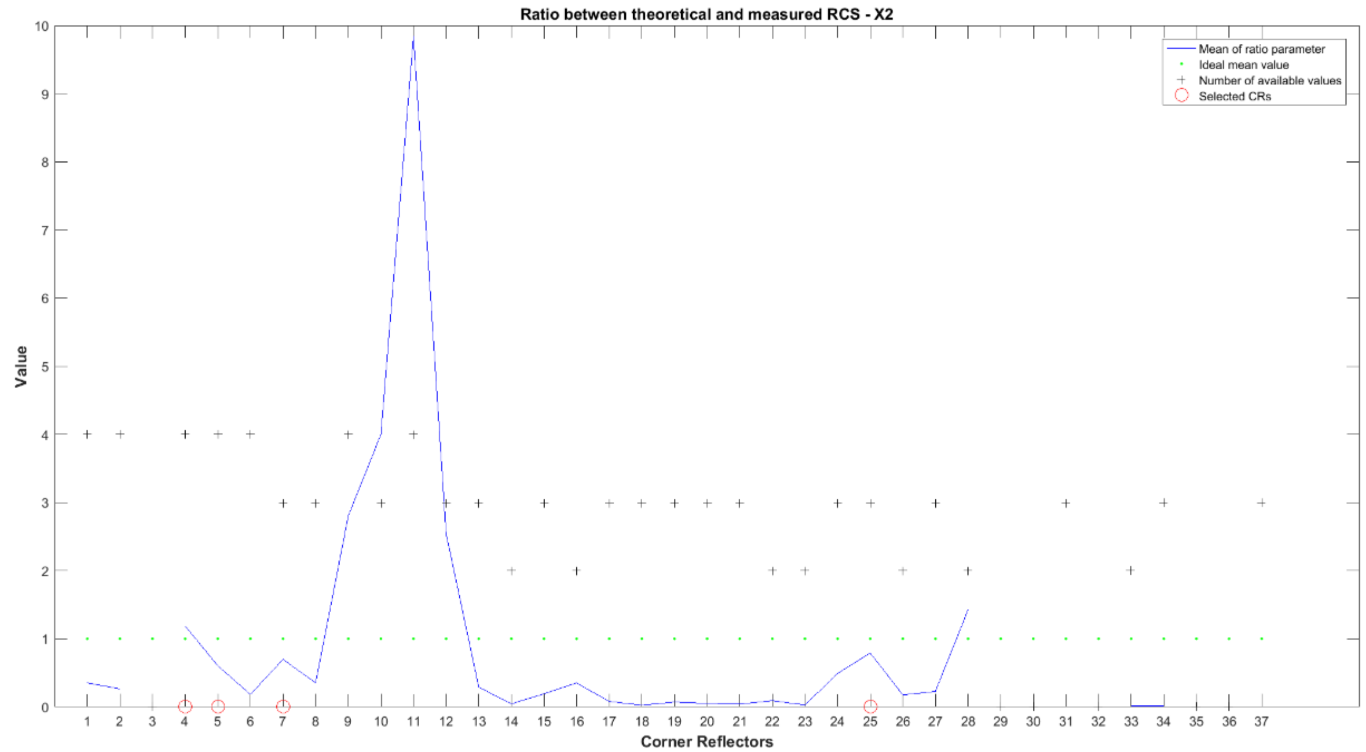

Figure 40. Results for X2 satellite per Corner Reflector.

The selected Corner Reflectors with mean value close to the ideal value are the 4, 9, 11, 12, 25 and 28.

The analysis of the filtering parameters with their correlation coefficient with the parameter R_δ is presented in the following figures.

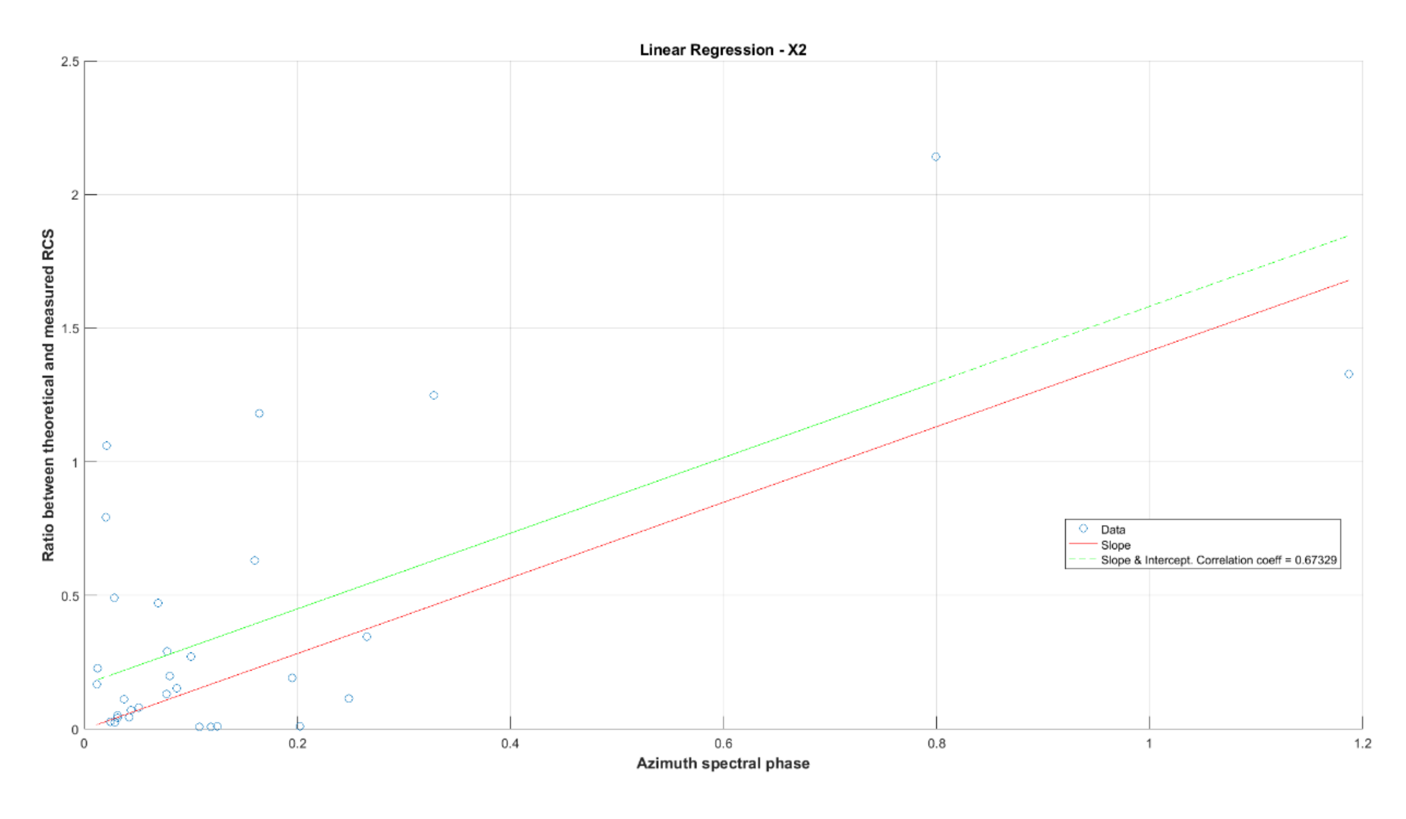

Figure 41. Linear regression of σ_{CASP} for X2 satellite.

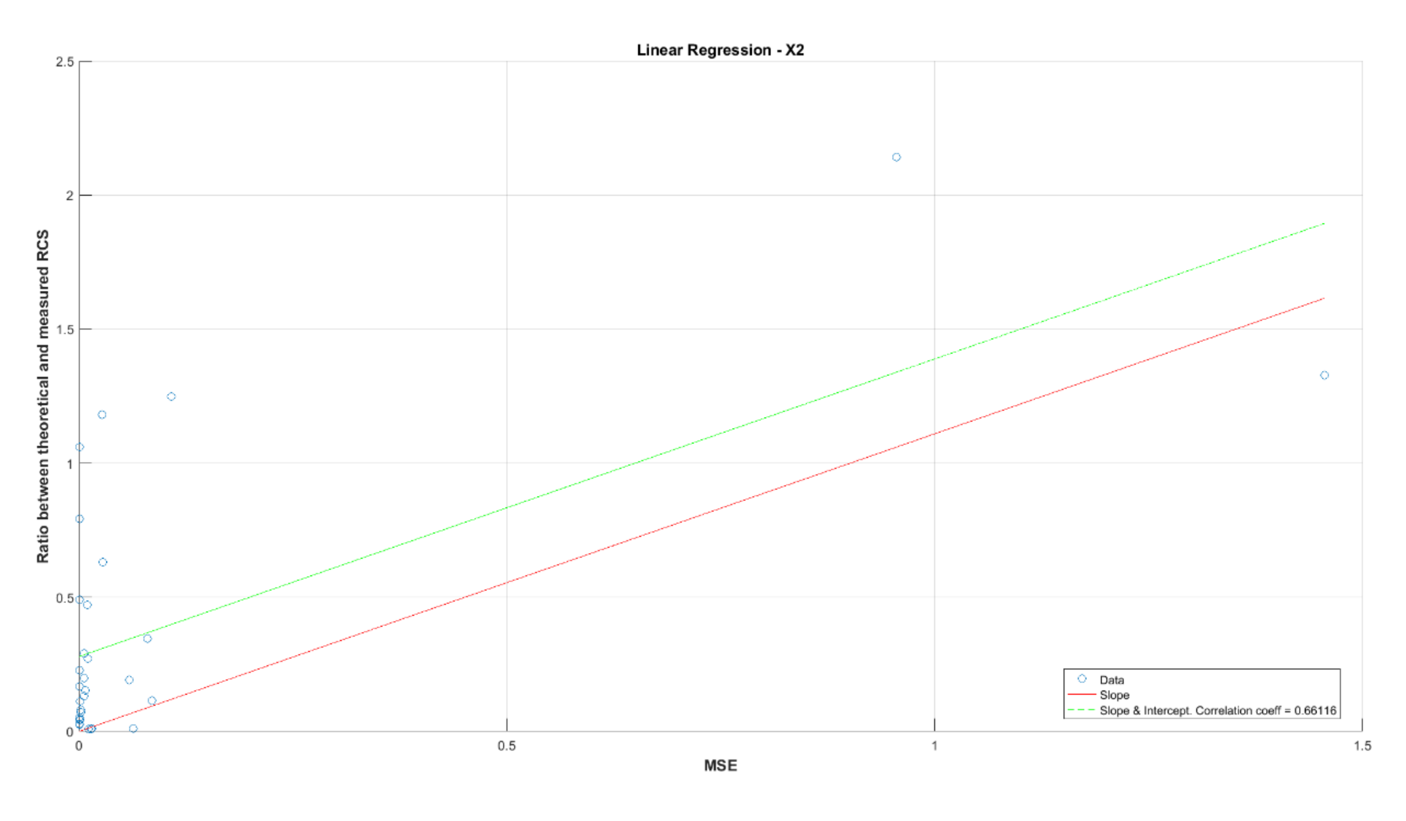

Figure 42. Linear regression of MSE_{CASP} for X2 satellite.

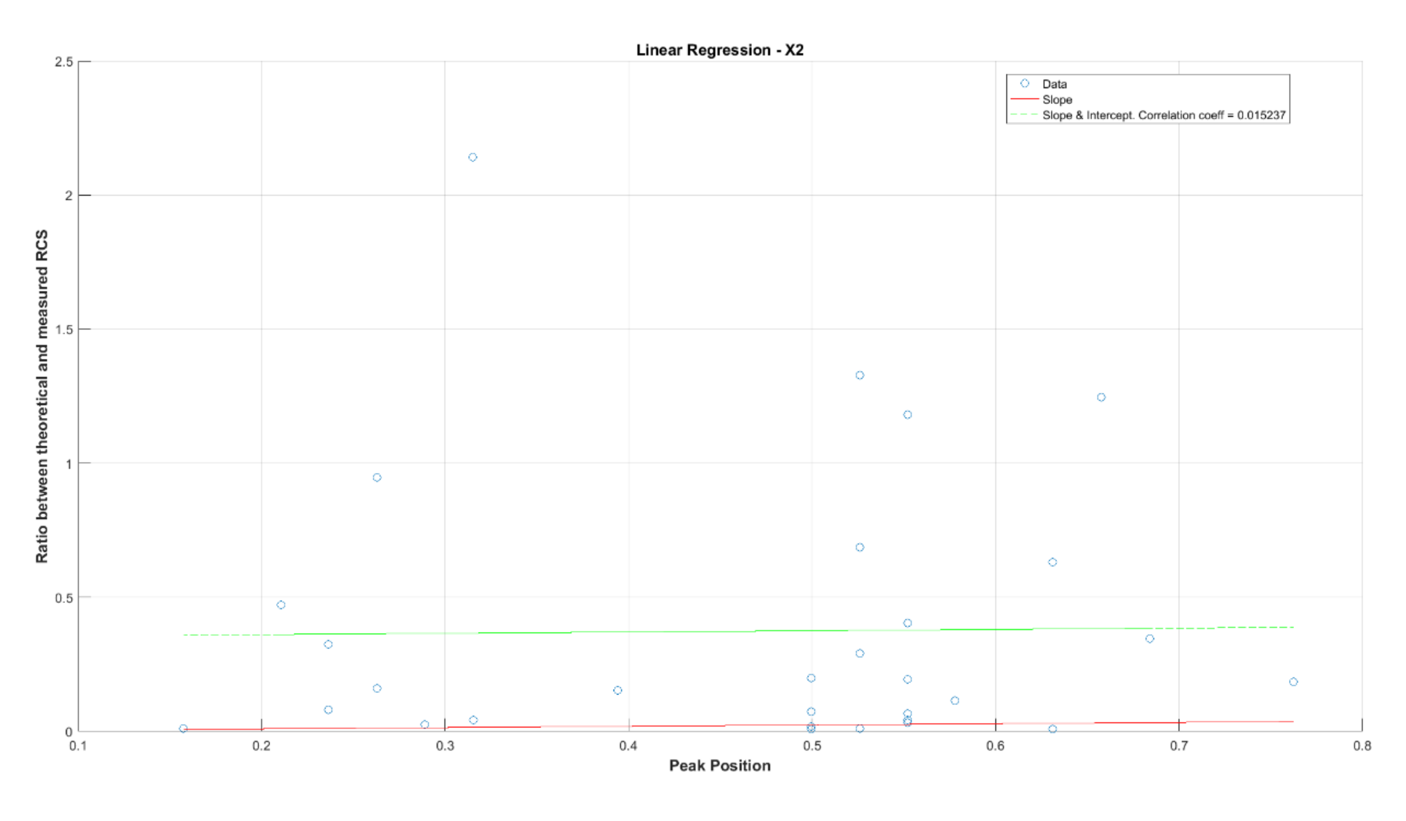

Figure 43. Linear regression of Peak Position for X2 satellite.

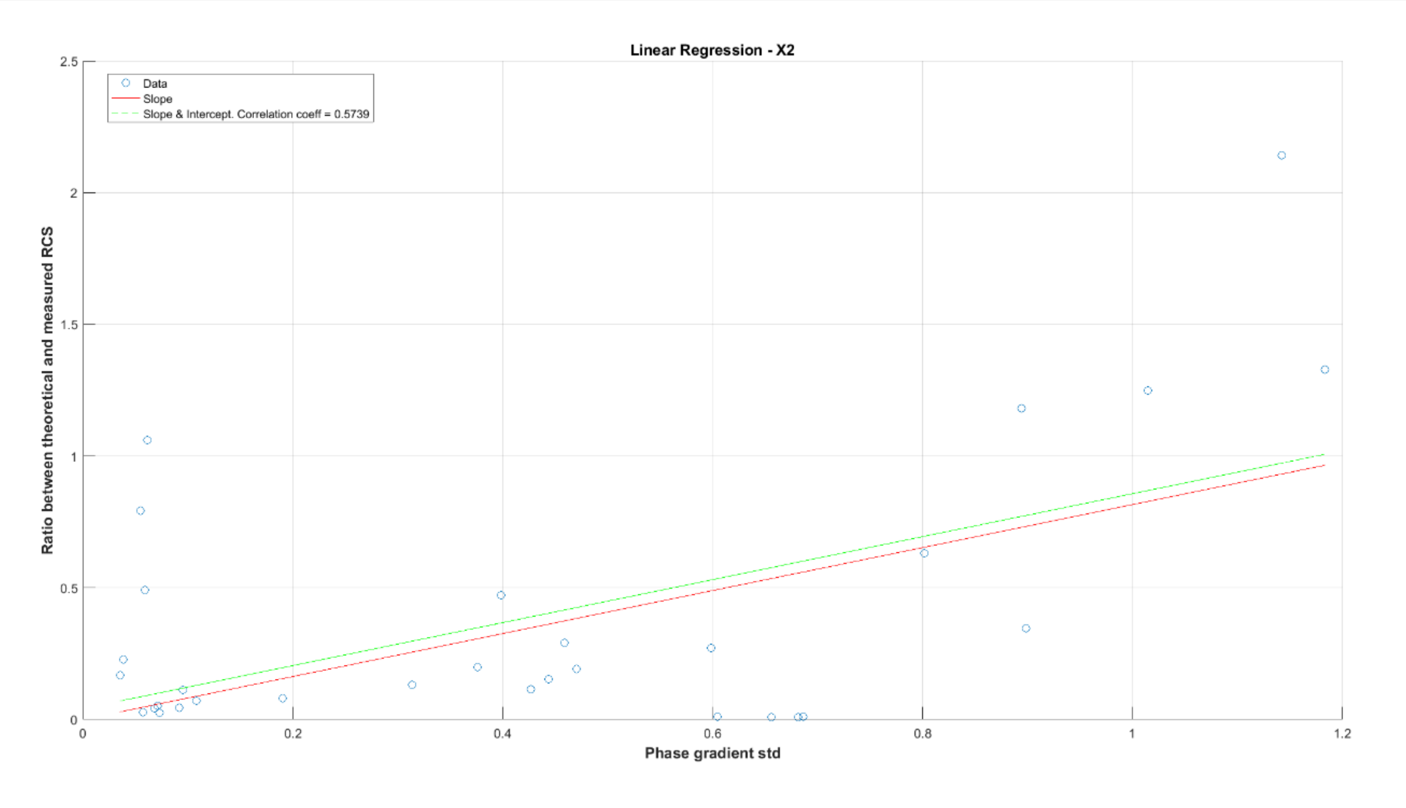

Figure 44. Linear regression of σ_{ASPG} for X2 satellite.

3.2.3.2 RESULTS FOR X4 SATELLITE

A set of 7 images have been acquired on the site for Corner Reflector selection: ds16743, ds16746, ds16751, ds16753, ds20063, ds20064, ds20388, ds20389.

The results per Corner Reflectors are presented in Figure 45.

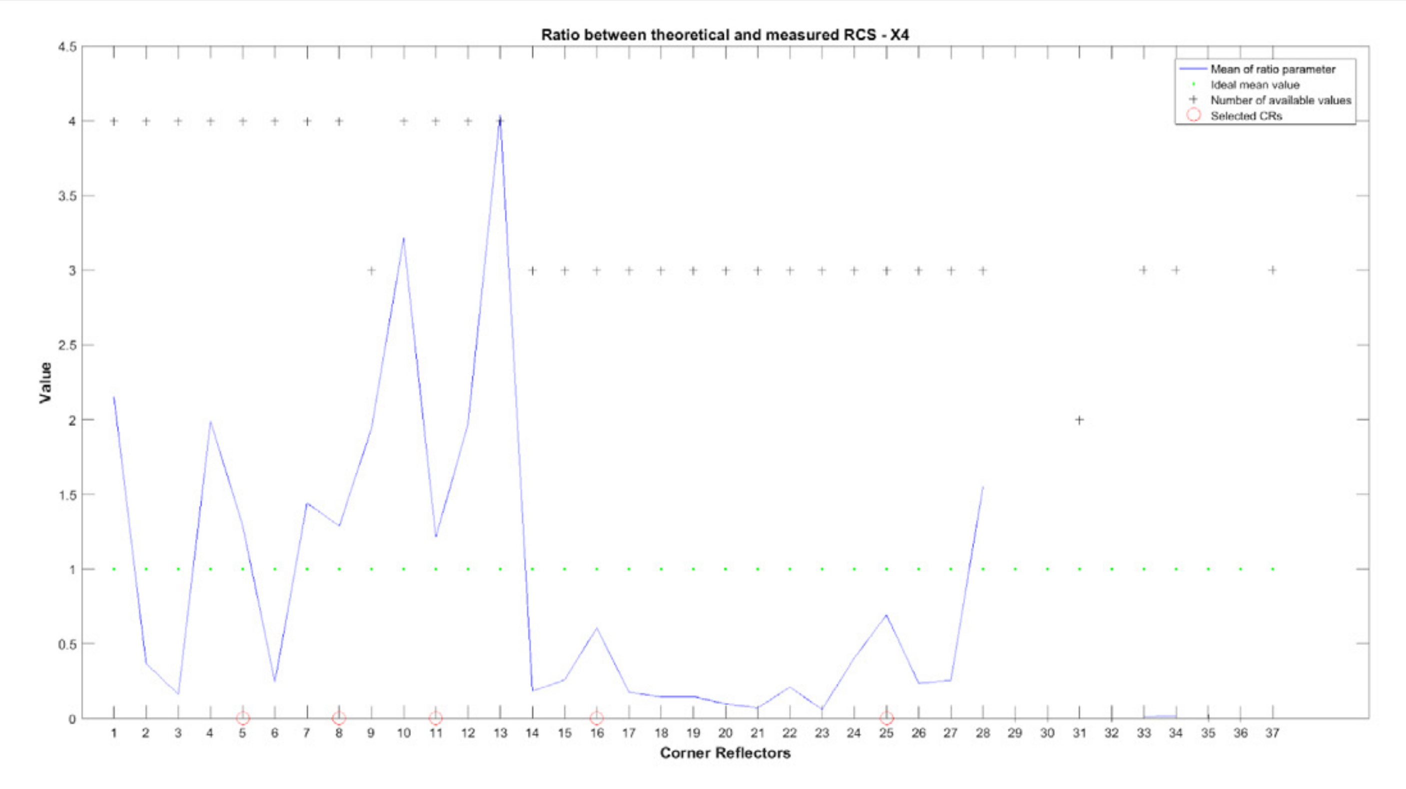

Figure 45. Results for X4 satellite per Corner Reflector.

The selected Corner Reflectors with mean value close to the ideal value are the 5, 8, 11, 16 and 25.

In the following the analysis of the filtering parameters with their correlation coefficient with the parameter R_{σ} is presented.

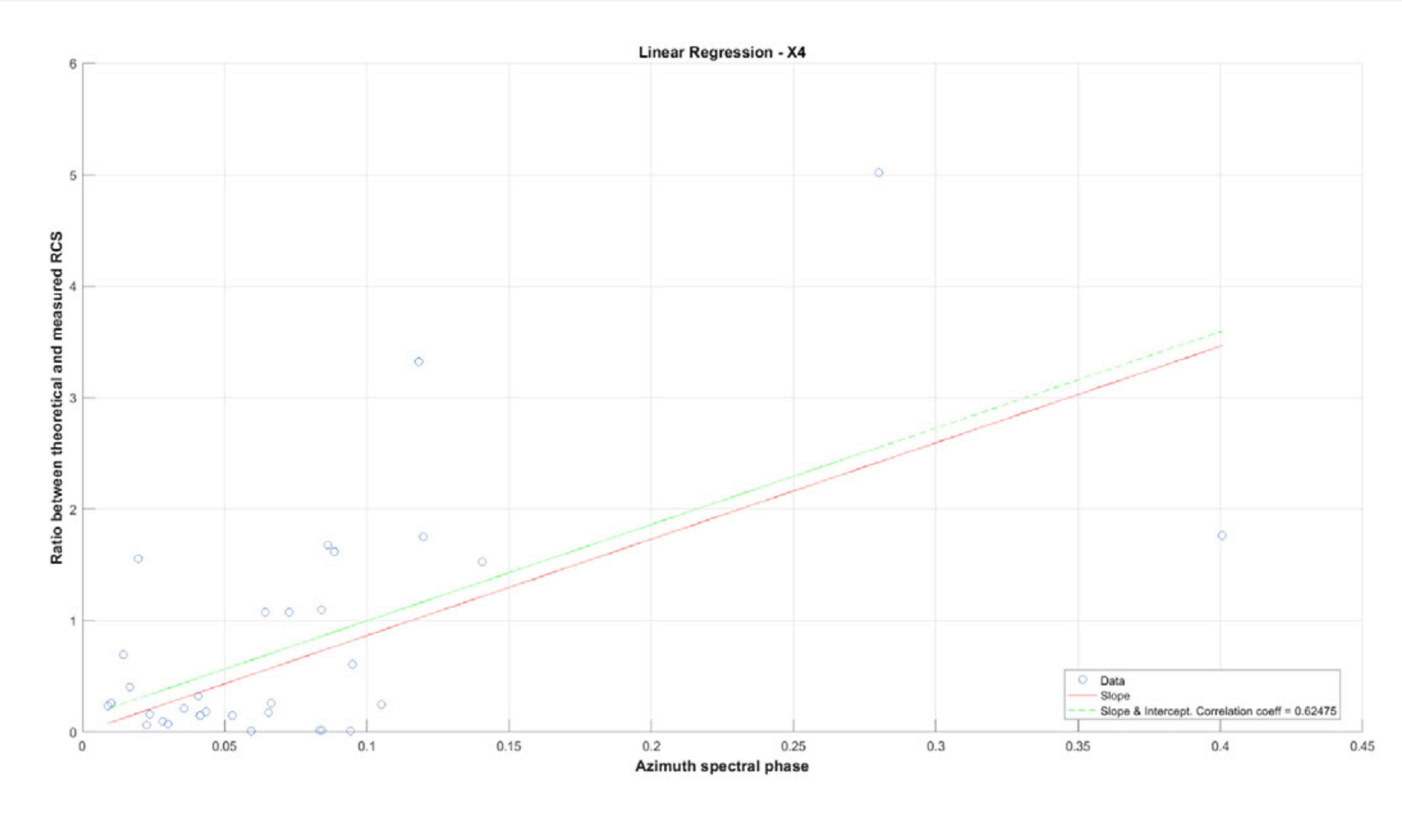

Figure 46. Linear regression of σ_{CASP} for X4 satellite.

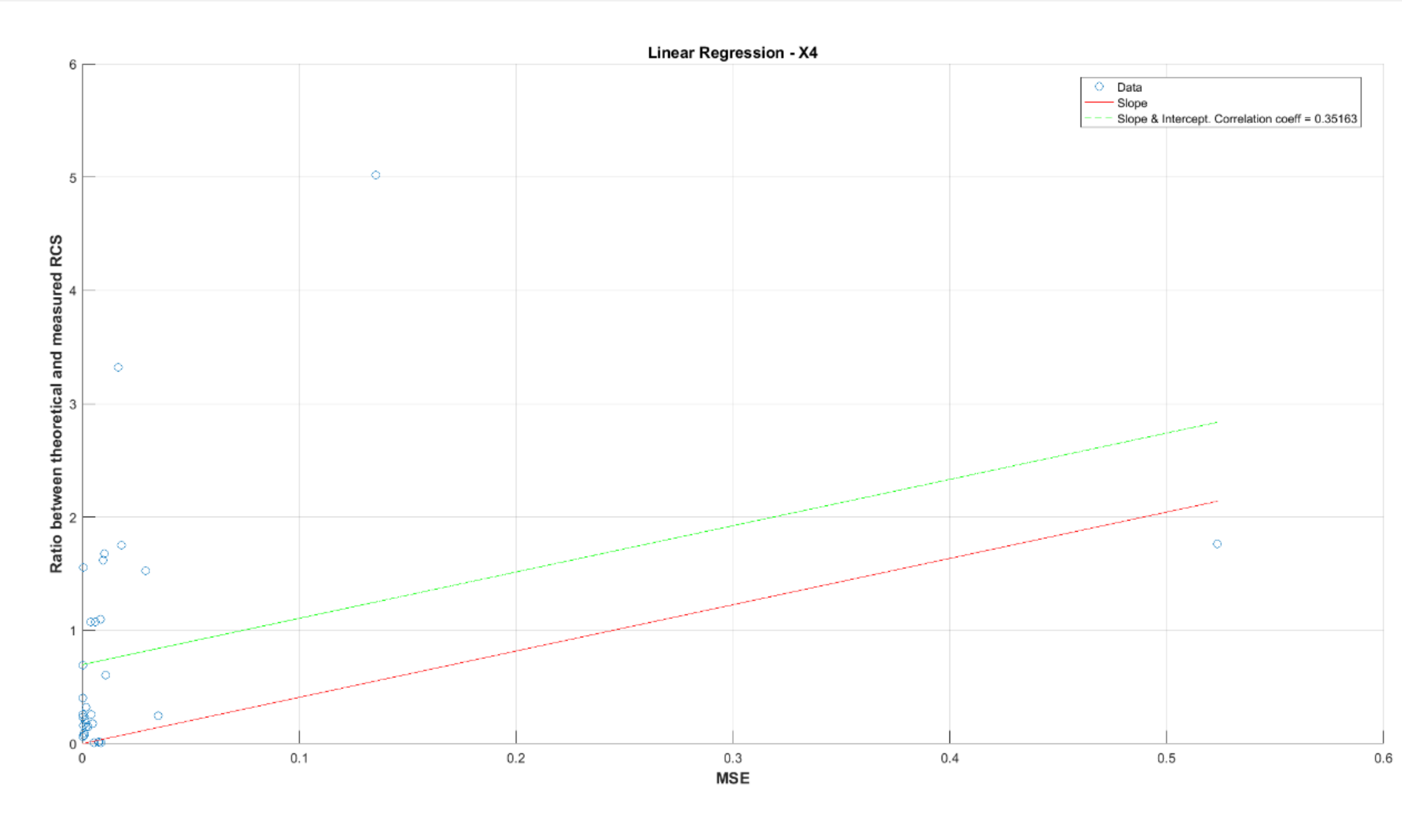

Figure 47. Linear regression of MSE_{CASP} for X4 satellite.

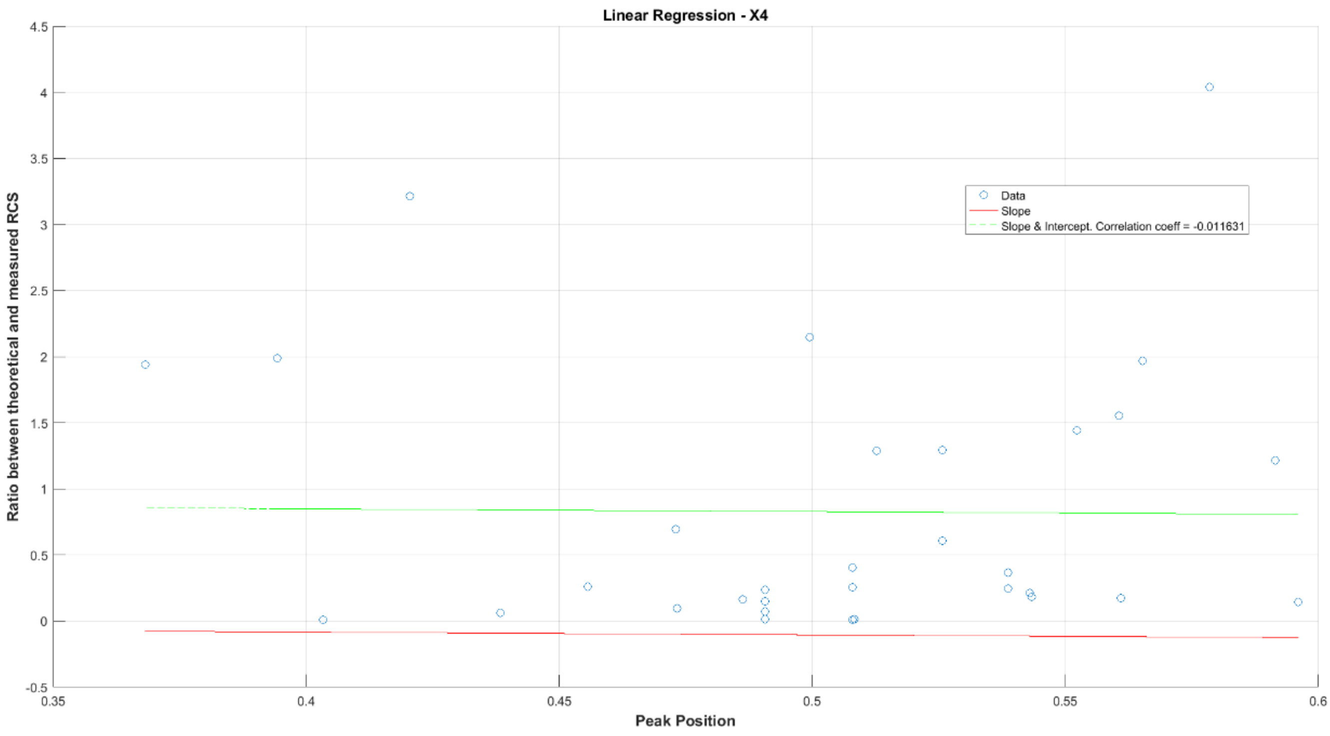

Figure 48. Linear regression of Peak Position for X4 satellite.

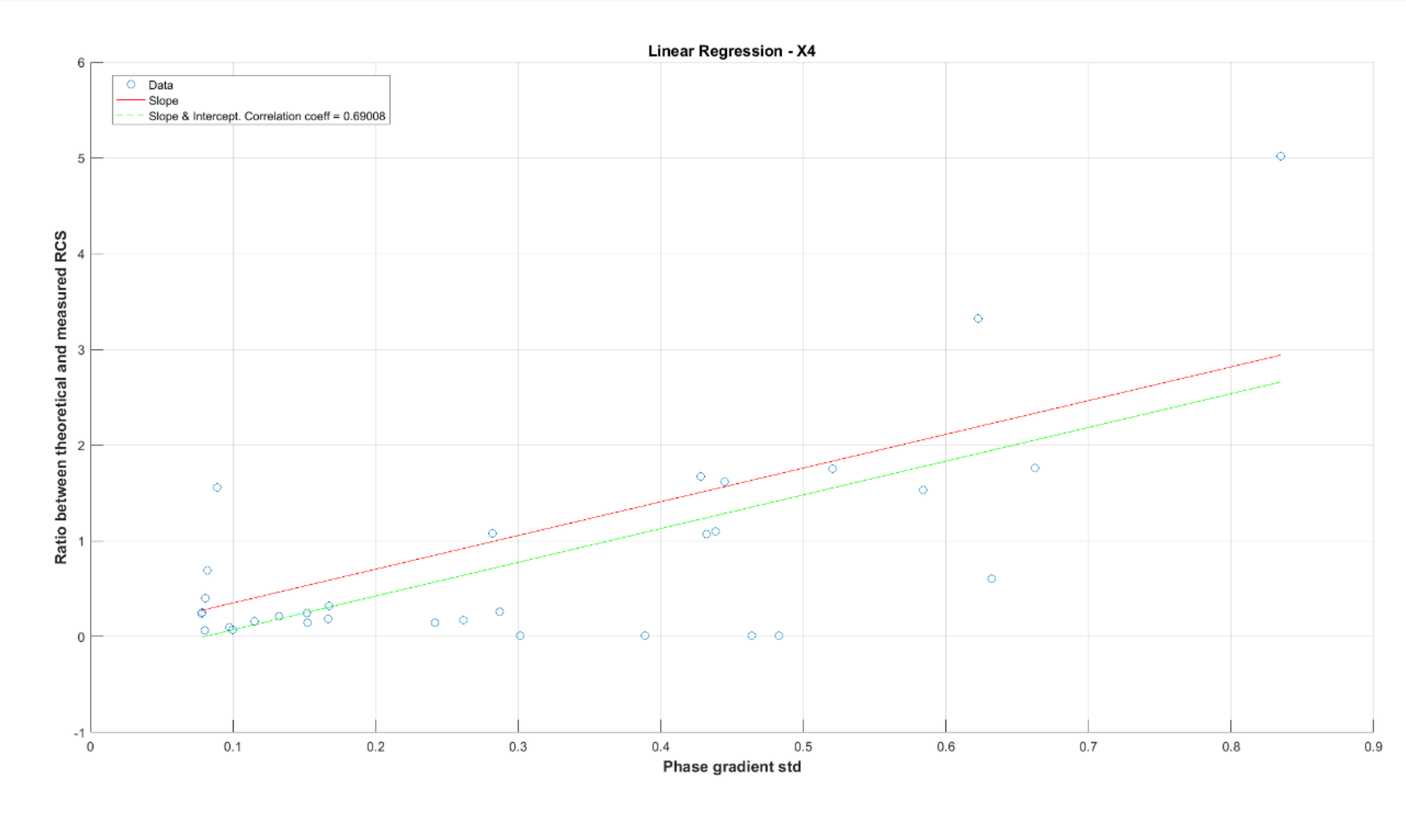

Figure 49: Linear regression of σ_{ASPG} for X4 satellite.

3.2.3.3 RESULTS FOR X5 SATELLITE

A set of 8 images have been acquired on the site for Corner Reflector selection: ds20065, ds20066, ds20067, ds20391, ds20392, ds21251, 21755, 21756.

The results per Corner Reflectors are presented in Figure 50.

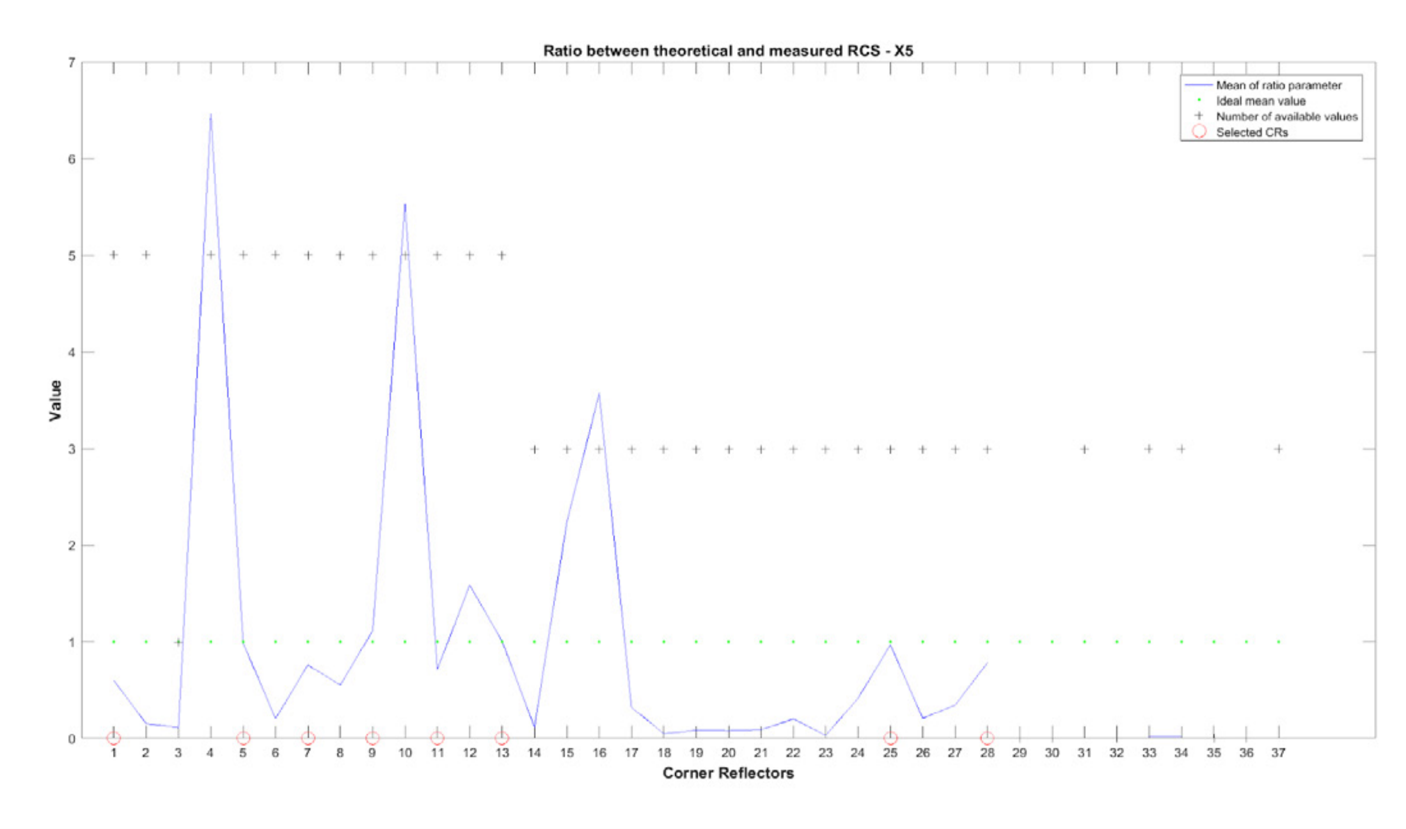

Figure 50. Results for X5 satellite per Corner Reflector.

The selected Corner Reflectors with mean value close to the ideal value are the 1, 5, 7, 9, 11, 13, 25 and 28.

In the following the analysis of the filtering parameters with their correlation coefficient with the parameter R_σ is presented.

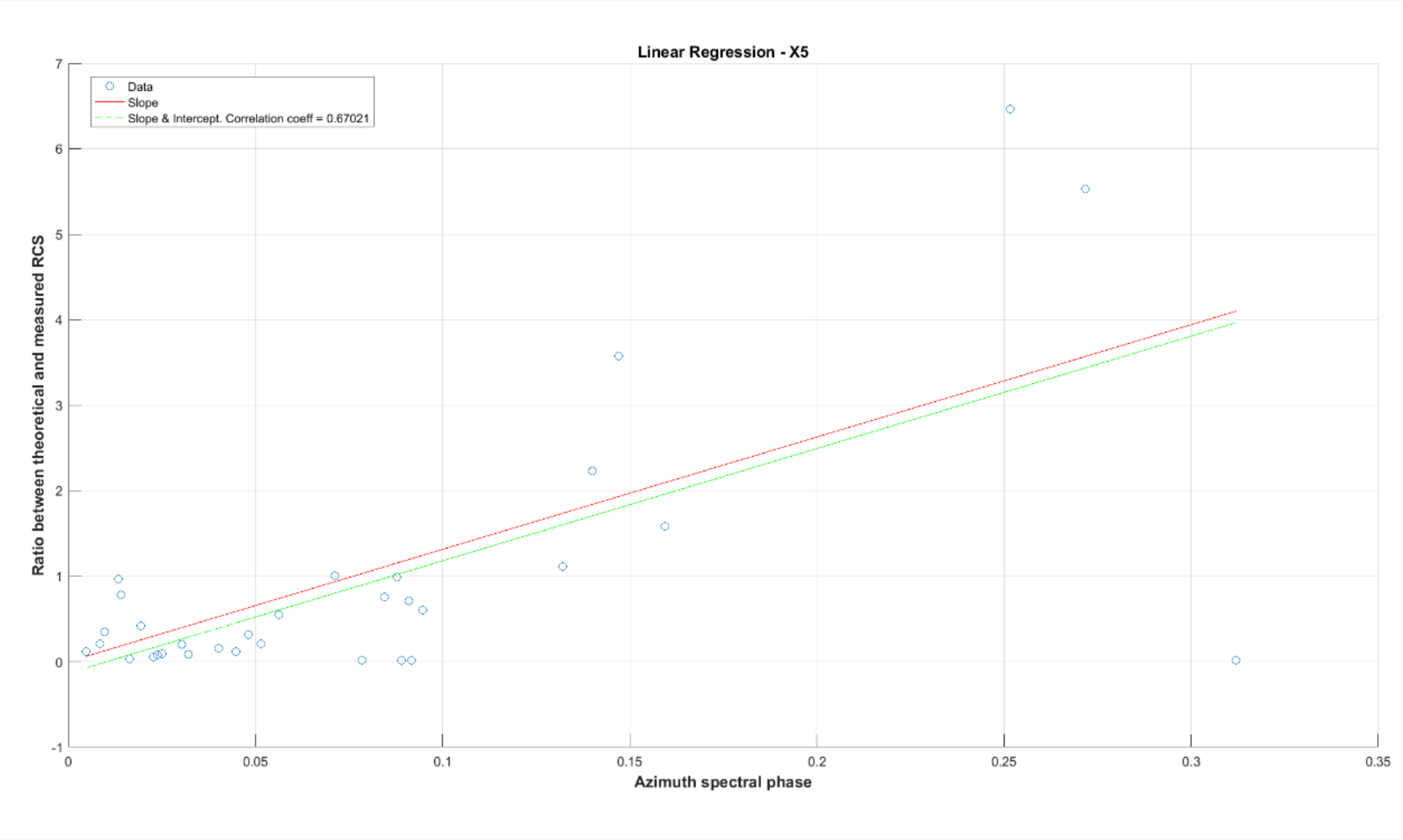

Figure 51. Linear regression of σ_{CASP} *for X5 satellite.*

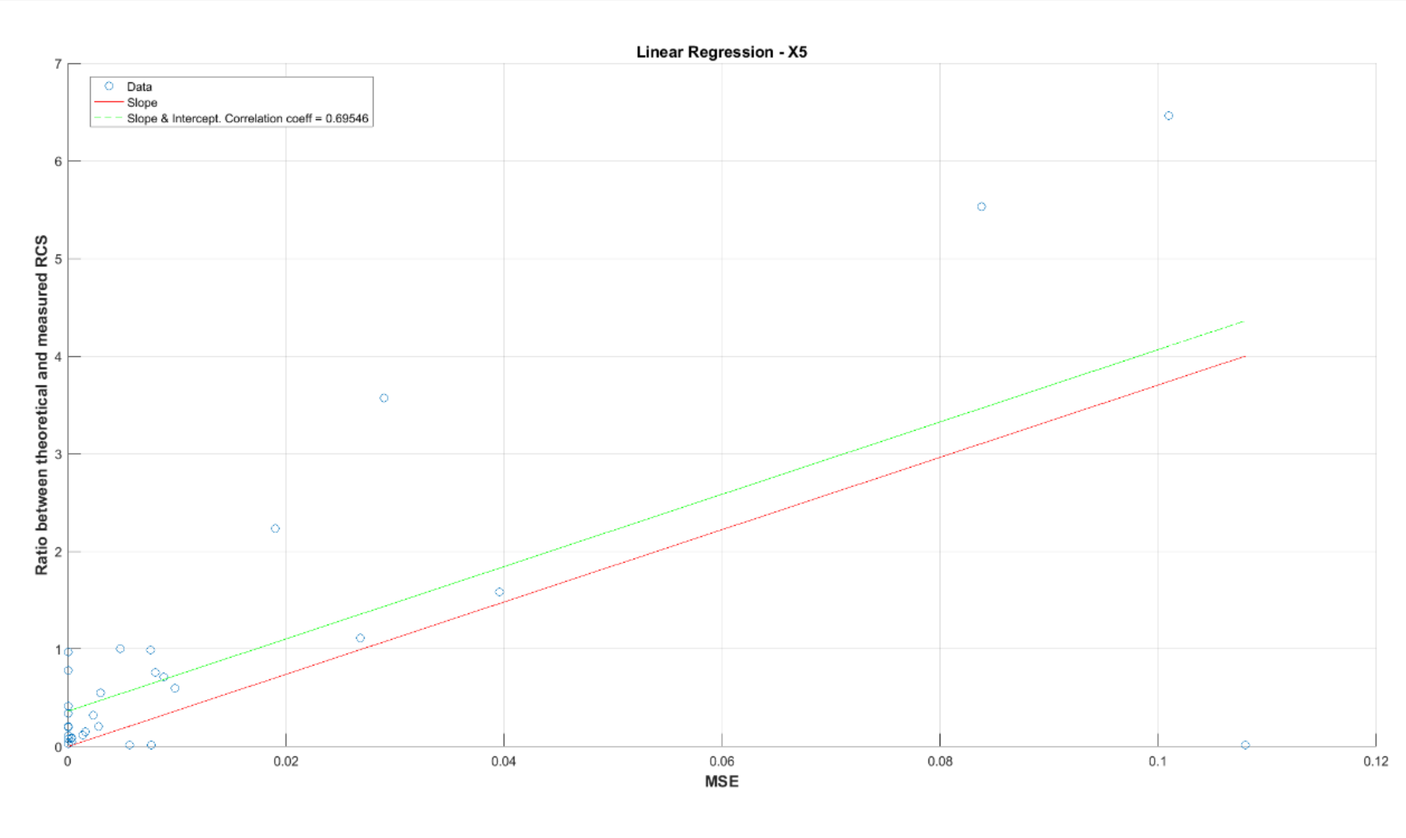

Figure 52. Linear regression of MSE_{CASP} for X5 satellite.

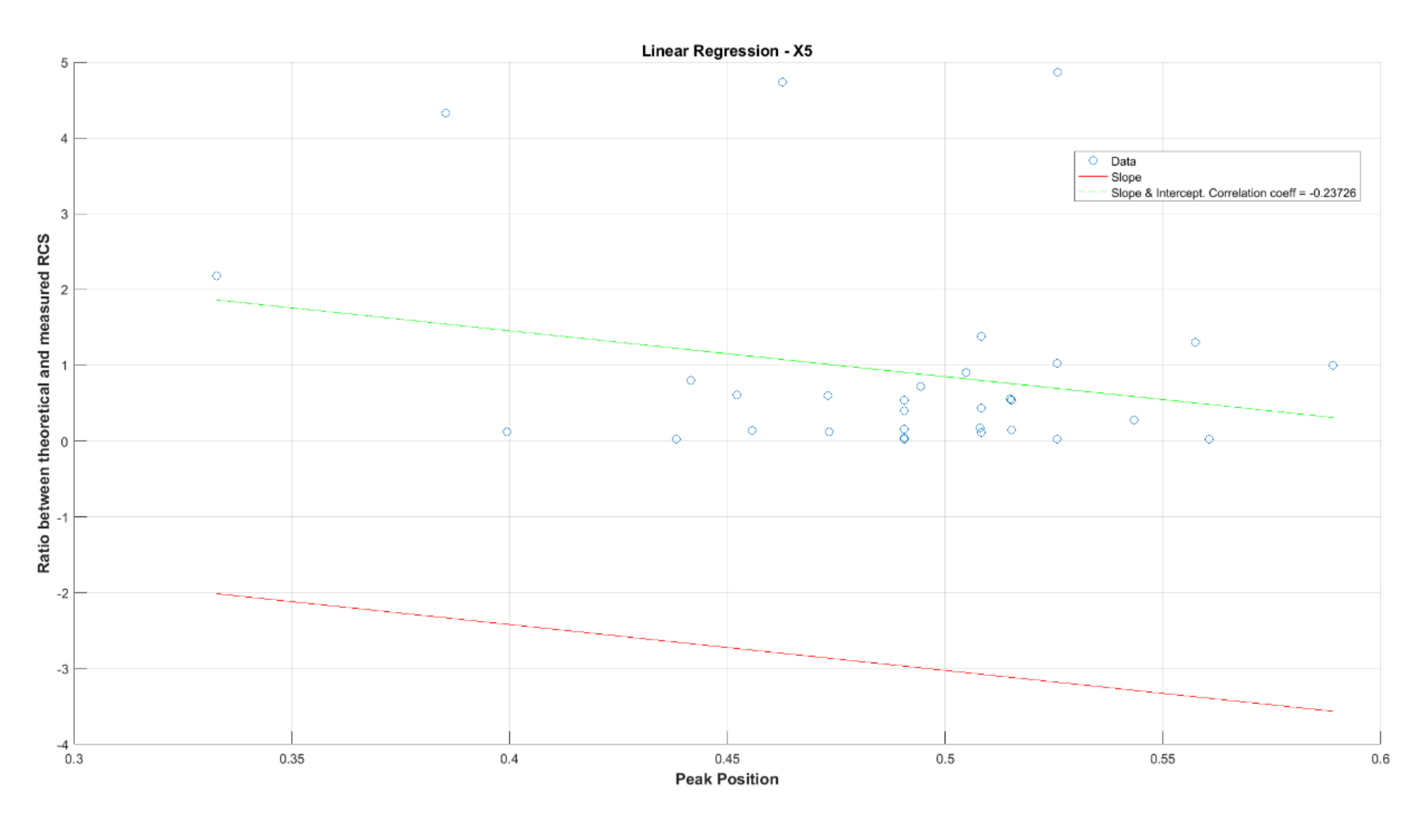

Figure 53. Linear regression of Peak Position for X5 satellite.

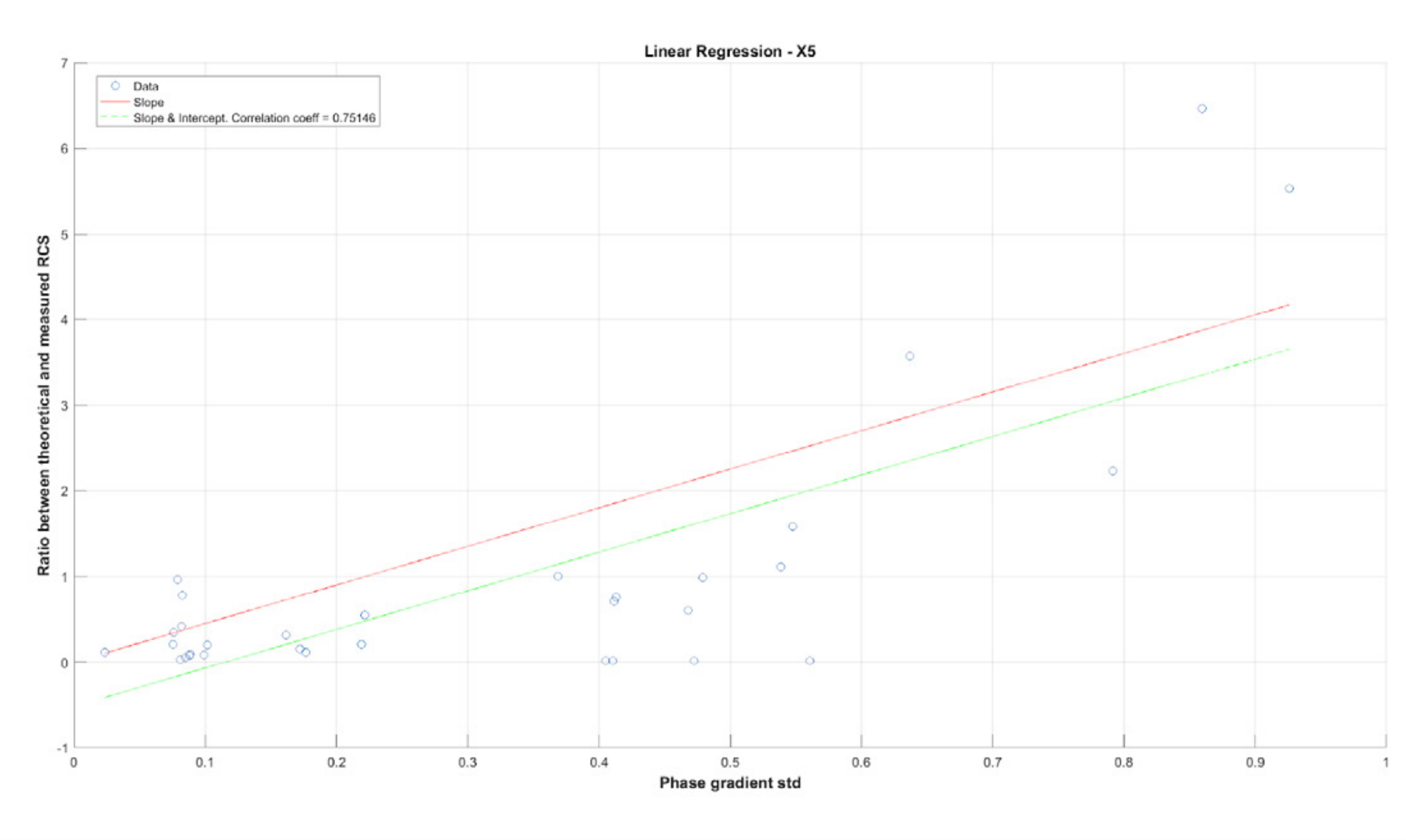

Figure 54. Linear regression of σ_{ASPG} for X5 satellite.

3.2.3.4 SUMMARY OF CORNER REFLECTOR SELECTION

Table 2 shows the number of selected Corner Reflectors for validation and the correlation between R_σ and the filtering parameters.

SATELLITE	SELECTED CRS	σ_{CASP} CORR COEFF (%)	MSE_{CASP} CORR COEFF (%)	PEAK POSITION CORR COEFF (%)	σ_{ASPG} CORR COEFF (%)
X2	4	67.3	66.1	-1.5	57.4
X4	5	62.5	35.1	-1.2	69
X5	8	67	69.5	-23.7	75.1

Table 2. Correlation between the filtering parameters and R_σ for X2, X4 and X5

CALIBRATION & VALIDATION OF ICEYE SENSORS

The results show that the best correlation with the theoretical results is obtained with the parameters σ_{CASP} and σ_{ASPG}, that overpass the 50% in at least 2 satellites.

Unexpectedly, the peak position parameter has a very low correlation with the parameter R_{σ}. The parameter MSE_{CASP} is not efficient to filter out the results affected by large errors, even if it reach a good correlation for X2 and X5, because most of estimations have low MSE_{CASP}. For these reasons these parameters will be discarded by the selection parameters for validation.

The thresholds that have been applied to filter out the bad RCS estimations during the validation step are the following:

$$\sigma_{CASP_{th}} = 0.3$$

$$\sigma_{ASPG_{th}} = 0.5\ .$$

3.2.4 VALIDATION ON CONGO FOREST

3.2.4.1 RESULTS FOR X2 SATELLITE

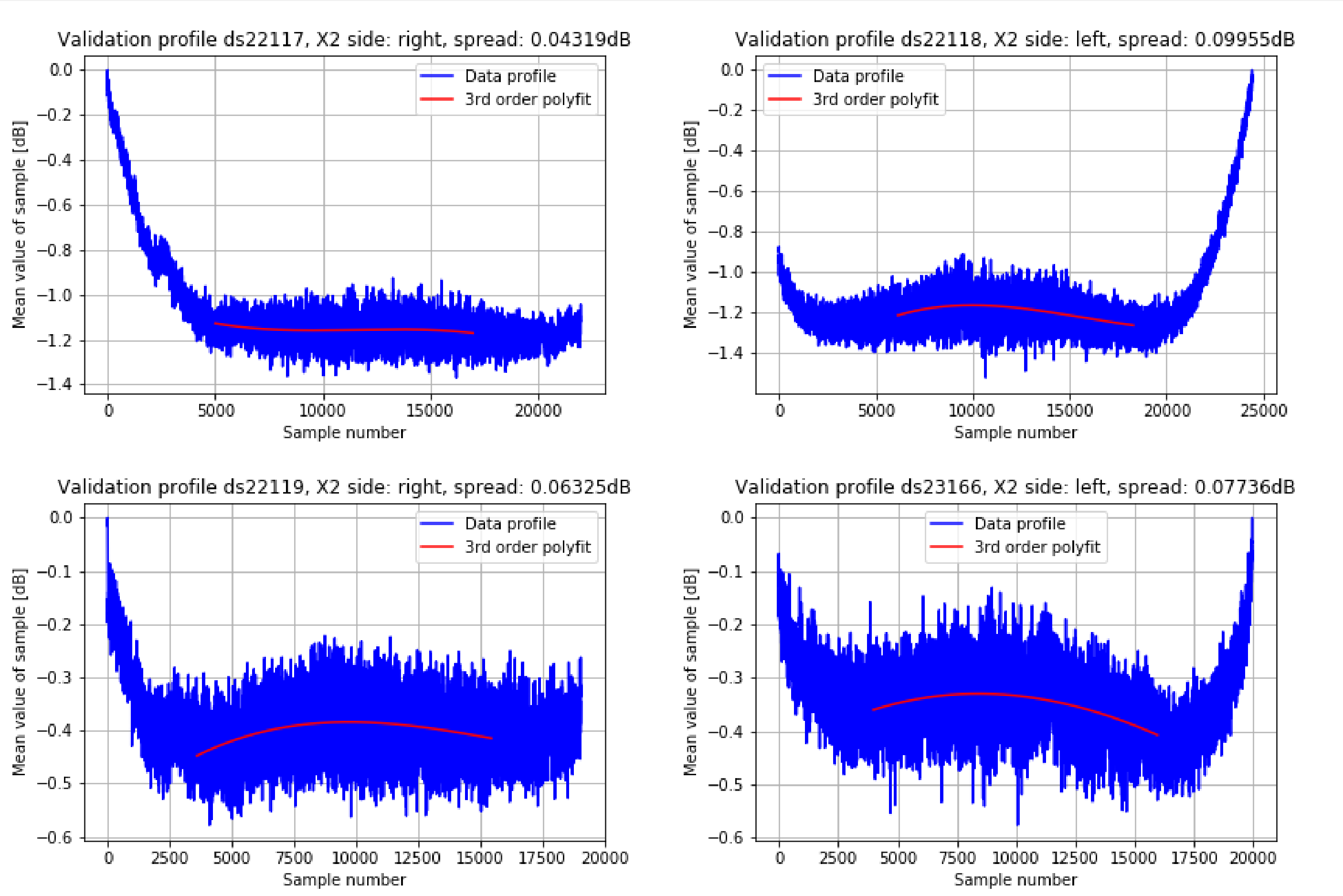

Figure 55. Radiometric validation results. Amplitude are profiles compensated by and non-homogenous areas masking. 3rd order polynomial fitting reflects 30 km swath length.

▶ CALIBRATION & VALIDATION OF ICEYE SENSORS

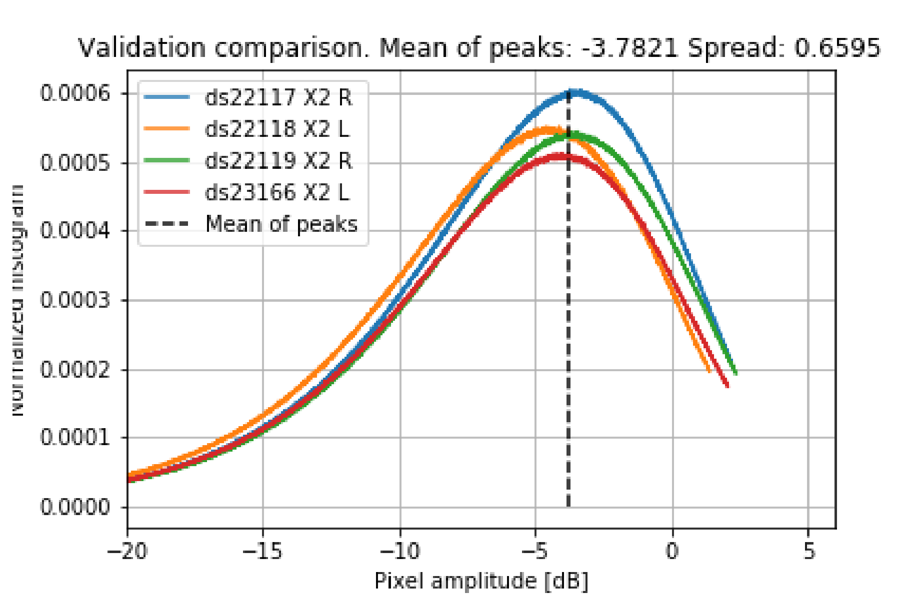

Figure 56. Comparison of sigma 0 for x2 satellite (Congo acquisitions) expressed in dB

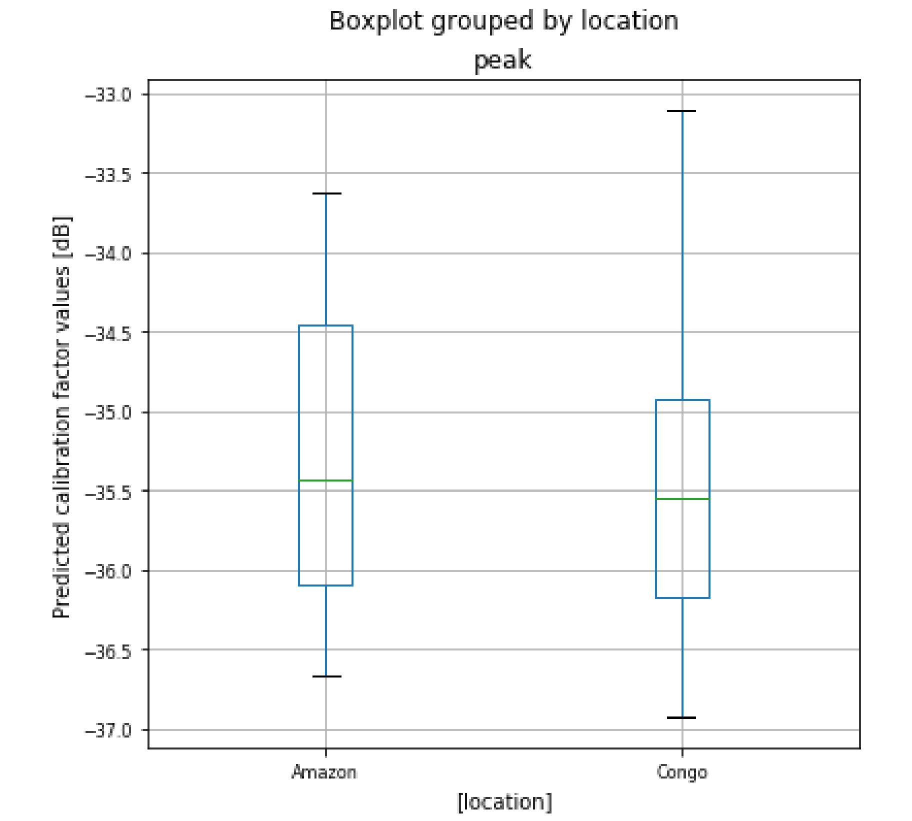

Figure 57. Comparison of predicted calibration factor values [dB] for x2 satellite between Amazon and Congo

3.2.4.2 RESULTS FOR X4 SATELLITE

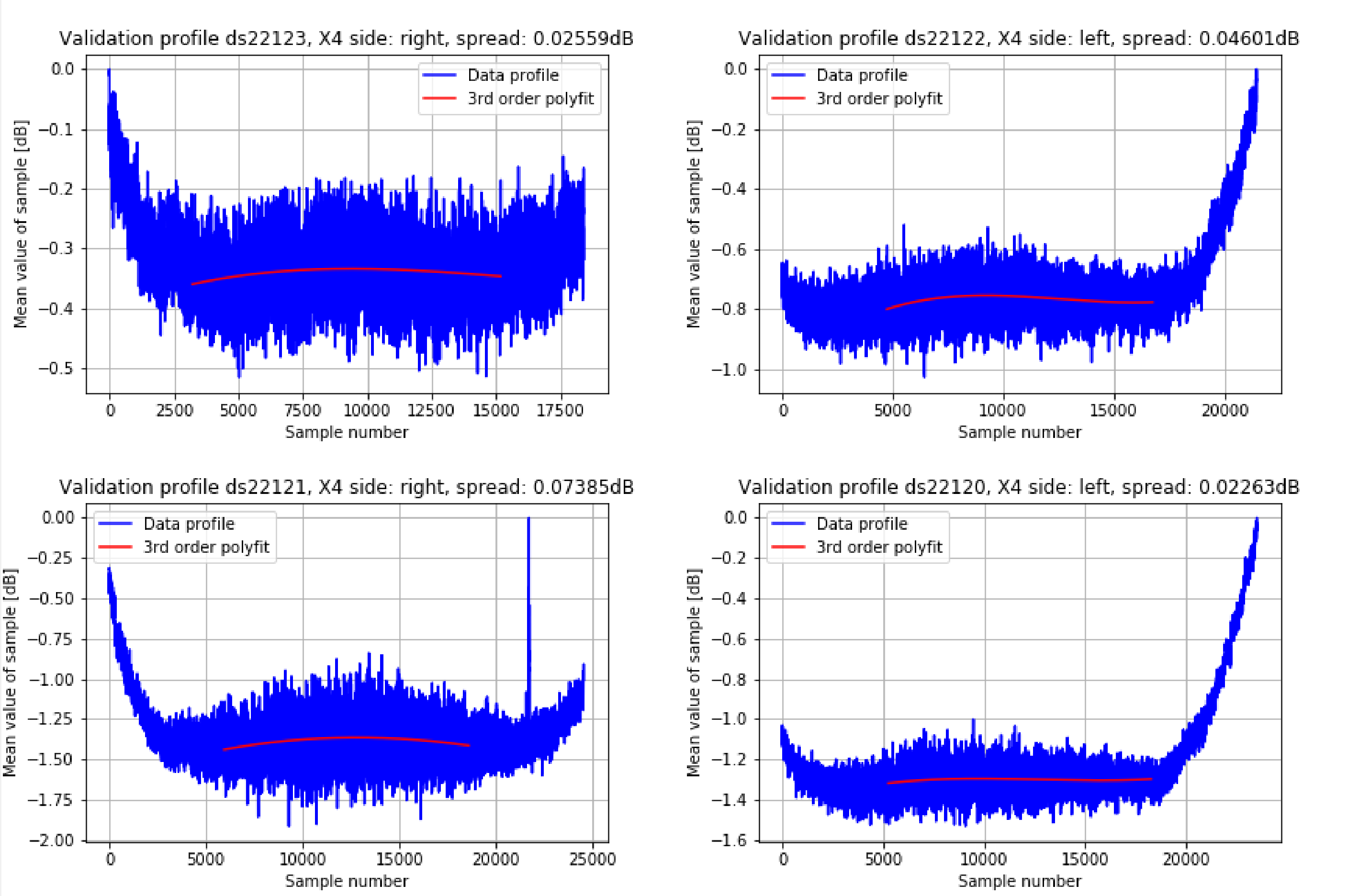

Figure 58. Radiometric validation results. Amplitude are profiles compensated by and non-homogenous areas masking. 3rd order polynomial fitting reflects 30 km swath length.

CALIBRATION & VALIDATION OF ICEYE SENSORS

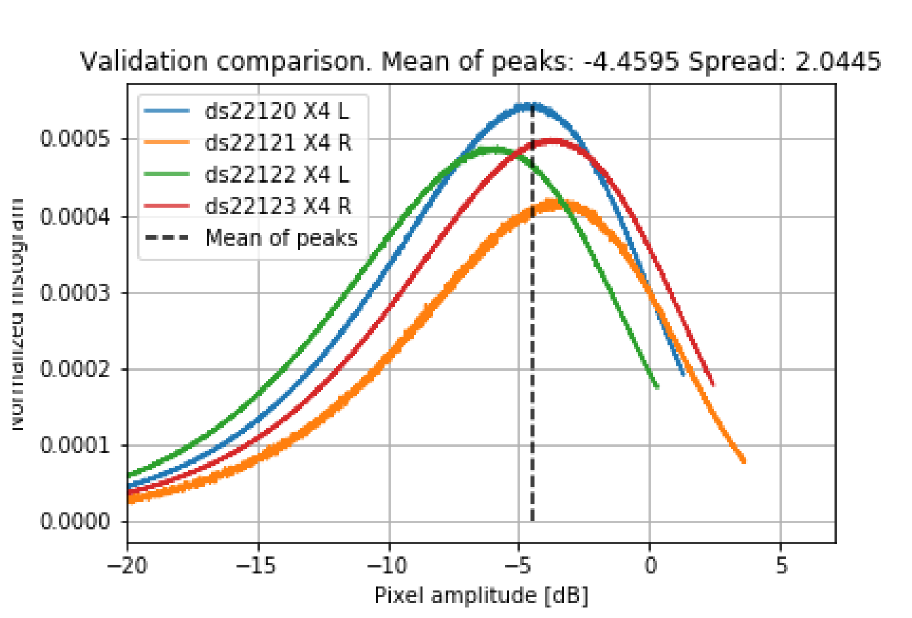

Figure 59. Comparison of sigma 0 for x4 satellite (Congo acquisitions) expressed in dB

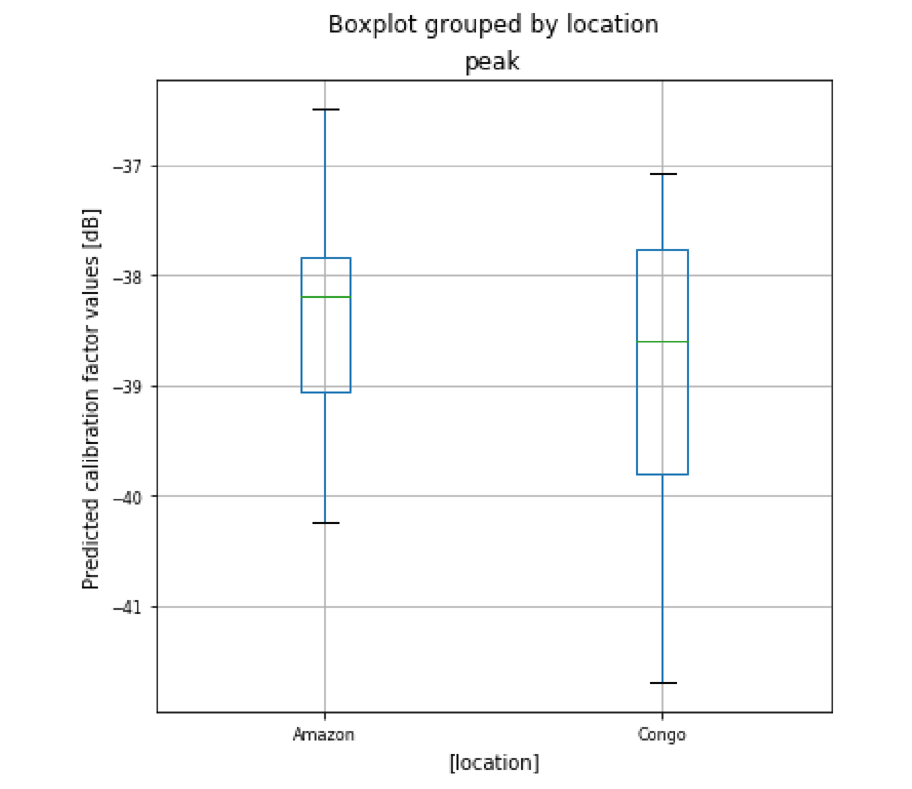

Figure 60. Comparison of predicted calibration factor values [dB] for x4 satellite between Amazon and Congo

3.2.4.3 RESULTS FOR X5 SATELLITE

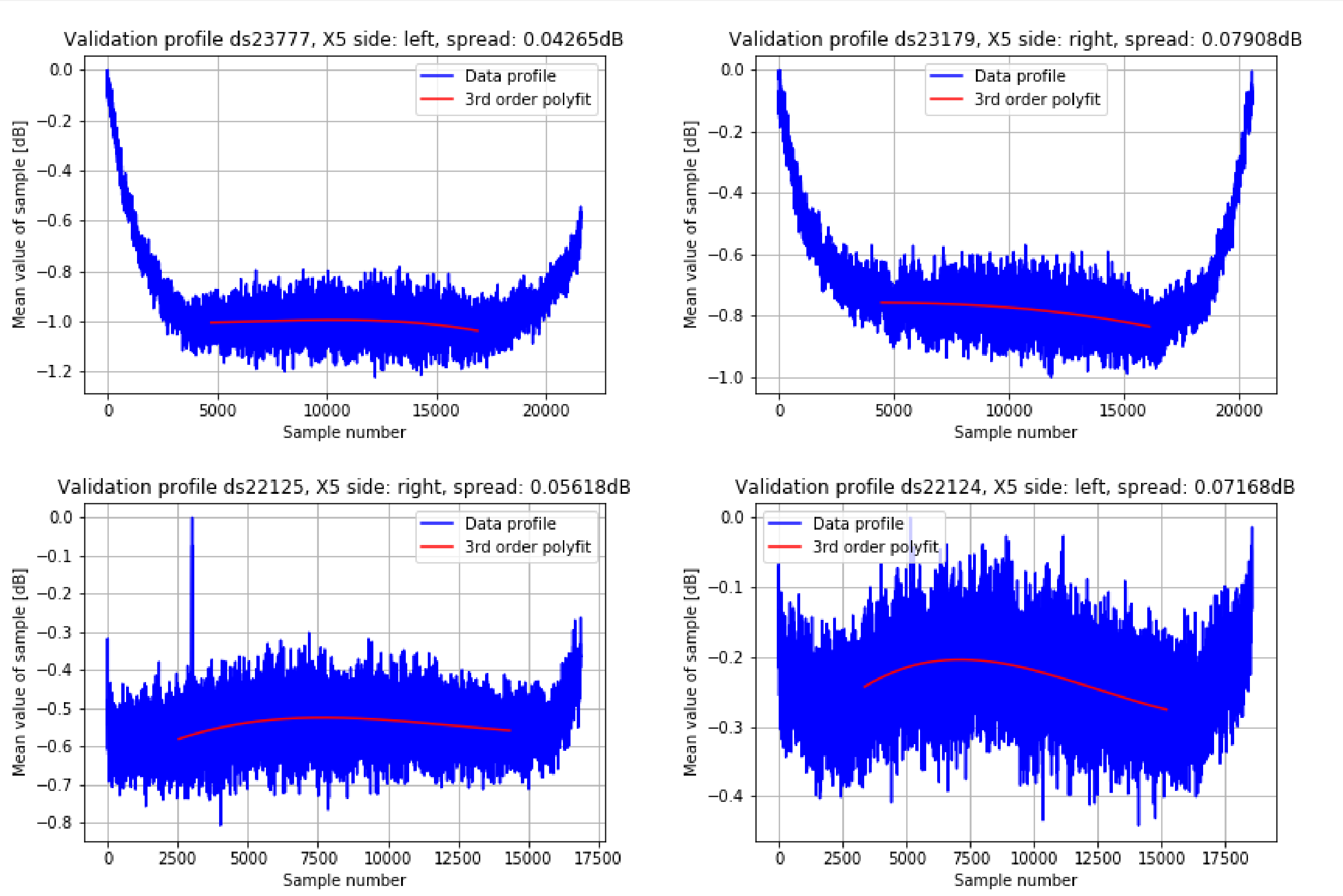

Figure 61. Radiometric validation results. Amplitude are profiles compensated by and non-homogenous areas masking. 3rd order polynomial fitting reflects 30 km swath length.

▶ CALIBRATION & VALIDATION OF ICEYE SENSORS

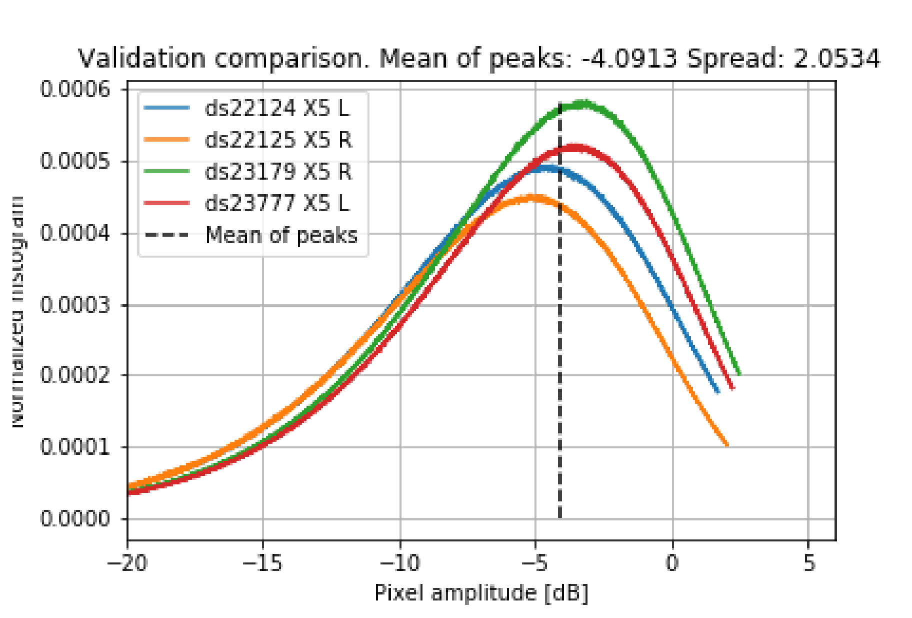

Figure 62. Comparison of sigma 0 for x5 satellite (Congo acquisitions) expressed in dB

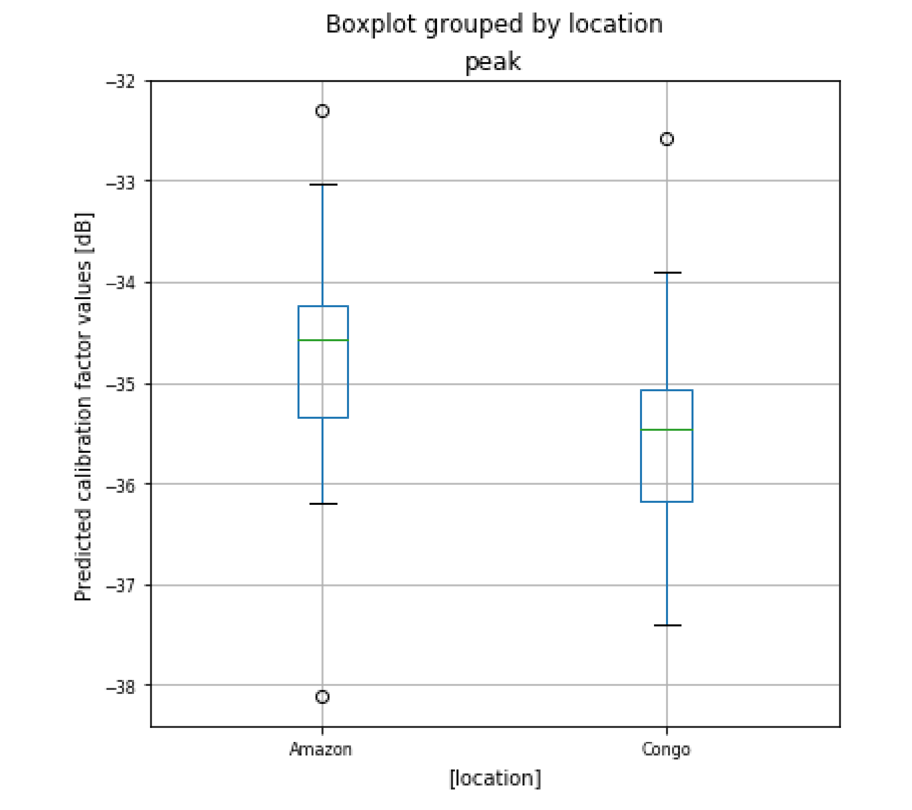

Figure 63. Comparison of predicted calibration factor values [dB] for x5 satellite between Amazon and Congo

CALIBRATION & VALIDATION OF ICEYE SENSORS

3.2.4.4 COMPARISON BETWEEN SATELLITES – CONGO FOREST

As a part of validation procedure, it is needed to verify if satellites present similar levels of pixel amplitudes after applying corresponding – new – calibration factors. For this purpose a number of images taken over Congo forest were reprocessed using new calibration constants. For each image, the normalized histogram of sigma nought has been calculated and compared on a single graph. As one can observe on figure 64 subsequent products represent low spread although a mean of - 4.28 dB which is over the target of -6.5 dB will still need to be investigated.

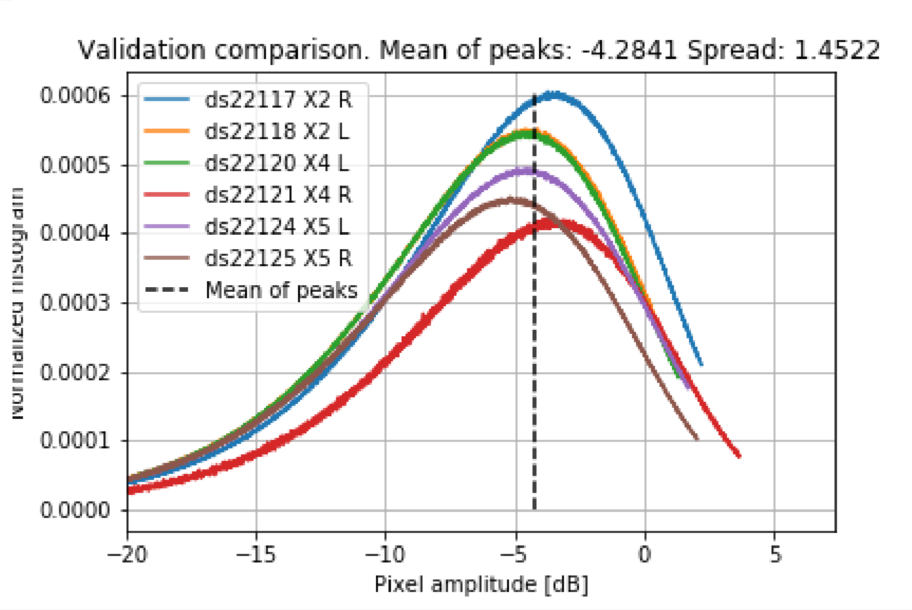

Figure 64. Comparison of sigma 0 for constellation satellites (X2, X4, X5) - Congo acquisitions

CALIBRATION & VALIDATION OF ICEYE SENSORS

3.2.5 VALIDATION ON CORNER REFLECTOR ANALYSIS

The next sections present the validation results for the satellites X2, X4 and X5 in Stripmap and Spotlight modes.

Unfortunately, few images acquired over the Amazon or Congo forest in Spotlight mode were available for calibration purposes. For this reason, it has not yet been possible to estimate the calibration constant for Spotlight. At this stage, the validation has been performed using the current calibration factor and the calibration factor estimated for Stripmap.

In the future a large amount of data acquired over the Amazon forest will be collected, allowing the proper calibration analysis.

The validation is performed analyzing the convergence of the cumulative ratio between the theoretical RCS value and the measured RCS R_σ. If the calibration constant has been estimated properly, the convergence $R_\sigma \rightarrow 1$ is expected. In fact, for $R_\sigma = 1$ the estimated calibration constant is equal to the ideal constant.

The validation has been performed using the Calibration Factors calculated by the median and the mean of the peak position in the K distribution. The ratio convergence without and with filtering (using the filtering parameters σ_{CASP} and σ_{ASPG}) are presented in the following plots.

3.2.5.1 RESULTS FOR X2 SATELLITE – STRIPMAP MODE

A set of 8 images have been acquired on the site for validation: ds23761, ds24146, ds24345, ds25093, ds25937, ds25956, ds26907, 27020.

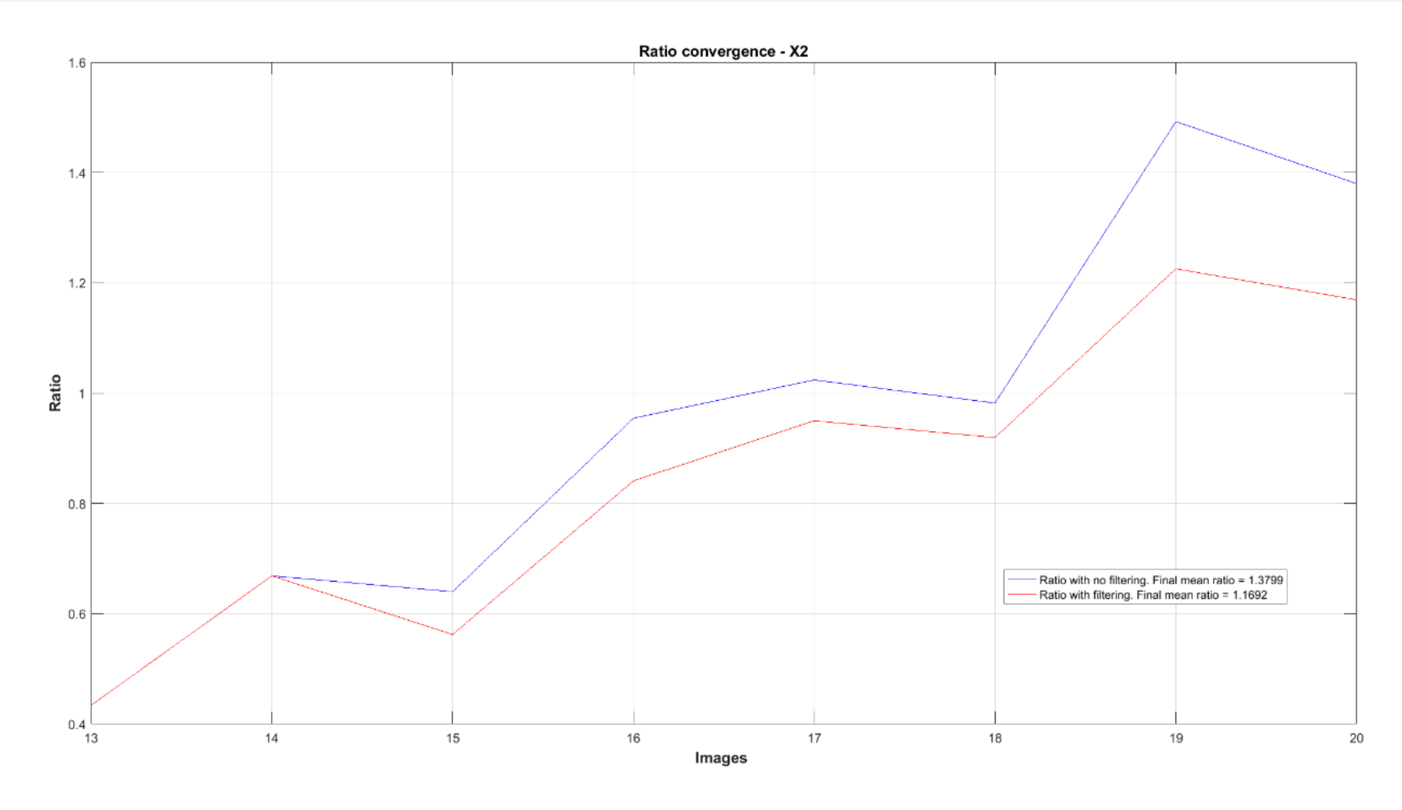

Figure 65. Ratio convergence using the old calibration constant – X2

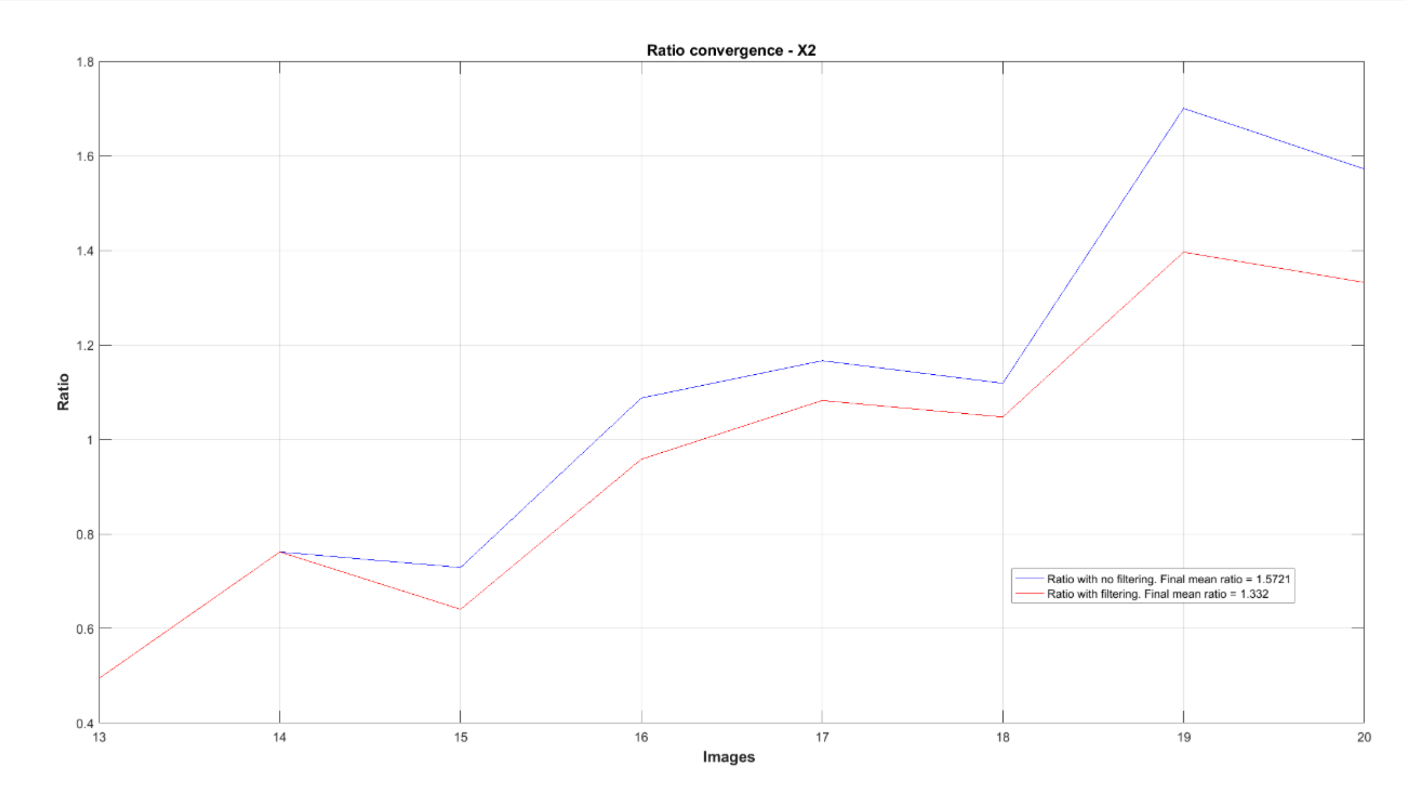

Figure 66. Ratio convergence using the new median value of calibration constant – X2

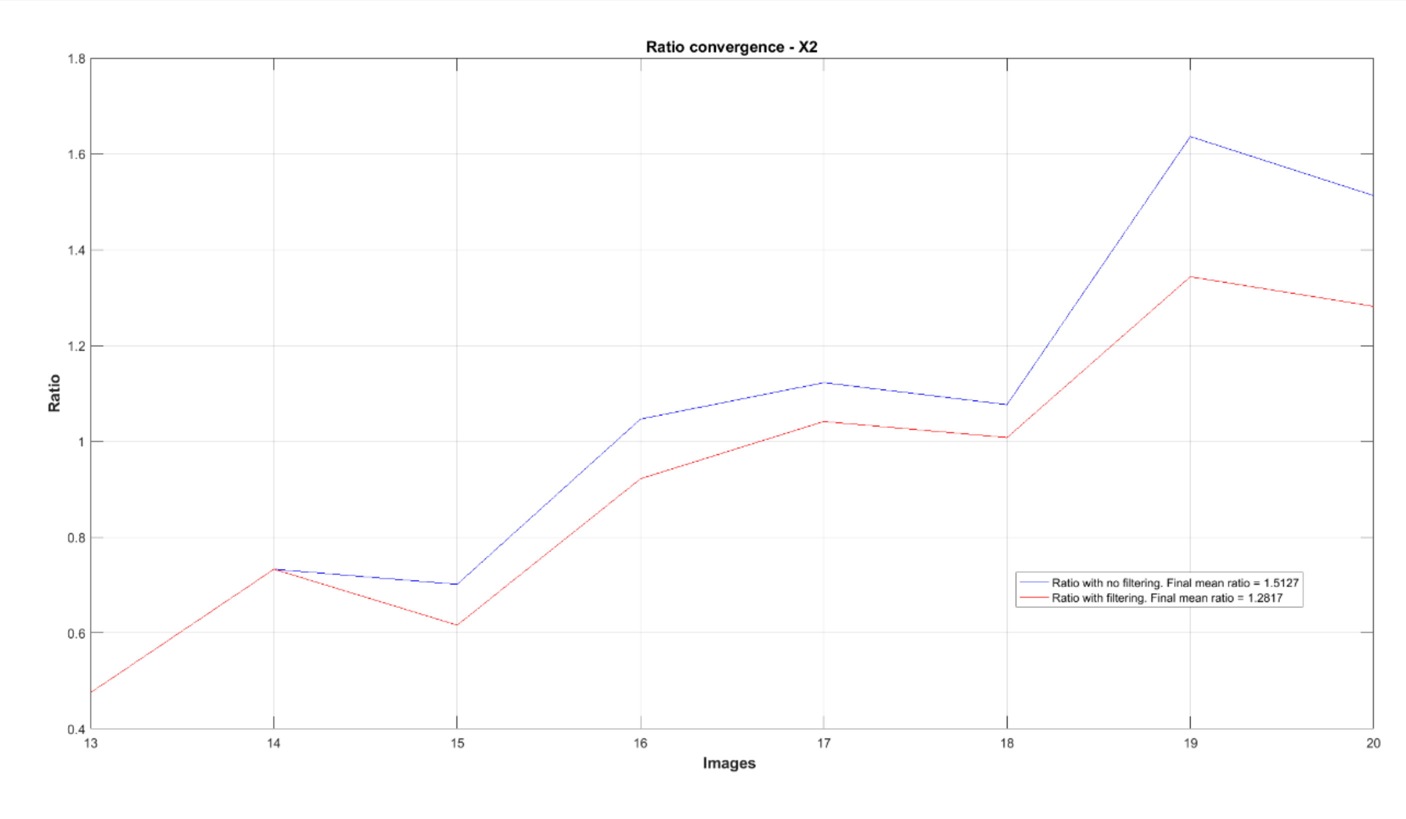

Figure 67. Ratio convergence using the new mean value of calibration constant – X2

The results for X2 must be considered preliminary, because the available images for validation are not enough.

3.2.5.2 RESULTS FOR X2 SATELLITE – SPOTLIGHT MODE

A set of 8 images have been acquired on the site for validation:
ds25091, ds25094, ds25626, ds25627, ds26770, ds26948, ds26952, 27022.

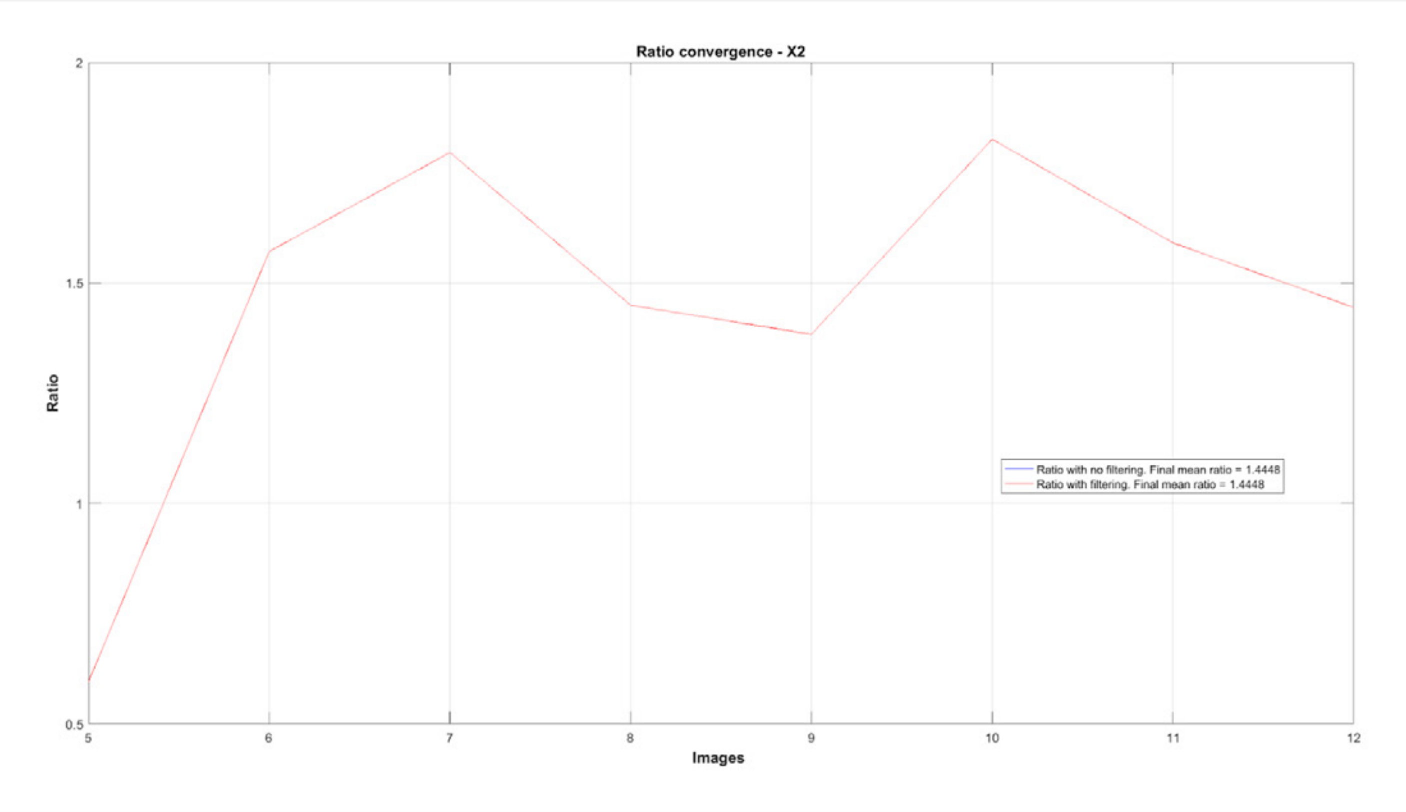

Figure 68. Ratio convergence using the old calibration constant – X2

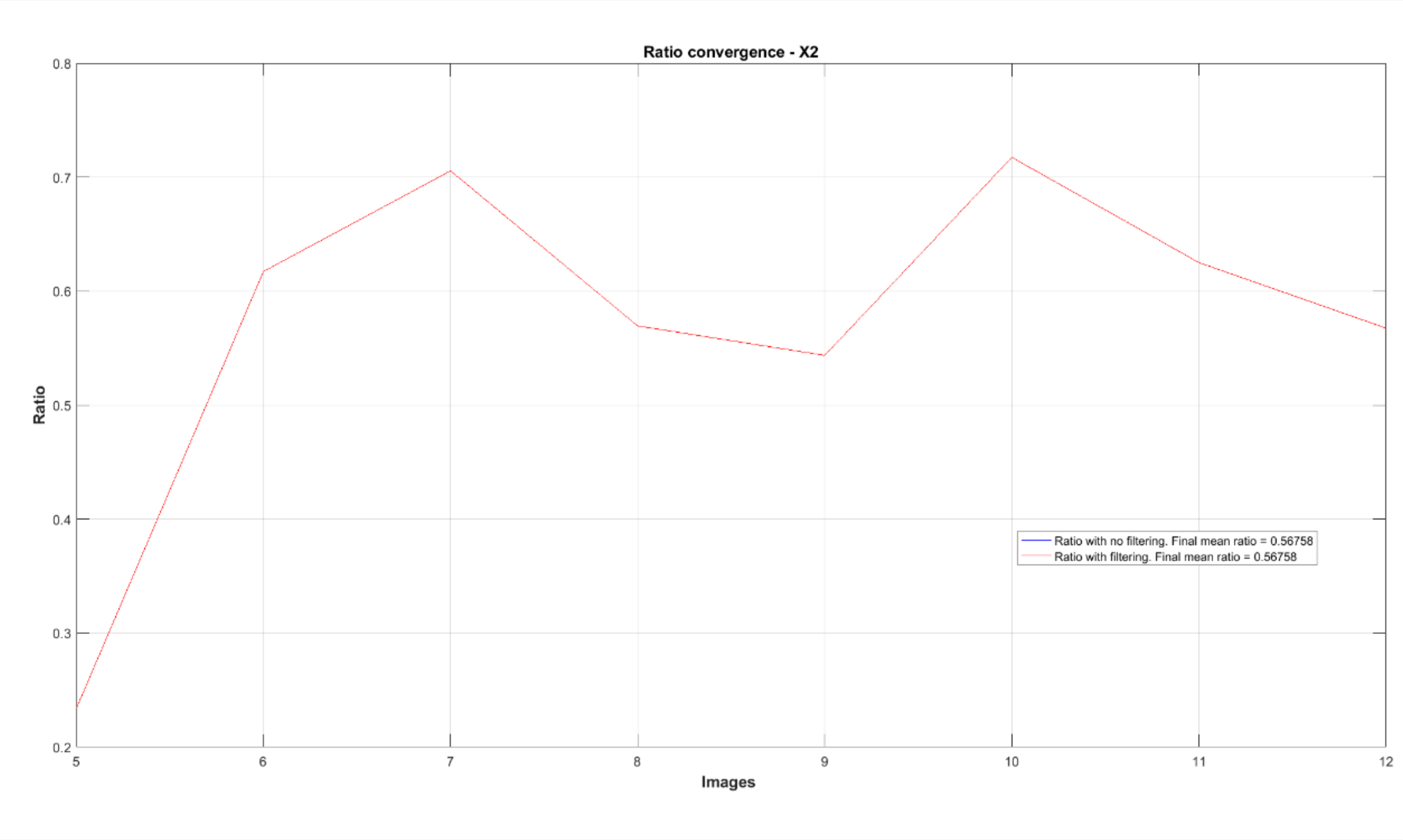

Figure 69. Ratio convergence using the new median value of calibration constant – X2

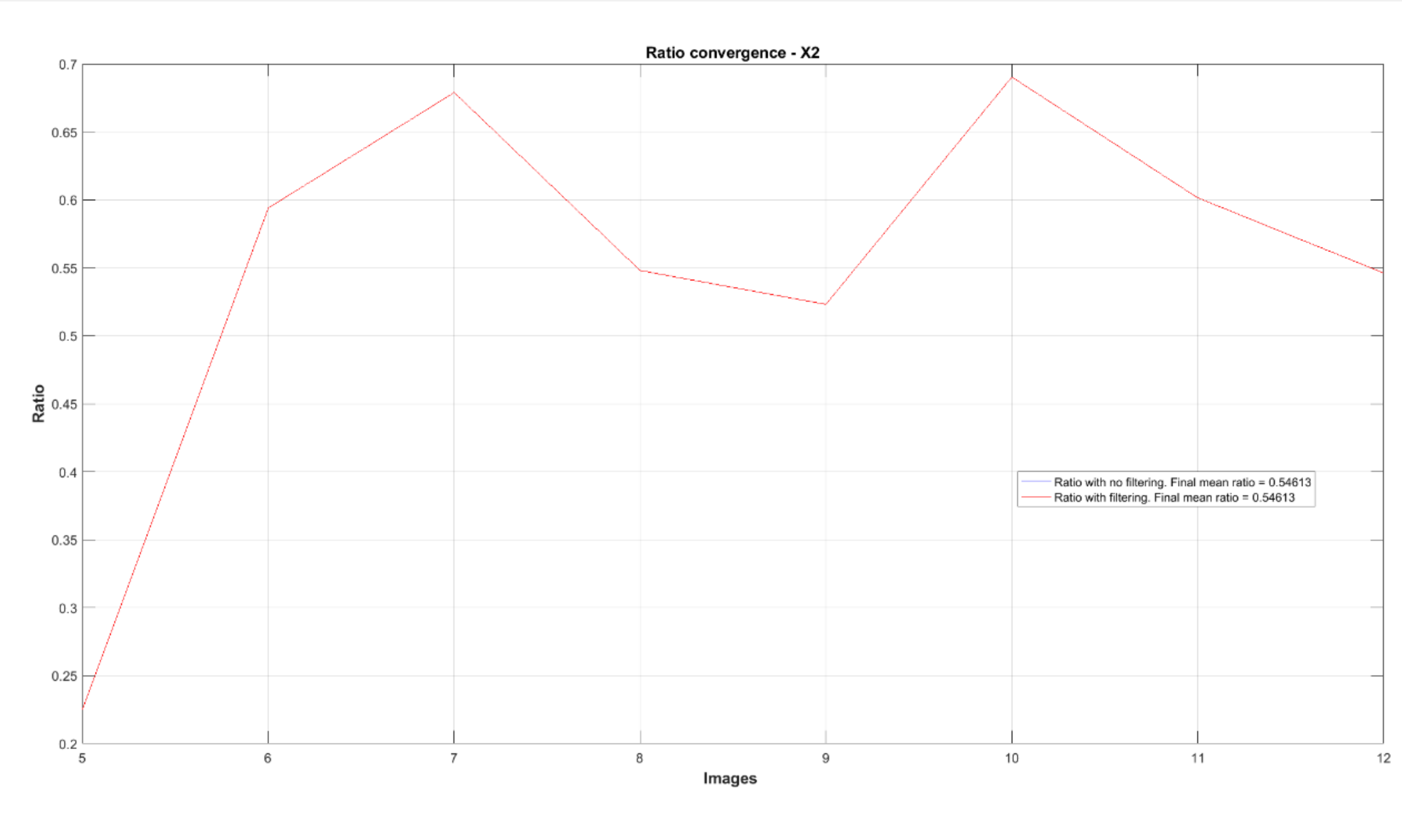

Figure 70. Ratio convergence using the new mean value of calibration constant – X2

The results show that the new calibration factor estimated for Stripmap mode is not representative of Spotlight images.

The results for X2 must be considered preliminary, because the available images for validation are not enough.

3.2.5.3 RESULTS FOR X4 SATELLITE – STRIPMAP MODE

A set of 13 images have been acquired on the site for validation: ds20389, ds21752, ds21753, ds22799, ds22806, ds23764, ds24335, 24338, ds24339, ds25085, ds25958, ds26307, 26308.

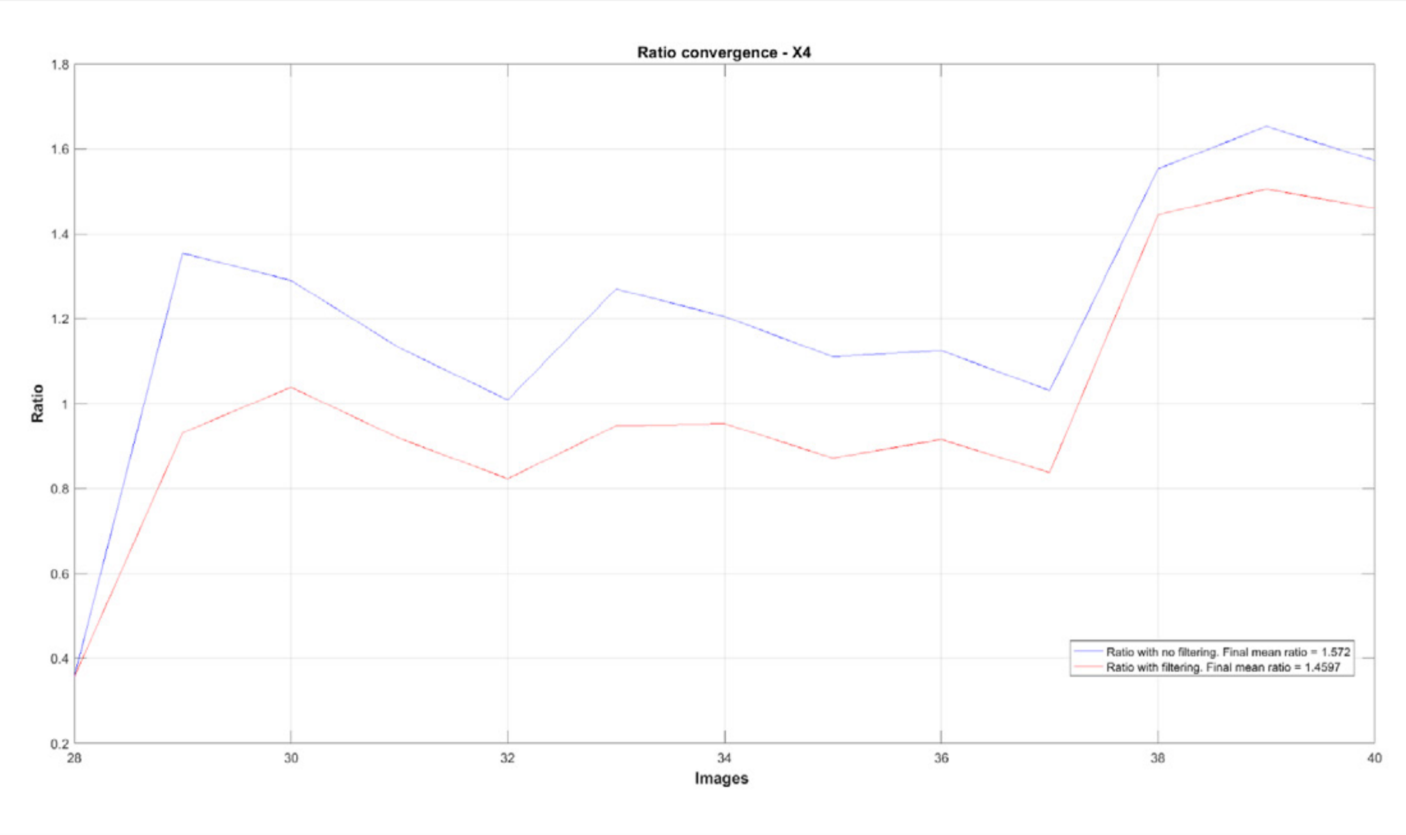

Figure 71. Ratio convergence using the old calibration constant – X4

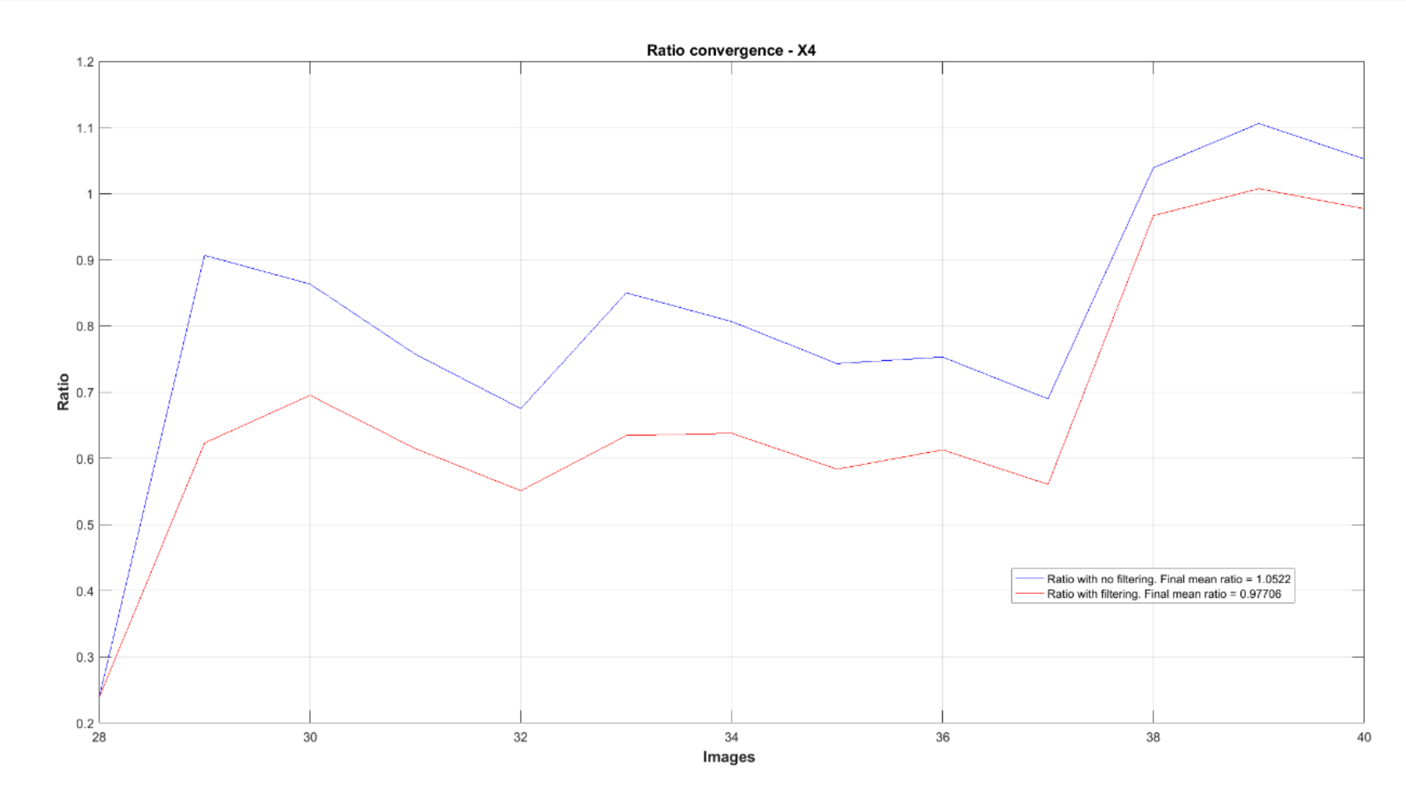

Figure 72. Ratio convergence using the new median value of calibration constant – X4

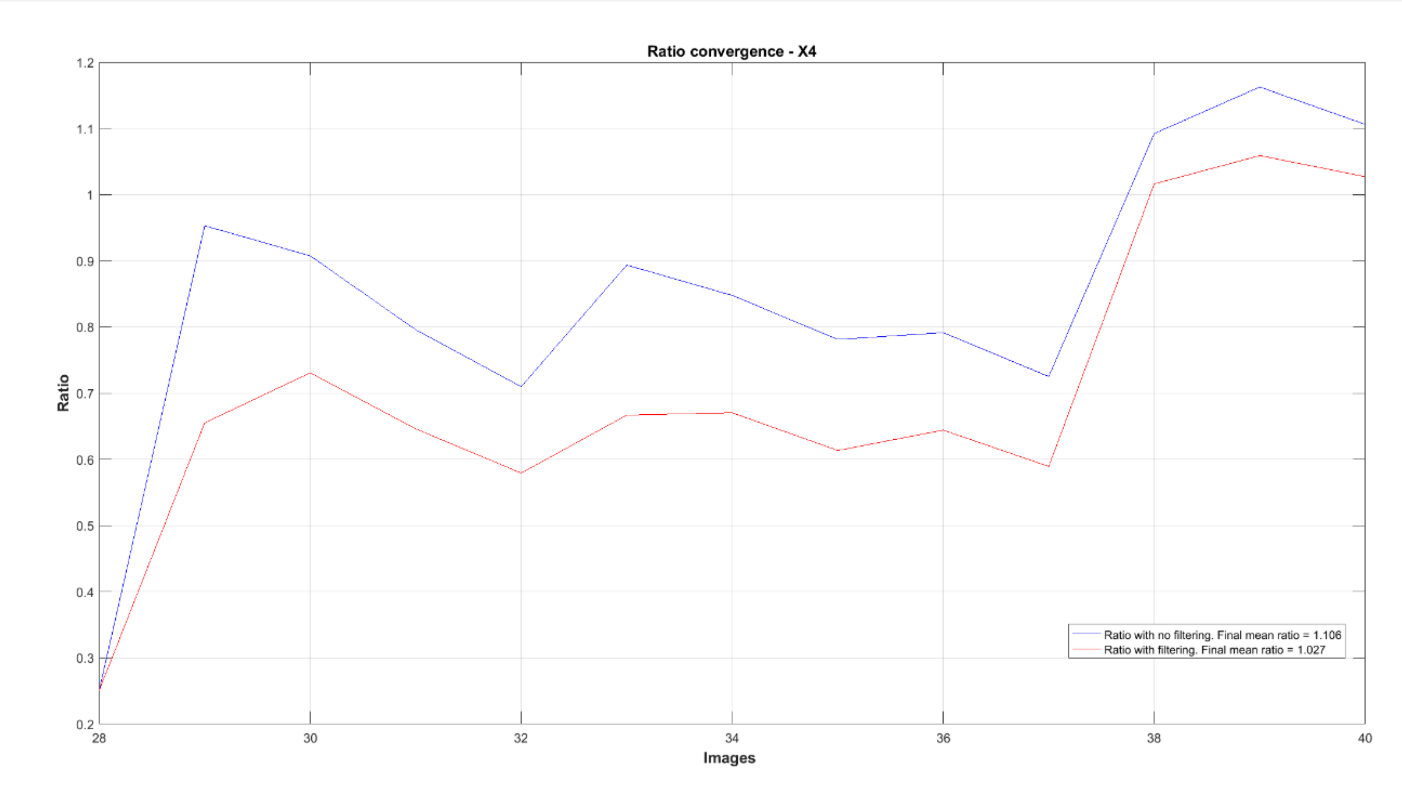

Figure 73. Ratio convergence using the new mean value of calibration constant – X4

The calibration of X4 finds a confirmation in the validation results, because the ideal calibration factor has a difference less than 3% from the estimated value.

3.2.5.4 RESULTS FOR X4 SATELLITE – SPOTLIGHT MODE

A set of 11 images have been acquired on the site for validation: ds23266, ds23267, ds23762, ds23763, ds24336, ds24337, ds25086, 25087, ds25957, ds26309, 27023.

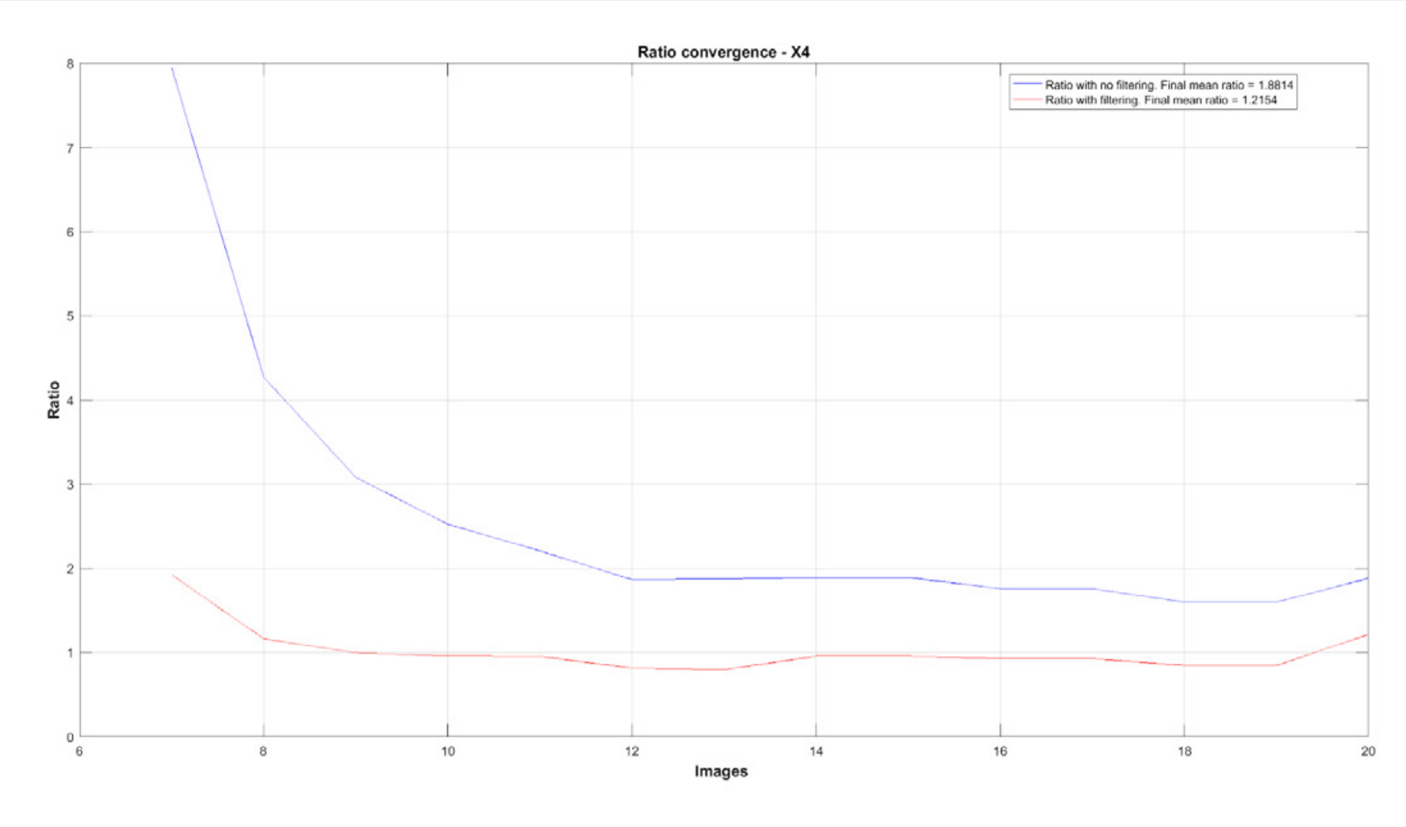

Figure 74. Ratio convergence using the old calibration constant – X4

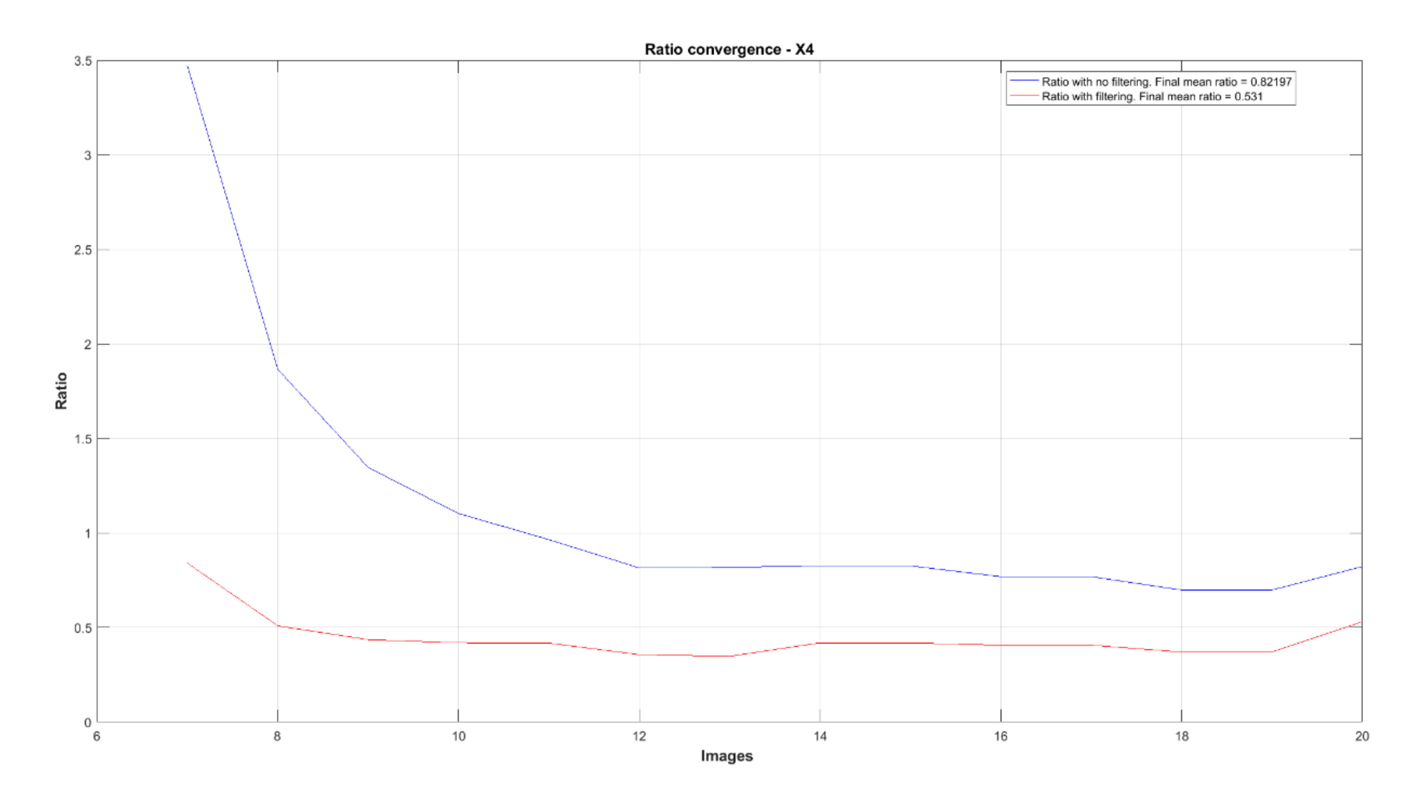

Figure 75. Ratio convergence using the new median value of calibration constant – X4

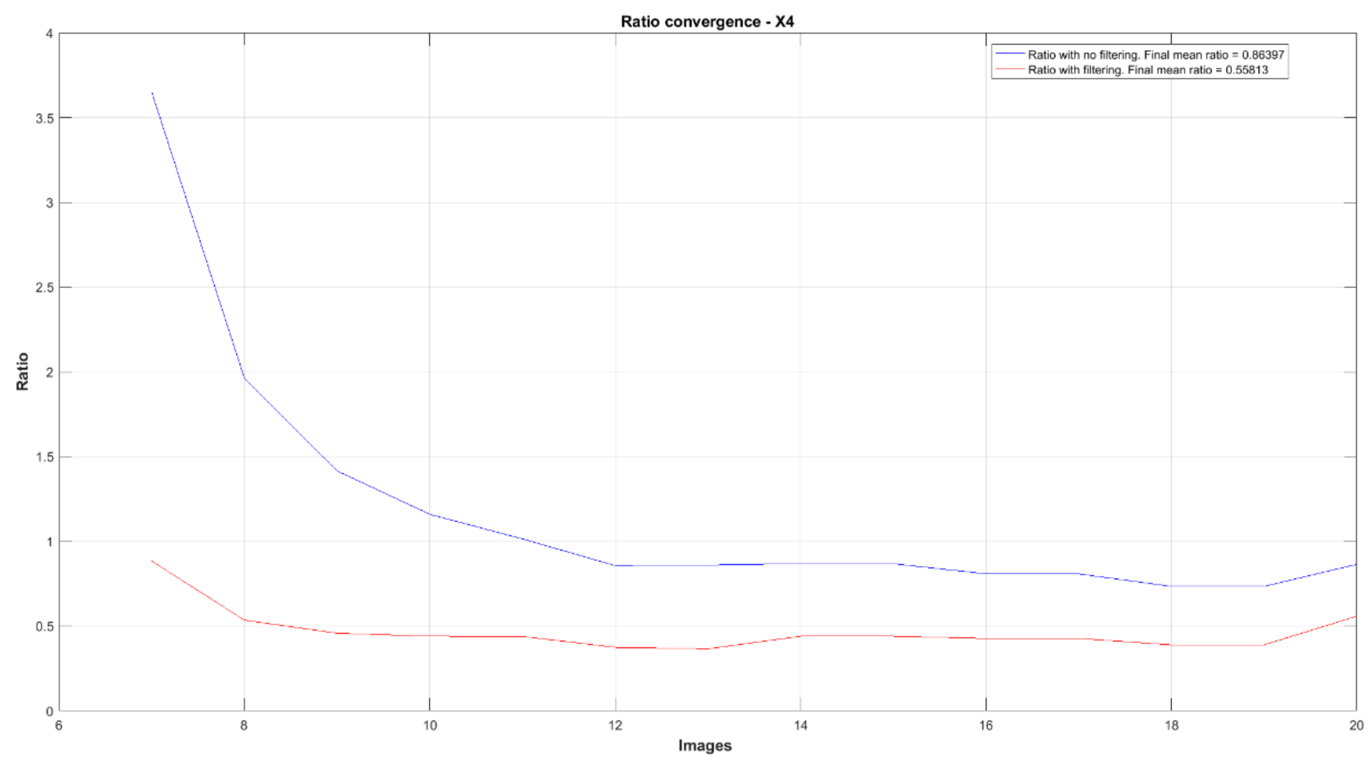

Figure 76. Ratio convergence using the new mean value of calibration constant – X4

The results show that the new calibration factor estimated for Stripmap mode is not representative of Spotlight images.

3.2.5.5 RESULTS FOR X5 SATELLITE – STRIPMAP MODE

A set of 11 images have been acquired on the site for validation: ds22801, ds23765, ds23766, ds23767, ds24342, ds24343, ds24344, 25088, ds25960, ds25961, ds26314.

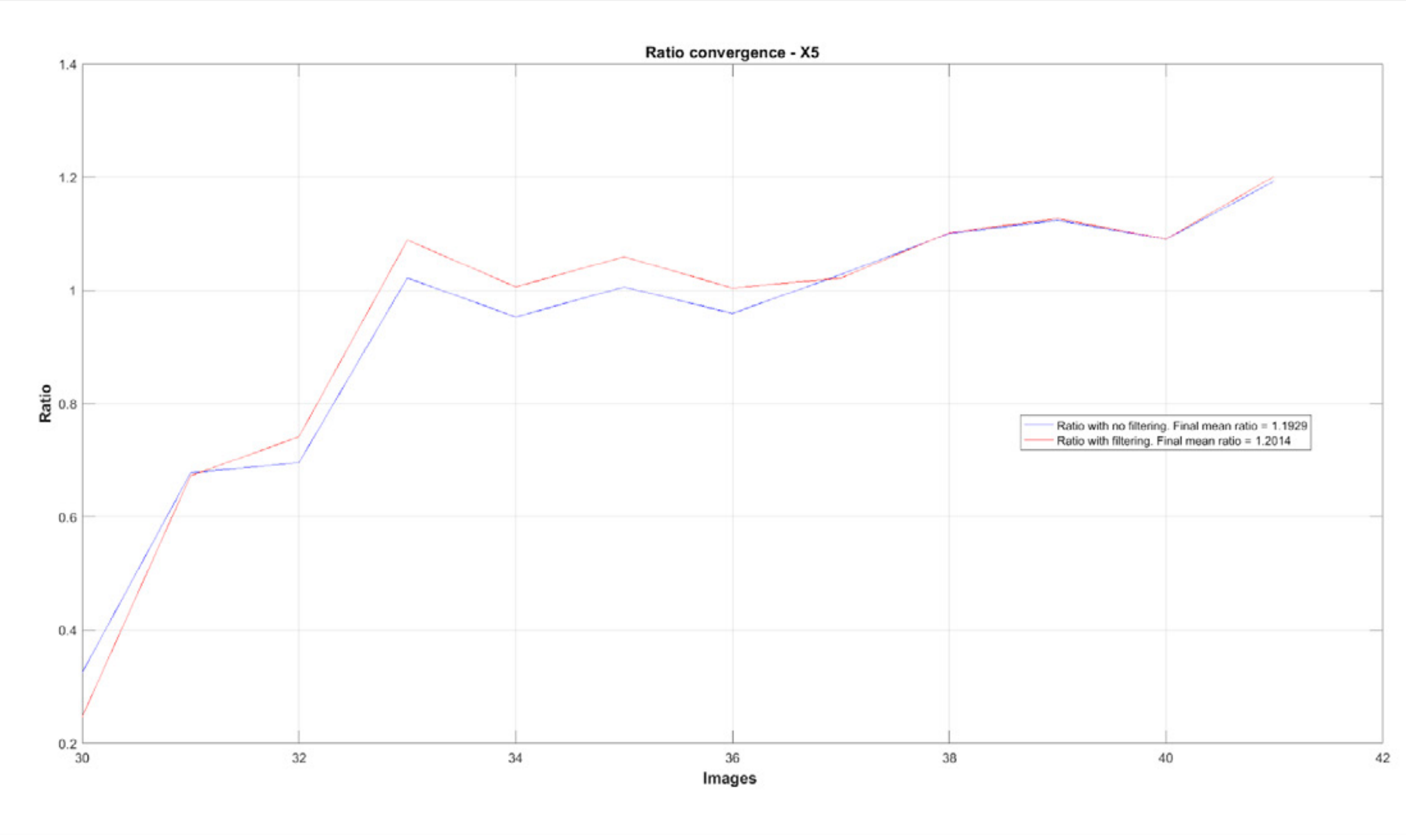

Figure 77. Ratio convergence using the old calibration constant – X5

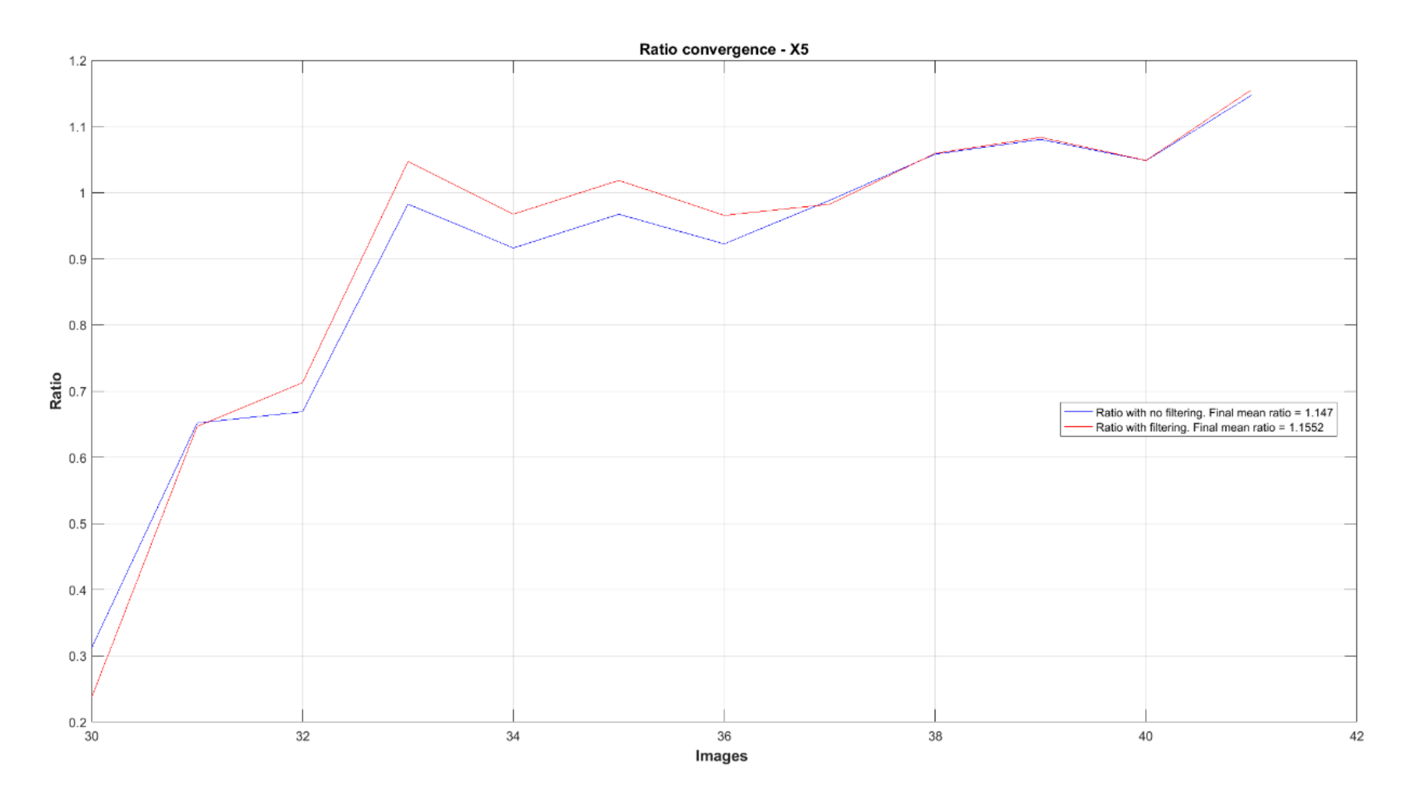

Figure 78. Ratio convergence using the new median value of calibration constant – X5

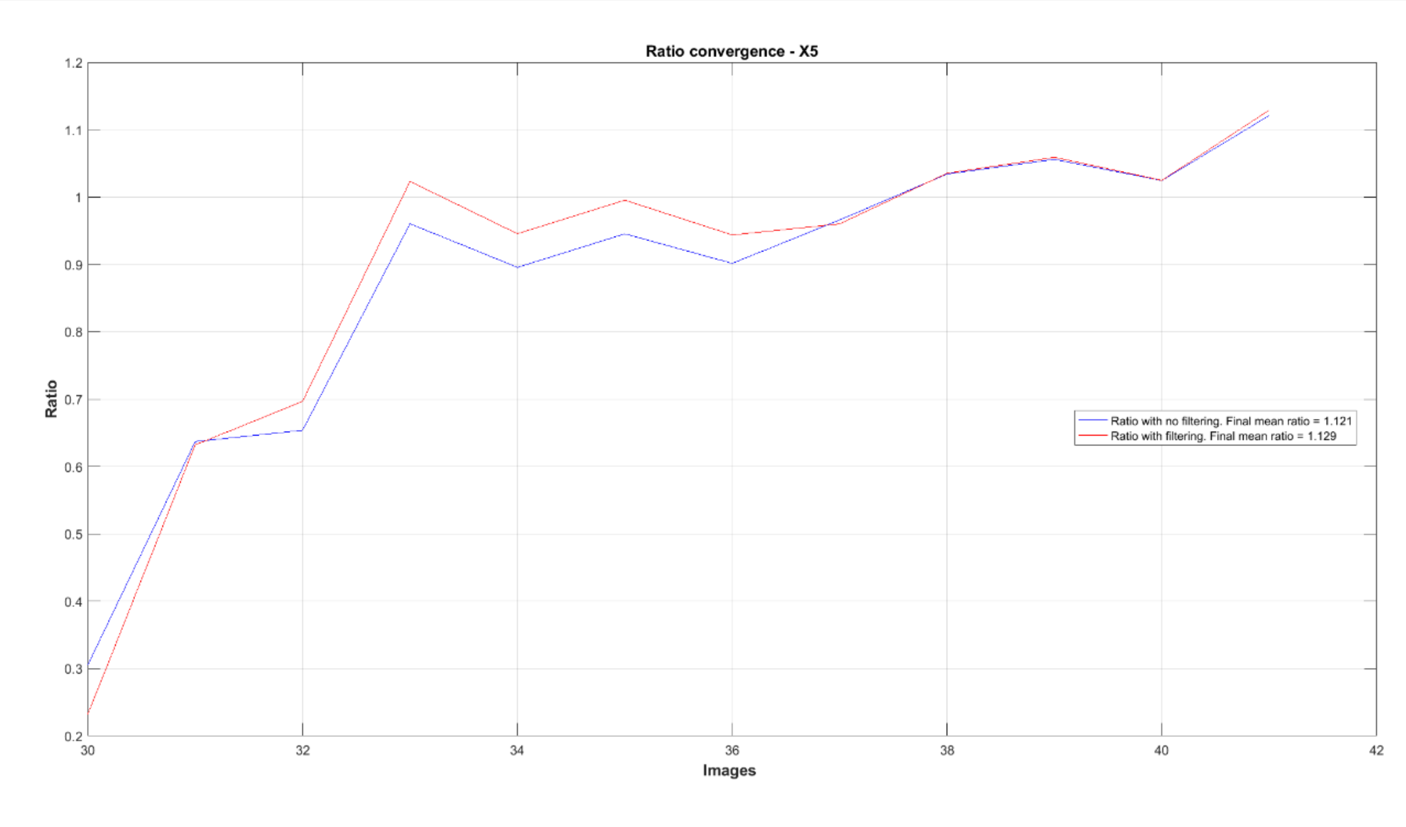

Figure 79. Ratio convergence using the new mean value of calibration constant – X5

The calibration of X5 seems to have a slight divergence from the ideal calibration factor, showing a difference of 10-15%.

3.2.5.6 RESULTS FOR X5 SATELLITE – SPOTLIGHT MODE

A set of 14 images have been acquired on the site for validation: ds21758, ds22802, ds22803, ds23269, ds24341, ds25089, ds25090, 25632, ds25959, ds25733, ds26311, ds26885, ds27024, ds27025.

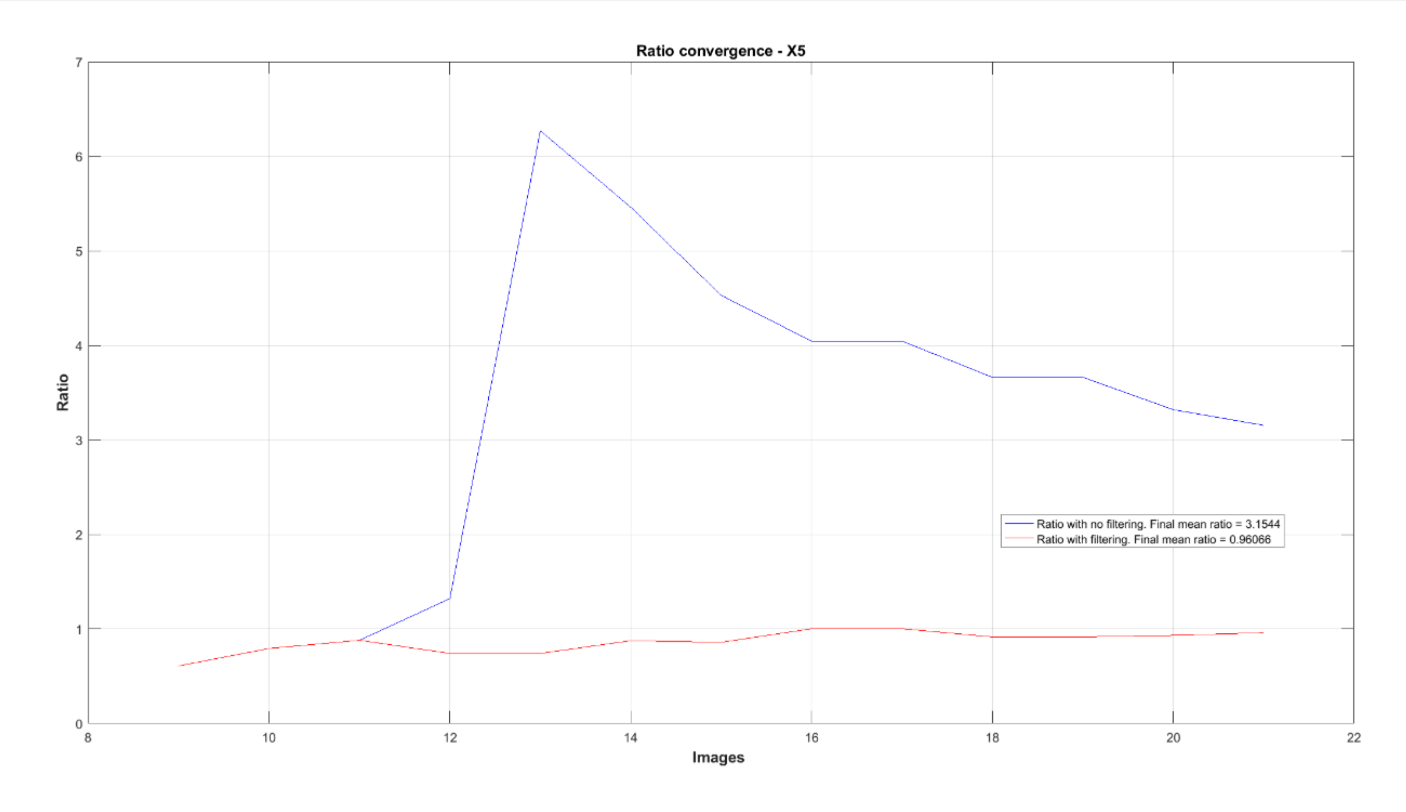

Figure 80. Ratio convergence using the old calibration constant – X5

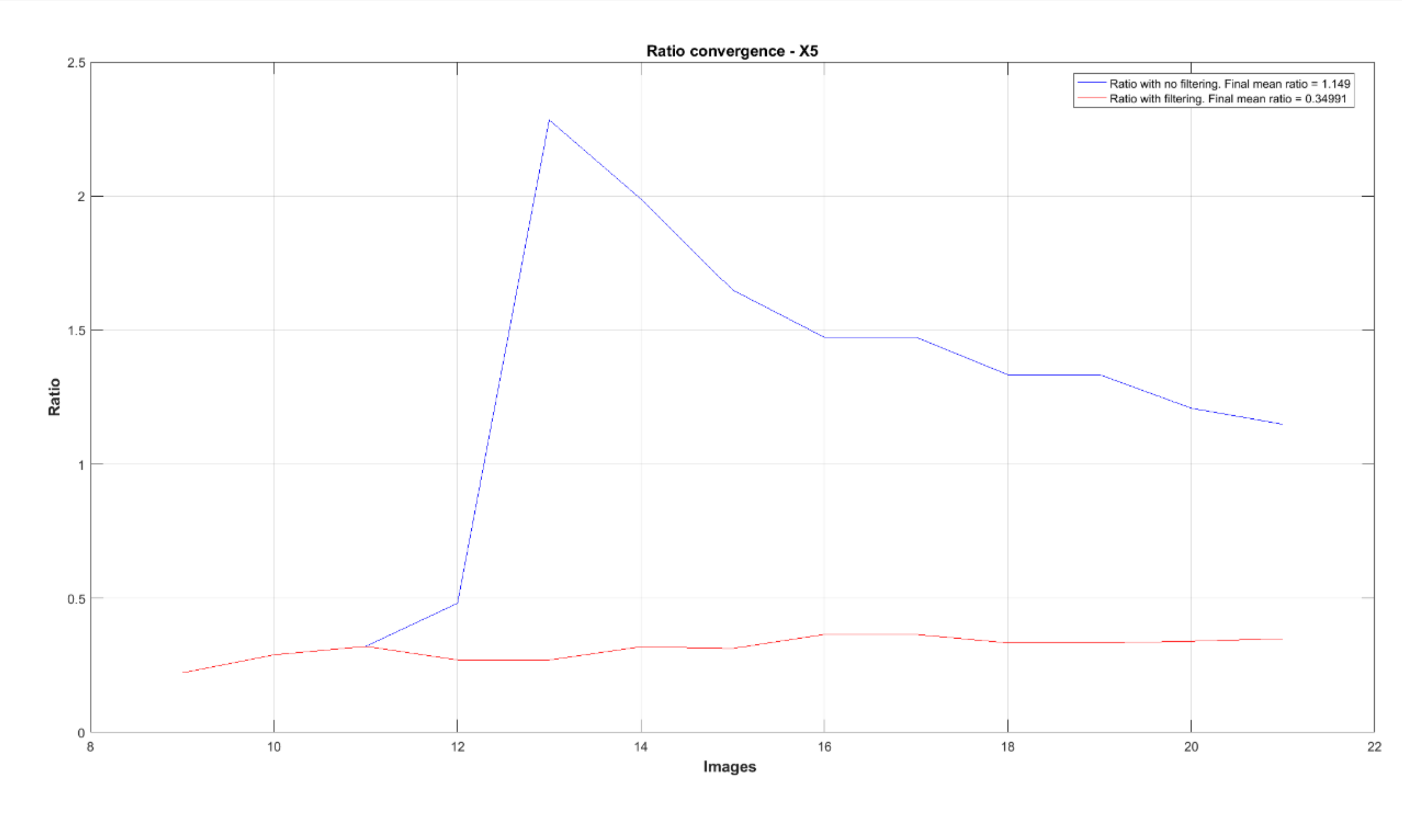

Figure 81. Ratio convergence using the new median value of calibration constant – X5

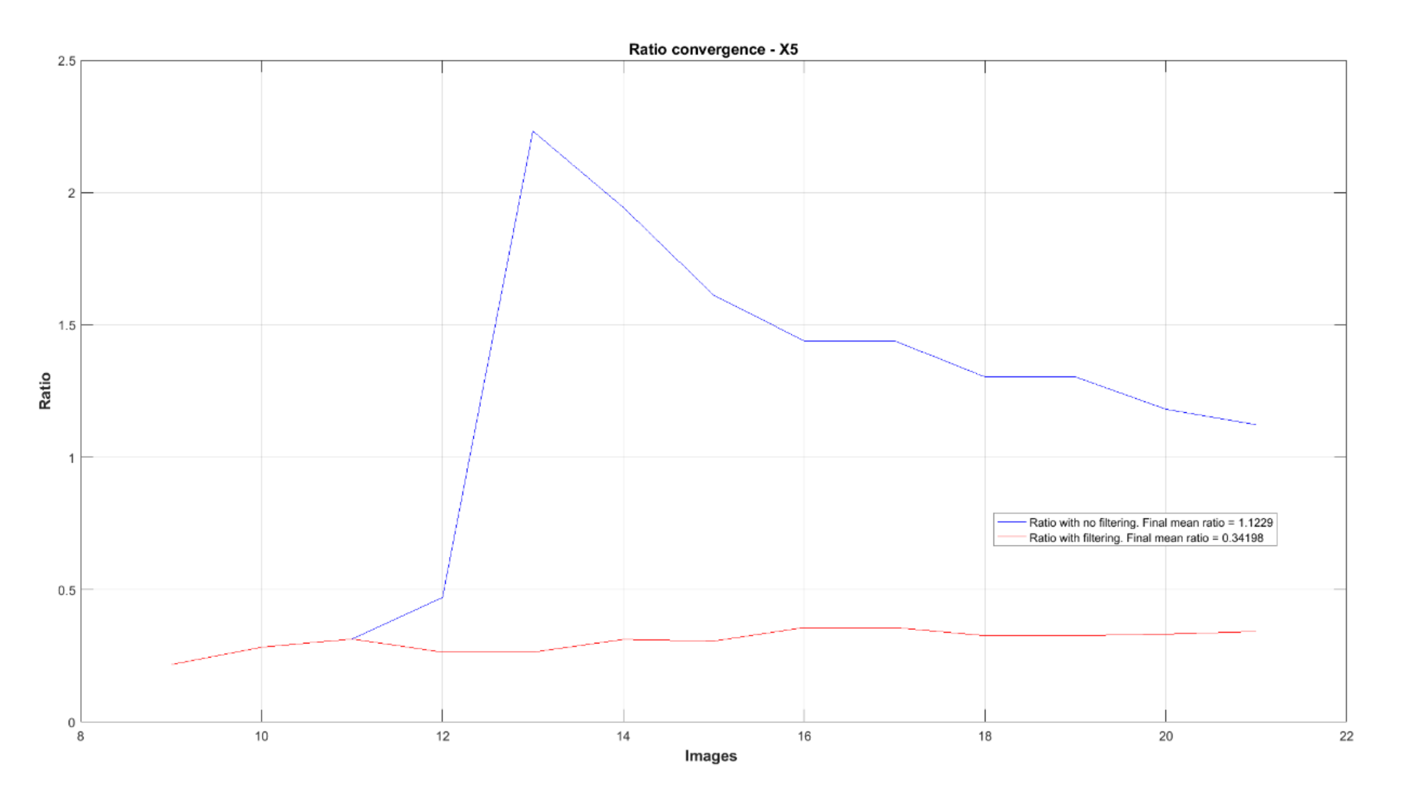

Figure 82. Ratio convergence using the new mean value of calibration constant – X5

Also for X5, the results show that the new calibration factor estimated for Stripmap mode is not representative of Spotlight images.

3.2.5.7 SUMMARY OF VALIDATION PERFORMED ON CORNER REFLECTORS

Table 3 shows the final validation results obtained by applying the filtering parameters. Note that for X2 the low amount of available images did not allow a full validation, that will be performed in the near future. Moreover, the lack of Spotlight images acquired over the Amazon or Congo forest did not allow the calculation of the calibration factor for Spotlight mode, and the validation has been performed using the calibration factor calculated for Stripmap mode.

ACQUISITION MODE	CALIBRATION FACTOR	X2 $R\sigma$	X4 $R\sigma$	X5 $R\sigma$
SM	Current K	1.17 (*)	1.46	1.2
SM	New median K	1.33 (*)	0.98	1.16
SM	New mean K	1.28 (*)	1.03	1.13
SL	Current K	1.44	1.22	0.96
SL	New median K	0.57 (**)	0.53 (**)	0.35 (**)
SL	New mean K	0.54 (**)	0.56 (**)	0.34 (**)

Table 3. Validation results obtained applying the filtering rules: R_σ for X2, X4 and X5

(*) Preliminary results due to a low number of available images in the validation dataset.

(**) Results obtained with the calibration factor calculated for Stripmap images. Calibration factor on Spotlight images has been not yet calculated due to the lack of SL images over the Amazon forest.

APPENDIX A. CALIBRATION/ VALIDATION SCHEME

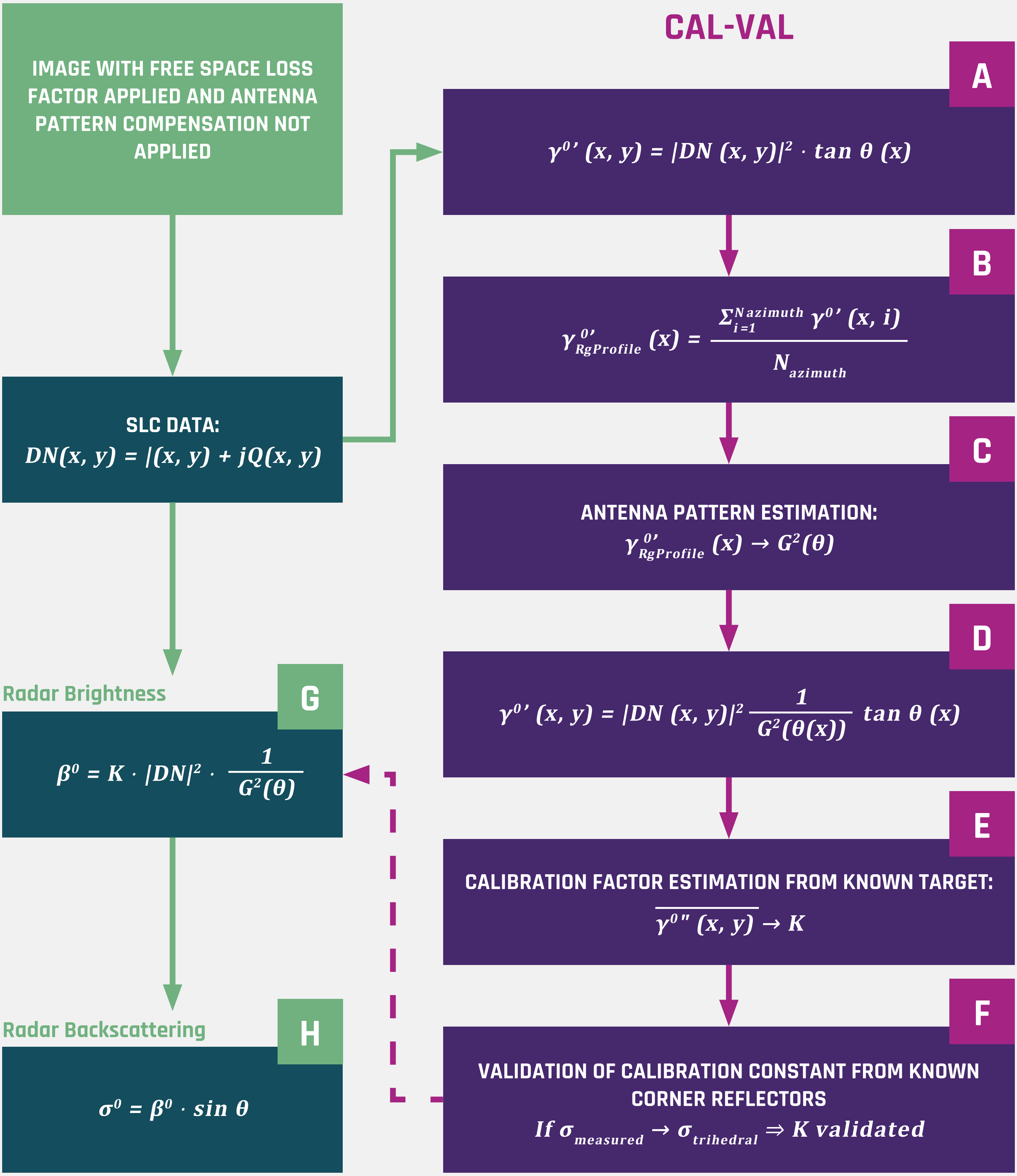

Figure 83. Scheme of Cal-Val methodology used to calibrate ICEYE's sensors

APPENDIX B. REFERENCE DOCUMENTS

▶ REFERENCE DOCUMENTS

[1] J.E. Laycock, H. Laur, “ERS-1 SAR Antenna Pattern Estimation”, Doc. No ES-DPE-OM-JL01, Issue 1, Rev. 1, September 2004.

[2] H. Laur, P. Bally, P. Meadows, J. Sànchez, B. Schättler, E.Lopinto, D.Esteban, “Derivation of the backscattering coefficient sigma0 in ESA SAR PRI Products”, Doc. No ES-TN-RS-PM-HL09, Issue 2, Rev. 5e, 18 February 2003.

[3] N. Miranda, P. Meadows, “Radiometric calibration of S-1 Level-1 Products generated by the S-1 IPF”, Doc. No ESA-EOPG-CSCOP-TN-0002, Issue 1, Rev. 0, 21 May 2015.

[4] M. Bachmann, M. Schwerdt, B. Bräutigam, “TerraSAR-X Antenna Calibration and Monitoring Based on a Precise Antenna Model,” IEEE Transactions on Geoscience and Remote Sensing, Vol. 48 , Issue 2, Pag. 690-701, 18 December 2009.

[5] A.W. Doerry, “Reflectors for SAR Performance Testing”, SANDIA Report SAND2008-0396, January 2008, https://prod.sandia.gov/techlib-noauth/access-control.cgi/2008/080396.pdf.

[6] Garthwaite, M. C., Nancarrow, S., Hislop, A., Thankappan, M., Dawson, J. H., Lawrie, S., “The Design of Radar Corner Reflectors for the Australian Geophysical Observing System: A single design suitable for InSAR deformation monitoring and SAR calibration at multiple microwave frequency bands”, GEOSCIENCE AUSTRALIA, RECORD 2015/03, GeoCat 8275, March 2015.


www.ICEYE.com